A Laboratory Investigation of Open-Channel Dispersion Processes for Dissolved, Suspended, and Floating Dispersants

GEOLOGICAL SURVEY PROFESSIONAL PAPER 433-E

Prepared in cooperation with the U.S. Atomic Energy Commission

A Laboratory Investigation of Open-Channel Dispersion Processes for Dissolved, Suspended, and Floating Dispersants

By W. W. SAYRE *and* F. M. CHANG

TRANSPORT OF RADIONUCLIDES BY STREAMS

GEOLOGICAL SURVEY PROFESSIONAL PAPER 433-E

Prepared in cooperation with the U.S. Atomic Energy Commission

UNITED STATES GOVERNMENT PRINTING OFFICE, WASHINGTON : 1968

UNITED STATES DEPARTMENT OF THE INTERIOR

STEWART L. UDALL, *Secretary*

GEOLOGICAL SURVEY

William T. Pecora, *Director*

For sale by the Superintendent of Documents, U.S. Government Printing Office
Washington, D.C. 20402 - Price 60 cents (paper cover)

CONTENTS

ILLUSTRATIONS

TABLES

SYMBOLS[1]

Symbol	*Definition*	*Dimensions*	*Units*
A_m	Area under experimental concentration-distribution curve, determined by planimetering.	----------	----------
A_t	Theoretical area under concentration-distribution curve—assuming perfect mixing and sampling.	----------	----------
B	Width of a rectangular channel.	L	ft
C	Concentration, by weight, of dispersant in water.	----------	ppb or ppm
C_v	Coefficient of variation, ratio of standard deviation to mean.	----------	----------
E	Mean rate of energy dissipation per unit mass of fluid, given by $\overline{U}gS$.	L^2/T^3	ft^2 per sec^3
$f(\cdot;\cdot)$	A probability-density function. The symbol(s), in the parentheses, preceding the semicolon designates the variable(s) with respect to which probability is distributed. The symbol following the semicolon designates the specific point in space or time to which the probability applies.	T^{-1} or L^{-1}	sec^{-1} or ft^{-1}
F	Sensitivity of fluorometer, expressed in fluorometer units per unit of concentration.	----------	----------
g	Acceleration of gravity.	L/T^2	ft per sec^2
I	Random variable denoting the time required for a particle of dispersant to travel from the source at $x=0$ to the sampling nozzle.	T	sec
K_x, K_y, K_z	Coefficients of dispersion in the x, y, and z directions.	L^2/T	ft^2 per sec
K_C	Component of K_x due to differential convection.	L^2/T	ft^2 per sec
K_T	Component of K_x due to turbulence.	L^2/T	ft^2 per sec
L	Length scale of smallest eddies whose energy is converted directly into heat by viscous dissipation.	L	ft
L_t	Lagrangian integral time scale of turbulence.	T	sec
L_x, L_z	Length scale for large-scale turbulence components in the x and z directions.	L	ft
L_m	Length of initial increment of dispersion distance within which the one-dimensional Fickian diffusion theory does not apply.	L	ft
O	Random variable denoting the duration of the time interval between the release of a particle of dispersant from the source and its registration by the detection system.	T	sec
q	Volumetric rate of release of dispersant from a continuous point source.	L^3/T	ml per sec
Q	Volumetric rate of discharge of water in the channel.	L^3/T	ft^3 per sec
R	Random variable denoting the time lag between the arrival of a particle of dispersant at the sampling nozzle and its registration by the detection system.	T	sec
R	Reynolds number, defined as $\overline{U}y_n/\nu$ in a wide, open channel and as $\overline{U}D/\nu$ in a pipe.	----------	----------
$R_{u_i'}(\tau)$	Lagrangian correlation coefficient, which correlates the fluctuating component u_i' of the velocity of a fluid particle at the times t and $t+\tau$.	----------	----------
S	Slope of the energy gradient in a uniform open-channel flow.	----------	----------
t	Time.	T	sec
$\bar{t}$	Mean traveltime of a dispersing substance over a prescribed distance.	T	sec
T	Water temperature.	----------	°C

[1] Special symbols, subscripts, superscripts, and overscores if not given here, are defined where they first appear in the text.

Symbol	Definition	Dimensions	Units
U	Time-averaged local velocity of flow in the x direction.	L/T	ft per sec
$\overline{U}$	Average velocity of flow in the cross section.	L/T	ft per sec
U^*	Difference between the local velocity U and the cross-sectional average velocity $\overline{U}$.	L/T	ft per sec
U_p	Time-averaged local velocity of a suspended sediment particle.	L/T	ft per sec
U_s	Time-averaged velocity of a particle floating on the water surface.	L/T	ft per sec
U_τ	Shear velocity in a wide, open channel, defined as $\sqrt{\tau_0/\rho}$ or $\sqrt{gy_nS}$.	L/T	ft per sec
V_p	Settling velocity of a sediment particle in quiescent water.	L/T	ft per sec
W	Weight of dispersing substance.	F	gm
x	Longitudinal distance.	L	ft
y	Vertical distance.	L	ft
y_n	Normal depth; depth of flow in a channel with uniform flow.	L	ft
z	Lateral distance.	L	ft
β	Sediment suspension parameter, defined as $V_p/\kappa U_\tau$.	----------	----------
γ	Specific weight of water.	F/L^3	lb per ft^3
ϵ	Local eddy diffusivity, sometimes called the kinematic eddy viscosity.	L^2/T	ft^2 per sec
ϵ_p	Local eddy diffusivity for sediment particles.	L^2/T	ft^2 per sec
ϵ_y	Local vertical eddy diffusivity.	L^2/T	ft^2 per sec
$\bar{\epsilon}_y$	Vertical eddy diffusivity averaged over the depth of flow.	L^2/T	ft^2 per sec
ζ	Eccentricity of source, the lateral displacement of a point source from the centerline of the channel.	L	ft
κ	Von Karman turbulence coefficient.	----------	----------
ν	Kinematic viscosity.	L^2/T	ft^2 per sec
ξ	Longitudinal displacement from a yz plane moving in the x direction at velocity $\overline{U}$, defined as $x-\overline{U}t$.	L	ft
σ_t^2	Variance of a concentration distribution with respect to time.	T^2	sec^2
σ_x^2, σ_z^2	Variances of longitudinal and lateral concentration distributions.	L^2	ft^2
τ	Time.	T	sec
τ_0	Shear stress at the bed, defined as $\gamma y_n S$.	F/L^2	lb per ft^2

A LABORATORY INVESTIGATION OF OPEN-CHANNEL DISPERSION PROCESSES FOR DISSOLVED, SUSPENDED, AND FLOATING DISPERSANTS

By W. W. Sayre and F. M. Chang

ABSTRACT

The establishment of more reliable criteria for regulating the discharge of contaminants into streams and rivers requires an improved understanding of fluvial transport and dispersion processes. This requirement applies particularly to contaminants which are transported as part of the suspended or bed-material sediment load.

A series of experiments conducted in a rigid-boundary laboratory flume having an artificially roughened bed compared longitudinal dispersion of suspended silt-size sediment particles with longitudinal dispersion of a fluorescent dye solution. Additional information on dispersion in open channels was provided by lateral dispersion experiments with dye and by longitudinal and lateral dispersion experiments with floating polyethylene particles. Several dispersion theories for open-channel flows are reviewed, and the experimental data are analyzed in the light of these theories.

The experimental results indicate that in a channel with a rough boundary the longitudinal and lateral dispersion processes for dissolved dispersants and floating particles converge to a Fickian-type diffusion process quite rapidly with increasing dispersion distance. The experimentally determined values of the longitudinal dispersion coefficient for the dye closely correspond to values calculated by J. W. Elder's theory of longitudinal dispersion in open channels. Except in the sediment-dispersion experiments, the dispersion coefficients in each set of experiments were found to be approximately proportional to the product of the depth and the shear velocity. The longitudinal dispersion process for suspended silt-size particles, although it resembles the process for the dye, is modified by the tendency of the particles to settle toward the slower moving flow near the bed and eventually to be deposited on the bed. The longitudinal distribution of particle deposition can be calculated with satisfactory accuracy by a procedure based on T. R. Camp's theory of the influence of turbulence on sedimentation in settling tanks. The confining effect of the sidewalls on the lateral distribution of dye can be accounted for satisfactorily by the reflection-superposition principle in which channel boundaries are treated as reflecting barriers.

To compare the response characteristics of the different concentration-measuring systems used in the experiments, the response of the systems to rapidly changing concentrations was investigated both experimentally and analytically. The results indicate that the system output can be expressed as the convolution of the response function of the system to a unit impulse and the input to the system.

INTRODUCTION AND ACKNOWLEDGMENTS

With the growing demands on the Nation's water resources, it becomes increasingly imperative that rational criteria be applied to the problem of allocating available water supplies among all the various competing uses. As requirements grow, the allowable margin for error decreases. All too frequently the information necessary for making rational decisions is lacking.

One example of this problem is the use of streams and rivers as channels for the disposal of industrial, agricultural, and domestic wastes. Waterways have traditionally performed this function. If pollution is not controlled, however, the availability of water for other uses may be sharply curtailed. To control pollution, the release of potentially harmful contaminants into waterways must be regulated so that the capacity of the flow to maintain the concentration of contaminants within permissible limits is not exceeded. This regulation requires knowledge of the rates at which stream systems are capable of transporting and dispersing contaminants. In general, transport and dispersion rates depend on the physical and chemical nature of the contaminant, and on the physiographic characteristics of, and the flow discharge in, the stream system. However, the relationships between these factors and the transport and dispersion processes are extremely complex. Due to inadequate understanding of both the relationships and the processes, criteria for predicting transport and dispersion rates are often unreliable.

With the introduction since World War II of radioactive wastes and the new generation of agricultural pesticides and herbicides, the need for improved criteria for predicting transport and dispersion rates has become more acute. This is largely because many of these contaminants (1) have a tolerance level several orders of magnitude lower than that for most other pollutants, (2) are chemically very stable and

retain their toxicity for long periods of time before yielding to natural decay processes, and (3) cannot be removed by conventional water-treatment practices.

For a number of years the Water Resources Division of the U.S. Geological Survey in cooperation with the Division of Reactor Development and Technology of the U.S. Atomic Energy Commission has been engaged in investigations of dispersion processes in streams. As either a direct or indirect result of this program, the dispersion of dissolved contaminants has been investigated by Godfrey and Frederick (1963), Glover (1964), Yotsukura, Smoot, and Cahal (1964), and Yotsukura and Fiering (1964); available information on the uptake and transport of radionuclides by stream sediments was assembled by Sayre, Guy, and Chamberlain (1963); and Sayre and Hubbell (1965) investigated the transport and dispersion of contaminants which have become attached to bed-material sediment particles in an alluvial channel.

The principal objective of this investigation is to bridge the gap between what is known about the dispersion process for dissolved contaminants and what is known about the dispersion process for contaminants that are transported as part of the bed-material load. Dissolved contaminants are transported at the mean velocity of the stream and are dispersed by the mechanism of turbulent diffusion and by the differential convection currents associated with velocity gradients. Contaminants that are transported in colloidal suspension have been shown by Sayre and Hubbell (1963) to disperse in the same manner as dissolved contaminants and at essentially the same rate. On the other hand, contaminants which are transported as part of the bed-material load move in a sequence of steps of random length between which particles may remain buried for considerable periods. Hence, these contaminants are transported and dispersed at rates that are much less—frequently by several orders of magnitude—than the rates for dissolved or colloidally suspended contaminants. Between these two extremes are the contaminants that are transported mainly with the suspended-sediment load. These contaminants are either adsorbed by, or behave as, sediment particles in the silt- and fine-sand-size ranges. These particles may travel for long distances in suspension and, while in suspension, behave very much like fluid or colloidally suspended particles. However, they have a tendency to settle and eventually be deposited on the bed, where they behave as bed-material particles until they are reentrained in the flow.

This report describes a series of experiments conducted in a rigid-boundary laboratory flume having an artificially roughened bed. In the experiments the longitudinal dispersion of suspended silt-size particles was compared with the longitudinal dispersion of a fluorescent dye solution, under nearly identical conditions. Because of inconsistencies between the results of previous experiments on the longitudinal dispersion of dissolved dispersants and Elder's (1959) theory of longitudinal dispersion in an open channel, the artificial roughness on the flume bed was designed to create flow conditions that would satisfy as nearly as possible the requirement, specified in the theory, of no transverse velocity gradient. To provide additional information on dispersion processes in open channels, lateral dispersion experiments with fluorescent dye and longitudinal and lateral dispersion experiments with small polyethylene particles floating on the water surface were also performed. The application of several dispersion theories to open-channel flow situations is reviewed, and the experimental data are analyzed within the framework of these theories.

The experiments were conducted in the hydraulic laboratory of Colorado State University at Fort Collins. The basic plan of the experimental program was conceived, and the first experiments were conducted, under the supervision of D. W. Hubbell, hydraulic engineer, of the U.S. Geological Survey. Tsung Yang, R. S. McQuivey, and J. A. Danielson, graduate students at Colorado State University, participated extensively in the design of experimental equipment and in the collection and analysis of data.

THEORY OF DISPERSION IN OPEN-CHANNEL FLOW

The processes by which dissolved and suspended particulate matter are dispersed in open-channel flow have been subjected to considerable theoretical analysis in recent years. Owing to a number of complex factors that are almost invariably associated with open-channel flow—turbulence, velocity gradients in the vertical and horizontal directions, and secondary flows originating from bends or obstructions—theoretical treatments of the problem have been only partially successful. Not even for the relatively simple conditions of uniform flow in a straight channel of constant cross section has a theory been formulated that accounts adequately for all of the above factors. Nevertheless, a considerable amount of useful information is contained in the technical literature. However, this information is scattered among many publications and much of it is not oriented toward open-channel dispersion processes. In this section an attempt is made to synthesize the most pertinent existing theories into a coherent theoretical background for the convenience of the general user in interpreting the experimental results presented and analyzed in the following sections.

The dispersion process can be described rather rigorously in differential-equation form by the diffusion equation for turbulent flow, which is based on the principle of conservation of mass. Stated in tensor form for dispersion in a steady flow of incompressible fluid, and with the assumption that the fluid properties of the dispersant are identical with those of the transporting medium, this equation is

$$\frac{\partial \overline{C}}{\partial t}+\overline{U}_i\frac{\partial \overline{C}}{\partial x_i}=-\frac{\partial}{\partial x_i}\overline{c'u_i'}+\epsilon_M\frac{\partial^2\overline{C}}{\partial x_i\partial x_i}, \quad (1)$$

where

$C=\overline{C}+c'=C(x_1, x_2, x_3, t)$ is the local concentration of dispersant expressed as the sum of a slowly varying part, $\overline{C}$, and a rapidly fluctuating part, c',

t=time,

$U_i=\overline{U}_i+u_i'=U_i(x_1, x_2, x_3)$ is the local velocity of flow expressed as the sum of the time-averaged velocity $\overline{U}_i$ and a turbulent component, u_i',

x_i=distance and the index $i=1, 2, 3$ indicates direction in a rectangular coordinate system, and

ϵ_M=coefficient of molecular diffusivity.

A coefficient of turbulent diffusion, $\epsilon_{T_{ij}}=\epsilon_{T_{ij}}(x_1, x_2, x_3)$, may be defined as

$$\epsilon_{T_{ij}}\frac{\partial \overline{C}}{\partial x_j}\equiv-\overline{c'u_i'}. \quad (2)$$

Assuming that the processes of molecular and turbulent diffusion are independent and therefore additive, Mickelsen (1960), the turbulent and molecular diffusion coefficients can be combined by addition to give

$$\epsilon_{ij}(x_1, x_2, x_3)=\epsilon_{T_{ij}}+\epsilon_M. \quad (3)$$

Incorporation of equations 2 and 3 and elimination of the averaging bars permits equation 1 to be written in the form

$$\frac{\partial C}{\partial t}+U_i\frac{\partial C}{\partial x_i}=\frac{\partial}{\partial x_i}\left[\epsilon_{ij}\frac{\partial C}{\partial x_j}\right]. \quad (4)$$

In equation 3 the question of whether the processes of molecular and turbulent diffusion actually are independent is mainly of academic interest, because in ordinary open-channel flows ϵ_T is several orders of magnitude larger than ϵ_M. If, in addition, the coordinate axes are defined so that they coincide with the principal axes of the diffusion tensor, $\epsilon_{ij}=0$ for $i\neq j$. If we now define $\epsilon_{ij}=\epsilon_i$ for $i=j$, equation 4 simplifies further to

$$\frac{\partial C}{\partial t}+U_i\frac{\partial C}{\partial x_i}=\frac{\partial}{\partial x_i}\left[\epsilon_i\frac{\partial C}{\partial x_i}\right]. \quad (4a)$$

Consider a uniform flow in a straight channel of constant cross section so that the basic flow and turbulence structure does not change with respect to the direction of flow. If a coordinate system is chosen in which the subscripts 1, 2, and 3 indicate respectively the direction of flow, the direction normal to the channel bed, and the horizontal direction normal to the flow direction, it is evident that $U_2=U_3=0$. Furthermore, under these conditions it is to be expected that ϵ_i is a function of x_2 and x_3, but not of x_1. Equation 4 may now be written

$$\frac{\partial C}{\partial t}+U_1\frac{\partial C}{\partial x_1}=\epsilon_1\frac{\partial^2 C}{\partial x_1^2}+\frac{\partial}{\partial x_2}\left[\epsilon_2\frac{\partial C}{\partial x_2}\right]+\frac{\partial}{\partial x_3}\left[\epsilon_3\frac{\partial C}{\partial x_3}\right] \quad (5)$$

or, after switching to the more conventional form of Cartesian notation in which x_1, x_2, x_3 are replaced by x, y, z; U_1, U_2, U_3 by U, V, W; and ϵ_1, ϵ_2, ϵ_3 by ϵ_x, ϵ_y, ϵ_z,

$$\frac{\partial C}{\partial t}+U\frac{\partial C}{\partial x}=\epsilon_x\frac{\partial^2 C}{\partial x^2}+\frac{\partial}{\partial y}\left[\epsilon_y\frac{\partial C}{\partial y}\right]+\frac{\partial}{\partial z}\left[\epsilon_z\frac{\partial C}{\partial z}\right]. \quad (5a)$$

This is the basic Eulerian diffusion equation which applies to dispersion in uniform turbulent flow. In equation 5a U, ϵ_x, ϵ_y, and ϵ_z are generally functions of y and z.

Theoretical work relating to dispersion in open-channel flow has been devoted mainly to (1) analysis of the nature of ϵ_x, ϵ_y, and ϵ_z from the standpoint of fluid mechanics, (2) the analysis of certain limiting cases for which solutions to equation 5 can be obtained, and (3) the transformation of equation 5 into forms which are more amenable to solution.

Approaches yielding useful results have been based on (1) the semiempirical Fickian diffusion theory, (2) the theory of diffusion by continuous movements, (3) Kolmogoroff's theory of local similarity in turbulence, (4) the theory of longitudinal dispersion by differential convection due to a velocity gradient, and (5) diffusion theory as applied to the transport of suspended sediment. Because all these theories have a direct bearing on the experiments described in this paper, a review of the pertinent results and limitations is appropriate here.

FICKIAN DIFFUSION THEORY

In applying the Fickian diffusion theory to the process of dispersion in a turbulent flow, an exact analogy with the process of molecular diffusion is assumed. Thus, the coefficients ϵ_x, ϵ_y, and ϵ_z are assumed to be constants, which we shall call K_x, K_y, and K_z, and the time-average velocity, U, which we shall call $\overline{U}$, is

assumed to be the same everywhere in the flow field. In a real flow $\overline{U}$ is defined as the average velocity in a cross section. With these very drastic assumptions, equation 5a becomes

$$\frac{\partial C}{\partial t}+\overline{U}\frac{\partial C}{\partial x}=K_x\frac{\partial^2 C}{\partial x^2}+K_y\frac{\partial^2 C}{\partial y^2}+K_z\frac{\partial^2 C}{\partial z}. \quad (6)$$

The convection term, $\overline{U}\dfrac{\partial C}{\partial x}$, means that dispersion is occurring within a frame of reference which is moving at a velocity $\overline{U}$ in the x direction.

Two types of dispersion in open-channel flow are of particular interest: (1) longitudinal dispersion from an instantaneous plane source which is distributed uniformly over the cross section, and (2) lateral dispersion from a continuous point source.

The longitudinal dispersion reduces to a one-dimensional problem because, owing to the restrictions on equation 6 and the initial source conditions, C is no longer dependent on y and z. Equation 6 then becomes

$$\frac{\partial C}{\partial t}+\overline{U}\frac{\partial C}{\partial x}=K_x\frac{\partial^2 C}{\partial x^2} \quad (7)$$

for which a solution satisfying the initial condition is

$$C(x, t)=C_0 f(x; t) \quad (8)$$

where

C_0=source strength of dispersant, which in a rectangular channel of flow depth y_n and width B is equal to $W/\gamma By_n$, where W is the total weight of dispersant, and

$$f(x; t)=\frac{1}{2\sqrt{\pi K_x t}}e^{-\frac{(x-\overline{U}t)^2}{4K_x t}} \quad (8a)$$

The function $f(x; t)$ is the probability-density function of the normal probability law with mean $\bar{x}=\overline{U}t$, and variance $\sigma_x^2=2K_x t$. In comparing equation 8 with experimental results it is usually more convenient to consider C as a function of t with x as a parameter rather than as a function of x with t as a parameter. Then equation 8 becomes

$$C(t, x)=\frac{C_0}{\overline{U}}f(t; x) \quad (9)$$

where

$$f(t; x)=\overline{U}f(x; t)=\frac{\overline{U}}{2\sqrt{\pi K_x t}}e^{-\frac{(x-\overline{U}t)^2}{4K_x t}} \quad (9a)$$

in which $f(t; x)$ is the probability-density function for the distribution of dispersant flux with respect to t at a fixed value of x. The mean and variance of $f(t; x)$ as given by Yotsukura (1963) are

$$\bar{t}\equiv\int_0^\infty tf(t; x)dt=\frac{x}{\overline{U}}+\frac{2K_x}{\overline{U}^2} \quad (10)$$

and

$$\sigma_t^2\equiv\int_0^\infty (t-\bar{t})^2 f(t; x)dt=\frac{2K_x x}{\overline{U}^3}+8\left(\frac{K_x}{\overline{U}^2}\right)^2. \quad (11)$$

Experimental evidence of Yotsukura, Smoot, and Cahal (1964), Glover (1964), and Godfrey and Frederick (1963) indicates that the Fickian diffusion theory provides at best a crude representation of the longitudinal dispersion process in open channels. In general, the agreement between the Fickian theory and experimental observations is poor in the early stages of dispersion, but tends to improve with increasing dispersion time or distance from the source. Thus, under some conditions, for example dispersion in a uniform rectangular channel with straight alinement, equations 8 and 9 are useful as asymptotic solutions for large values of t and x respectively.

Let us turn now to lateral dispersion from a point source. Since it is assumed implicitly in equation 6 that the dispersion process in any one of the three coordinate directions is independent of the process in either or both of the other two directions, the joint probability-density function $f(x, y, z; t)$ is equal to the product of the one-dimensional probability-density functions, $f(x; t)$, $f(y; t)$, and $f(z; t)$. The solution of equation 6 for the initial condition of an instantaneous point source at the origin can then be written in the form

$$C(x, y, z, t)=\frac{W}{\gamma}f(x, y, z; t)=\frac{W}{\gamma}f(x; t)f(y; t)f(z; t) \quad (12)$$

where

$$f(x; t)=\frac{1}{2\sqrt{\pi K_x t}}e^{-\frac{(x-\overline{U}t)^2}{4K_x t}}, \quad (12a)$$

$$f(y; t)=\frac{1}{2\sqrt{\pi K_y t}}e^{-\frac{y^2}{4K_y t}}, \quad (12b)$$

and

$$f(z; t)=\frac{1}{2\sqrt{\pi K_z t}}e^{-\frac{z^2}{4K_z t}} \quad (12c)$$

The three functions $f(\cdot; t)$, where the dot represents an arbitrary variable with respect to which probability is distributed, are, like equation 8a, probability-density functions of the normal probability law. In a three-dimensional domain they are one-dimensional only in the sense of marginal probability-density functions. For example, the function

$$f(y; t)=\int_0^\infty\int_{-B/2}^{B/2} f(x, y, z; t)dzdx$$

describes the vertical distribution of all of the dispersant irrespective of position with respect to x and z. It does not apply to the distribution in any particular cross section.

Assuming that y_n/B is small and that there is sufficient turbulence to rapidly distribute the dispersant throughout the depth of flow, the concentration with respect to y soon tends to become uniform—that is, $f(y;\ t)\rightarrow 1/y_n$. Then equation 12 becomes

$$C(z,\ x,\ t)=\frac{W}{\gamma y_n}f(x;\ t)f(z;\ t). \tag{13}$$

The solution of equation 6 for a point source discharging continuously at a constant volumetric rate q so that $W=q\gamma C_0 dt$, where C_0 is the concentration of dispersant at the source, can be obtained by applying the superposition principle to equation 13 whereby

$$\begin{aligned}C(z,\ x)&=\int_{-\infty}^{t}C(z,\ x,\ t-t_1)dt_1\\&=\int_0^{\infty}C(z,\ x,\ \tau)d\tau\\&=\frac{qC_0}{y_n}\int_0^{\infty}f(x;\ \tau)f(z;\ \tau)d\tau.\end{aligned}$$

In the above operation the dispersion time $\tau=t-t_1$ of a particle of dispersant is the difference between the observation time, t, and the release time, t_1. Making the appropriate substitutions and performing the integration,

$$C(z,\ x)=\frac{qC_0}{2\pi y_n\sqrt{K_xK_z}}\,e^{\frac{\bar{U}x}{2K_x}}\,K_0\left[\frac{\bar{U}}{2K_x}\sqrt{x^2+\left(\frac{K_x}{K_z}\right)z^2}\right], \tag{14}$$

where $K_0(\ )$ is a modified Bessel function of the second kind, of order zero. Values of $K_0(\ )$ are tabulated in mathematical reference books such as Korn and Korn (1961). For

$$\left(\frac{K_x}{K_z}\right)\frac{z^2}{x^2}<<1 \text{ and } x>>\frac{2K_x}{\bar{U}},$$

equation 14 converges to

$$C(z,\ x)=\frac{qC_0}{\bar{U}y_n}f\left(z;\ \frac{x}{\bar{U}}\right), \tag{15}$$

in which $f\left(z;\ \frac{x}{\bar{U}}\right)$ is the probability-density function of the normal probability law given in equation 12c, wherein t is replaced by $x/\bar{U}$. Except close to the source, the conditions for convergence are usually easily obtainable in open-channel flow so that from a practical standpoint the difference between the two functions is generally scarcely distinguishable. The variance corresponding to equation 14,

$$\sigma_z^2=\frac{2K_z}{\bar{U}}\left(x+\frac{2K_x}{\bar{U}}\right), \tag{16}$$

is larger than the variance corresponding to equation 15,

$$\sigma_z^2=\frac{2K_zx}{\bar{U}}, \tag{17}$$

by the constant amount, $\frac{4K_zK_x}{\bar{U}^2}$.

In a channel of finite width, equations 14 and 15 apply only in the region extending downstream from the section where $f(y;\ t)\approx\frac{1}{y_n}$ to the section where a significant amount of dispersant reaches the sidewalls at $x\approx 0.01\bar{U}B^2/K_z$. In a rectangular channel of width B, if the sidewalls are assumed to behave as reflecting barriers, equations 14 and 15 may be extended to account for the confining effects of the walls. The solution for the general case in which the source is displaced a lateral distance, ζ, from the origin at the center of the channel is

$$\begin{aligned}C_1(z,\ x)=C(z-\zeta,\ x)+\sum_{n=1}^{\infty}C(nB-\zeta\\+(-1)^nz,\ x)+C(nB+\zeta-(-1)^nz,\ x),\end{aligned} \tag{18}$$

in which

$-B/2\leq z\leq B/2$ and
$n=$ the number of reflection cycles.

The $C(\cdot,\ x)$ terms on the right side of equation 18 are as defined by equations 14 or 15, but with z replaced by the first expression—for example, $nB-\zeta+(-1)^nz$—inside the parentheses. Downstream from $x\approx 0.15\bar{U}B^2/K_z$, where probably not more than two reflection cycles are contributing significantly to the value of $C_1(z,x)$, the dispersant becomes distributed uniformly across the channel and

$$C_1(z,\ x)=\frac{qC_0}{\bar{U}y_nB}=\text{constant}. \tag{19}$$

Experimental evidence of Orlob (1961), Sayre and Chamberlain (1964), and Patterson and Gloyna (1963) indicates that the Fickian diffusion model represents lateral dispersion considerably better than it represents longitudinal dispersion.

In summary, the Fickian diffusion theory gives, at best, an approximate kinematic description of dispersion in open channels. It provides little insight into the

actual mechanics of the dispersion process and no insight into how the value of the dispersion coefficients are related to flow and channel characteristics. Dispersion coefficients for a particular set of conditions are evaluated empirically from a set of observed concentration-distribution data by means of the definition

$$K_i \equiv \frac{1}{2} \operatorname*{Lim}_{t\to\infty} \frac{d\sigma_i^2}{dt} \tag{20}$$

or other relationships derived therefrom.

DIFFUSION BY CONTINUOUS MOVEMENTS

The theory of diffusion by continuous movements (Taylor, 1921), like the Fickian theory, is restricted to giving a kinematic description of dispersion, but the description is much more realistic because it is based on the turbulence properties of the flow. Taylor's equation for dispersion in one direction in a turbulence field that is spatially homogeneous and stationary in time is

$$\sigma_i^2(t) = 2\overline{u_i'^2} \int_0^t (t-\tau) R_{u_i'}(\tau) d\tau \tag{21}$$

where

$\sigma_i^2(t)$ = the variance at time t of the distribution in the i direction of a group of fluid particles that were located at the origin at time $t=0$,

$\overline{u_i'^2}$ = the mean of the squared instantaneous turbulent velocity components in the i direction,

t = dispersion time, and

$R_{u_i'}(\tau) \equiv \dfrac{\overline{u_i'(t)u_i'(t+\tau)}}{\overline{u_i'^2}}$ is the Lagrangian correlation coefficient which correlates values of u_i' for fluid particles at the times t and $t+\tau$.

Equation 21 describes the dispersion of the fluid particles about the mean position of the group. Thus, if the turbulence field is being convected at the time-averaged velocity $\overline{U}_i$, the dispersion refers to instantaneous displacement in the i direction from a point moving with velocity $\overline{U}_i$. In general, $\sigma_i^2(t)$ depends on the functional form of $R_{u_i'}(\tau)$ which, like all Lagrangian turbulence properties, is difficult to determine and is therefore usually not known. However, useful information can be obtained from equation 21 for the limiting conditions of (1) very small dispersion times where $\operatorname*{Lim}_{\tau\to 0} R_{u_i'}(\tau) = 1$ and equation 21 reduces to

$$\sigma_i^2(t) \approx \overline{u_i'^2} t^2 \tag{22}$$

and (2) large dispersion times where $\operatorname*{Lim}_{\tau\to\infty} R_{u_i'}(\tau) = 0$ and equation 21 reduces to

$$\sigma_i^2(t) \approx 2\overline{u_i'^2} L_{t_i} t - 2\overline{u_i'^2} \int_0^\infty \tau R_{u_i'}(\tau) d\tau, \tag{23}$$

where

$L_{t_i} \equiv \int_0^\infty R_{u_i'}(\tau) d\tau$ is the Lagrangian integral time scale of turbulence.

Given the homogeneity and stationarity of the turbulence, the second term on the right of equation 23 is a constant, so that as t becomes very large,

$$\sigma_i^2(t) \approx 2\overline{u_i'^2} L_{t_i} t, \tag{24}$$

which is equivalent to the variance given by the Fickian theory when the substitution $K_i = \overline{u_i'^2} L_{t_i}$ is made.

Equation 21 was originally derived to describe dispersion in a homogeneous turbulence field—one in which the statistical properties of the turbulence are the same at every point. Thus, at first glance it seems inapplicable to dispersion in open channels where the statistical properties of the turbulence generally vary with the distance from the boundary. However, Orlob (1958, 1961) showed that planes which are equidistant from the boundary in wide channels having uniform flow, for example the water surface, do indeed satisfy the criteria for a homogeneous turbulence field. Also, Batchelor and Townsend (1956) pointed out that, for steady uniform flows confined by rigid boundaries, the turbulence structure is homogeneous with respect to the longitudinal direction, and the instantaneous velocity of a fluid particle is necessarily a stationary random function of time as soon as the influence of the particle's initial position in the cross section has been lost. This says that the identity $U_x = \overline{U}_x + u_x'$, where $\overline{U}_x$ is the discharge velocity, (Q/A), is independent of x and becomes a stationary random function of time even though u_x' is a function of position in the cross section also. Therefore, under conditions of uniform flow, equation 21 applies to lateral and longitudinal dispersion in planes which are parallel to the bed in wide channels, and equation 23 applies to longitudinal dispersion in any uniform channel. A very significant aspect of this conclusion is that it gives theoretical support, if not proof, to the applicability of the Fickian diffusion theory to dispersion in open channels for large dispersion times.

ANALOGY WITH THEORY OF LOCAL SIMILARITY

One of the basic hypotheses in Kolmogoroff's (1941) theory of local similarity in turbulence is that at sufficiently large Reynolds numbers the small-scale turbulence is locally isotropic, and that within the

portion of the turbulence energy spectrum characterized by the local isotropy the statistical characteristics of the turbulent motion are uniquely determined by the mean rate of energy dissipation per unit mass of fluid, E, and the kinematic viscosity, ν. A major result of this hypothesis is the definition of the length scale

$$L=\left(\frac{\nu^3}{E}\right)^{1/4}, \tag{25}$$

which characterizes the size of the smallest eddies whose energy is converted directly into heat by viscous dissipation. Batchelor (1953) gave the term "universal equilibrium range" to the portion of the turbulence energy spectrum in which the similarity principle defined by equation 25 is applicable. In this range, which covers the high frequency portion of the spectrum, the removal of energy by viscous dissipation chiefly at the upper end of the range is exactly compensated by the insertion of energy due to inertia transfer from the lower frequency components at the lower end of the range.

Orlob (1958, 1961) assumed an analogy between molecular and turbulent diffusion in which the viscosity, ν, is replaced by a coefficient of turbulent diffusion, K. From dimensional considerations and the analysis of the lateral dispersion of small polyethylene particles on the water surface of an open channel, he arrived at the formula for the lateral dispersion coefficient at the surface,

$$K_{z_s}=0.0136E^{1/3}L_z^{4/3}, \tag{26}$$

which is similar in form to equation 25. In equation 26,

$E=\overline{U}gS$=mean rate of energy dissipation per unit mass of fluid in a broad open channel where $\overline{U}$ is the mean flow velocity, g is gravitational acceleration, and S is the slope of the energy gradient, and

$L_z=U_sL_{t_z}$=length scale for large-scale lateral turbulence components, defined as the product of the mean velocity at the water surface, U_s, and the Lagrangian integral time scale, L_{t_z}, for the lateral component of turbulence.

Hino (1961) carried the analysis a step further by deriving a modified form of equation 26,

$$K_{z_s}=\text{const}\,\varphi\left(\frac{\overline{U}}{U_\tau}\right)E^{1/3}L_z^{4/3}, \tag{26a}$$

in which

$$\varphi\left(\frac{\overline{U}}{U_\tau}\right)=\left(\frac{U_\tau}{U_s}\right)^{5/3}\left(\frac{U_s}{\overline{U}}\right)^{1/3}$$

accounts for the influence of boundary roughness and $U_\tau=\sqrt{gy_nS}$ is the shear velocity. Krenkel (1960) applied a similar model to that of Orlob in analyzing the longitudinal dispersion of a tracer solution in open-channel flow.

The physical justification for Orlob's analogy remains obscure despite (1) the fact that Orlob's and Krenkel's data are reasonably well represented by equations based on Kolmogoroff's similarity concept and (2) the resemblance of equation 26 to the empirical "Four-Thirds Law" which has found application in large-scale dispersion phenomena in the atmosphere and in the ocean (Richardson, 1920; Richardson and Stommel, 1948). As pointed out by von Karman and Lin (1949), turbulent diffusion is associated with the low-frequency end of the turbulence energy spectrum where the relationships among the turbulence characteristics and the energy transfer mechanisms are quite different from those in the universal equilibrium range. However, this observation does not necessarily rule out the validity of Orlob's analogy.

From a practical standpoint, equation 26 is not readily applicable to predicting dispersion in open channels because the length scale L_t, although necessarily related to the dimensions of the flow field, is difficult to determine. On the basis of his data, Orlob (1958) proposed the empirical formula

$$L_z\approx 7y_n^{4/3}.$$

Yotsukura, Smoot, and Cahal (1964) suggested that in a broad open channel

$$L_x\approx y_n,$$

which does not seem to be compatible with Orlob's formula.

In summary, there is not yet sufficient evidence to either prove or disprove the validity of extending Kolmogoroff's similarity hypothesis to include dispersion by turbulence. If the extension is justified, an adequate method for predicting L_t in open-channel flows remains to be determined.

LONGITUDINAL DISPERSION BY DIFFERENTIAL CONVECTION DUE TO A VELOCITY GRADIENT

In this class of theories the basic Eulerian dispersion equation,

$$\frac{\partial C}{\partial t}+U\frac{\partial C}{\partial x}=\epsilon_x\frac{\partial^2 C}{\partial x^2}+\frac{\partial}{\partial y}\left(\epsilon_y\frac{\partial C}{\partial y}\right)+\frac{\partial}{\partial z}\left(\epsilon_z\frac{\partial C}{\partial z}\right), \tag{5a}$$

is converted by assumptions and transformations into simpler forms that permit an evaluation of the longitudinal dispersion coefficient, K_x, in terms of param-

eters which describe the flow. This value of K_x can then be used in equation 8 to predict the dispersion pattern. Considering longitudinal dispersion from an instantaneous plane source, which extends across the channel in a two-dimensional flow so that all $\frac{\partial}{\partial z}$ terms equal zero, and assuming that the rate of spread of dispersant in the longitudinal direction due to turbulence is very small in comparison to the rate of spread due to differential convection imposed by a velocity gradient, equation 5a becomes

$$\frac{\partial C}{\partial t}+U\frac{\partial C}{\partial x}=\frac{\partial}{\partial y}\left(\epsilon_y\frac{\partial C}{\partial y}\right). \tag{27}$$

Elder (1959), following the method derived by Taylor (1954) for longitudinal dispersion in a turbulent axisymmetric pipe flow, introduced the transformations

$$U^*(y)=U-\overline{U},$$

which is the difference between the local time-averaged velocity U at y and the mean velocity in the cross section $\overline{U}$, and

$$\xi=x-\overline{U}t,$$

which is the longitudinal displacement from the plane moving at velocity $\overline{U}$ about which dispersion is occurring. Taylor and Elder furthermore assumed that at large dispersion times in the transformed system $\frac{\partial C}{\partial t}\approx 0$, and that

$$C=C_1(\xi)+C_2(y)$$

where $\left|\frac{\partial C_1}{\partial \xi}\right|=$constant. With these assumptions, equation 27 becomes

$$U^*\frac{\partial C_1}{\partial \xi}=\frac{\partial}{\partial y}\left(\epsilon_y\frac{\partial C_2}{\partial y}\right). \tag{28}$$

Upon defining a coefficient of longitudinal dispersion due to convection, K_C, in terms of the rate of transfer of dispersant across a section at ξ,

$$-K_C\frac{\partial C_1}{\partial \xi}\equiv\frac{1}{y_n}\int_0^{y_n}U^*C_2dy,$$

and substituting this definition into equation 28, equation 28 can be integrated twice to obtain

$$K_C=-\frac{1}{y_n}\int_0^{y_n}U^*\int_0^{y}\frac{1}{\epsilon_y}\int_0^{y}U^*dydydy. \tag{29}$$

Ellison (1960) integrated equation 29 by parts and obtained

$$K_C=\frac{1}{y_n}\int_0^{y_n}\frac{1}{\epsilon_y}\left(\int_0^{y}U^*dy\right)^2dy, \tag{29a}$$

which is a more convenient form for computational purposes. Taking the origin at the water surface and employing the von Karman–Prandtl logarithmic velocity-distribution equation,

$$\frac{U^*}{U_\tau}=\frac{1}{\kappa}\left(\ln(1-y/y_n)+1\right), \tag{30}$$

and also the Reynolds analogy, which states the equivalence of mass and momentum transfer,

$$\epsilon_y\equiv\frac{-\overline{v'c'}}{\frac{\partial C}{\partial y}}\approx\frac{-\overline{u'v'}}{\frac{\partial U}{\partial y}}\approx\frac{-U_\tau^2y/y_n}{\frac{\partial U}{\partial y}}, \tag{31}$$

Elder (1959) integrated equation 29 and obtained

$$K_C=0.404\frac{y_nU_\tau}{\kappa^3}. \tag{32}$$

In equations 30 through 32, $U_\tau=\sqrt{\tau_0/\rho}=\sqrt{gy_nS}$ is the shear velocity and κ is the von Karman turbulence coefficient. The experimental results of Al-Saffar (1964), and the results of Kalinske and Pien (1944), who obtained fairly good agreement between ϵ_y evaluated by means of equation 31 and

$$\epsilon_y=\frac{U}{2}\frac{d\sigma_y^2}{dx}$$

from dispersion experiments in a flume, provide empirical justification for applying Reynolds' analogy.

If it is assumed that the turbulence is isotropic, the coefficient of longitudinal dispersion due to turbulence, which was neglected in the development leading to equation 32, can also be estimated. Using equations 30 and 31,

$$K_T\approx\overline{\epsilon_y}=\frac{1}{y_n}\int_0^{y_n}\epsilon_ydy=\frac{\kappa}{6}y_nU_\tau. \tag{33}$$

Following Taylor, Elder assumed that the convection and turbulence components of dispersion are additive, whereupon he obtained for the total coefficient of longitudinal dispersion in a rectangular channel having uniform two-dimensional flow,

$$K_x=K_C+K_T=\left[\frac{0.404}{\kappa^3}+\frac{\kappa}{6}\right]y_nU_\tau. \tag{34}$$

If the parabolic velocity-distribution function

$$\frac{U^*}{U_\tau}=\frac{1}{\kappa}\left[-3\left(\frac{y}{y_n}\right)^2+1\right], \tag{30a}$$

obtained by integrating equation 31 with

$$\epsilon_y=\frac{\kappa}{6}y_nU_\tau,$$

is used instead of the logarithmic distribution function in equation 29, then

$$K_C=0.457\frac{y_nU_\tau}{\kappa^3}. \tag{32a}$$

In view of the generally accepted observation that the value of K_C is extremely sensitive to small changes in velocity distribution, the agreement with equation 32 is remarkably close.

The assumptions made in going from equation 27 to equation 28 are rather gross; however, they seem to be approximately true at large dispersion times. Therefore, equations 29 and 34 should be considered applicable only in the limiting case of large dispersion times.

Aris (1956) approached the problem of evaluating K_x in a more rigorous fashion. By taking the p'th moment of equation 5a with respect to ξ, where $\xi=x-\overline{U}_t$ as before, so that

$$C_p(y, z, t)=\int_{-\infty}^{\infty}\xi^pC(\xi, y, z, t)d\xi, \tag{35}$$

and averaging the resulting equation over the cross-sectional area, A, of the channel so that

$$m_p(t)=\overline{C}_p=\frac{1}{A}\iint_A C_p(y, z, t)dydz, \tag{36}$$

Aris derived an equation in m_p for which he was able to obtain solutions for $p=0$, $p=1$, and $p=2$. Employing the definition of the dispersion coefficient he was then able to obtain

$$K_x\equiv\frac{1}{2}\operatorname*{Lim}_{t\to\infty}\frac{d\sigma_\xi^2}{dt}=\frac{\bar{\epsilon}_y}{2}\operatorname*{Lim}_{t\to\infty}\frac{d}{dt}\left(\frac{m_2}{m_0}-\left(\frac{m_1}{m_0}\right)^2\right).$$

Fischer (1964a) showed that this result for a rectangular channel with two-dimensional flow and isotropic turbulence becomes

$$K_x=\bar{\epsilon}_y+K_C$$

where K_C and $\bar{\epsilon}_y$ are identical with the functions obtained by Elder which are given in equations 29 and 33. The result of Aris' analysis strengthens considerably the credibility of the results obtained by Taylor and Elder. Aris' method, in its more general form, also appears to be applicable to three-dimensional uniform flow where $U=U(y, z)$, even though the mathematical difficulties are apt to be quite formidable.

Yotsukura and Fiering (1964, 1966) obtained some particular solutions of equation 27 by means of a numerical methods technique with the aid of a digital computer. The longitudinal concentration distribution curves generated in the solutions resembled experimental curves in that they were highly skewed in the upstream direction at small dispersion times and tended to approach a normal distribution as an asymptotic limit at large dispersion times. Because Yotsukura and Fiering used a different velocity distribution function, their results cannot be compared quantitatively with Elder's.

Perhaps the most significant contribution of the differential convection theories has been to identify y_nU_τ as an important parameter which relates both K_x and $\bar{\epsilon}_y$ to flow conditions. However, experimentally determined values of K_x/y_nU_τ ranging from 3 to 24 in laboratory flumes and from 15 to 800 in canals and natural streams have been reported in the literature by Glover (1964), Yotsukura, Smoot, and Cahal (1964), and Godfrey and Frederick (1963). Such a wide variation indicates the existence of other major influences such as velocity variation with respect to z, variation in κ, boundary roughness, scale effect, and nonuniformity of the channel. Fischer (1964a) discusses several possible causes for these disparities.

If, as is suggested by the results of some experimental investigations, K_C/y_nU_τ is a function of $\overline{U}/U_\tau$, dimensional considerations suggest that $y_n\overline{U}$ is perhaps a more significant parameter than y_nU_τ. Indeed, some investigators (Orlob, 1958; Yotsukura and others, 1964) have found that for given sets of data a significant correlation exists between the Schmidt number $\mathbf{S}=K_t/\nu$ and the Reynolds number $\mathbf{R}=y_n\overline{U}/\nu$. However, as with the experimentally determined $K_x/y_nU\tau$ values, here also the disparities among various sets of data encompass approximately two orders of magnitude.

APPLICATIONS OF DIFFUSION THEORY IN SUSPENDED-SEDIMENT TRANSPORT

The basic differential equation for the dispersion of suspended sediment, when the concentration by volume is small, is

$$\frac{\partial C}{\partial t}+U_{p_i}\frac{\partial C}{\partial x_i}=\frac{\partial}{\partial x_i}\left[\epsilon_{p_i}\frac{\partial C}{\partial x_i}\right], \tag{37}$$

which is the same as equation 4 except that the subscript p here indicates reference to sediment particles. Upon introduction of the same simplifying assumptions as before, for a wide channel with uniform two-dimensional flow, and a uniform distribution of dispersant in the z direction, equation 37 becomes

$$\frac{\partial C}{\partial t}+U_p\frac{\partial C}{\partial x}=\epsilon_{p_x}\frac{\partial^2C}{\partial x^2}+\frac{\partial}{\partial y}\left(\epsilon_{p_y}\frac{\partial C}{\partial y}\right)+V_p\frac{\partial C}{\partial y}. \tag{38}$$

With the exception of the term $V_p\dfrac{\partial C}{\partial y}$, where V_p is the settling velocity of the sediment particles, equation 38 has the same form as the corresponding equation for a fluid dispersant. Additional assumptions implicit in equation 38 are that all the sediment particles have

identical transport characteristics, that V_p is the same in turbulent and quiescent fluid, and that $U_p=U$ at a point. With respect to the last assumption, however, it should be noted that the cross-sectional average velocity of sediment in the x direction is

$$\overline{U}_p=\frac{\int_0^{y_n} UCdy}{\int_0^{y_n} Cdy}, \tag{39}$$

which is different from the cross-sectional average velocity of flow, $\overline{U}$.

Although equation 38 in its complete form has never been solved, certain special cases which permit drastic simplifications have been solved. For example, for the steady-state equilibrium conditions where both $\frac{\partial C}{\partial t}$ and $\frac{\partial C}{\partial x}$ equal zero, equation 38 reduces to the well-known equation

$$\epsilon_{p_y}\frac{\partial C}{\partial y}+V_pC=0, \tag{40}$$

which for many years has served as the basis for computing the vertical distribution of suspended sediment in alluvial channels. For a turbulence tank in which $\frac{\partial C}{\partial x}=0$ and ϵ_{p_y}=constant, Dobbins (1944) obtained a formal solution to the equation

$$\frac{\partial C}{\partial t}=\epsilon_{p_y}\frac{\partial^2 C}{\partial y^2}+V_p\frac{\partial C}{\partial y}, \tag{41}$$

which agreed well with the results of experiments in which the transient response to the shift from one steady state to another was investigated.

Experience in comparing predictions based on equations 40 and 41 with experimental results (Task Committee on Preparation of Sedimentation Manual, 1963) indicates that the theory is basically sound. Experiments by Brush (1962) on the dispersion of sediment particles in a submerged jet show, furthermore, that ϵ_{p_i} tends to approach ϵ_i as the particle diameter, d, decreases, becoming approximately equal when $d\approx 0.2$ mm. This result is in essential agreement with an analysis based on the equation of motion of a particle in a turbulent flow field (Tchen, 1947; Hinze, 1959), which shows that $\epsilon_{p_i}\approx\epsilon_i$ when $\nu L_{t_i}/d^2\geq$ about 3.5. Therefore, in most instances ϵ_{p_y}, like ϵ_y, can be evaluated by means of Reynolds' analogy (eq 31). Some comparisons of ϵ_y computed from Reynolds' analogy and ϵ_{p_y} computed from equation 40 using experimental data were given by Vanoni (1946).

A very rough approximation of K_{x_p} for the longitudinal dispersion of suspended sediment was obtained by Elder (1959) by means of equation 29 with $U^*=U-\overline{U}_p$, where U_p is defined by equation 39. Assuming a parabolic velocity distribution, where ϵ_y is a constant, according to Reynolds' analogy, Elder obtained

$$K_{x_p}=\frac{(U_{max}y_n)}{7560\epsilon_y}(64+21\beta-308\beta^2-210\beta^3-35\beta^4), \tag{42}$$

where $\beta=V_p/\kappa U_\tau$. In the derivation of equation 42 it was also assumed that no deposit of sediment on the bed occurs and that the dispersing particles are distributed vertically according to the probability-density function

$$f\left(\frac{y}{y_n}\right)=\left[\frac{y/y_n}{1-y/y_n}\right]^\beta\frac{\sin\pi\beta}{\pi\beta} \qquad \text{where } 0<\beta<1. \tag{43}$$

Equation 43 is obtained by solving equation 40 for steady-state equilibrium where the diffusivity term,

$$\epsilon_{p_y}=\epsilon_y=U_\tau\kappa y(1-y/y_n),$$

is obtained by solving equation 31 for a logarithmic velocity distribution. Equation 42 has not been verified experimentally.

If it is assumed instead that the particles are distributed vertically according to the probability-density function

$$f\left(\frac{y}{y_n}\right)=\frac{6\beta e^{6\beta y/y_n}}{e^{6\beta}-1}, \tag{44}$$

which results from solving equation 40 for a constant diffusivity

$$\epsilon_{p_y}=\bar{\epsilon}_y=\frac{\kappa}{6}y_nU_\tau,$$

then equation 29 leads to

$$K_{x_p}=\frac{-6y_nU_\tau}{\kappa^3}\left[\frac{1}{6}(f(\beta))^2-\frac{7}{20}f(\beta)+\frac{3}{28}\right] \tag{45}$$

where

$$f(\beta)=\frac{e^{6\beta}(18\beta^2-6\beta+1)-1}{6\beta^2(e^{6\beta}-1)}.$$

Equations 42 and 45 give nearly identical results for the ratio K_{x_p}/K_x. As shown in figure 56, K_{x_p}/K_x has an asymptotic value of unity as β approaches zero, rises to a weak maximum of 1.0055 at $\beta\approx 0.033$, and decreases rapidly to zero near $\beta=0.5$.

Although diffusion theory has not as yet (1965) been successfully applied to predicting longitudinal and lateral dispersion of suspended sediment particles, successful application of diffusion theory in some other areas of sediment transport suggest that such an application is possible.

DESCRIPTION OF THE EXPERIMENTS

All the experiments were conducted in a recirculating flume 150 feet long having a rectangular cross section

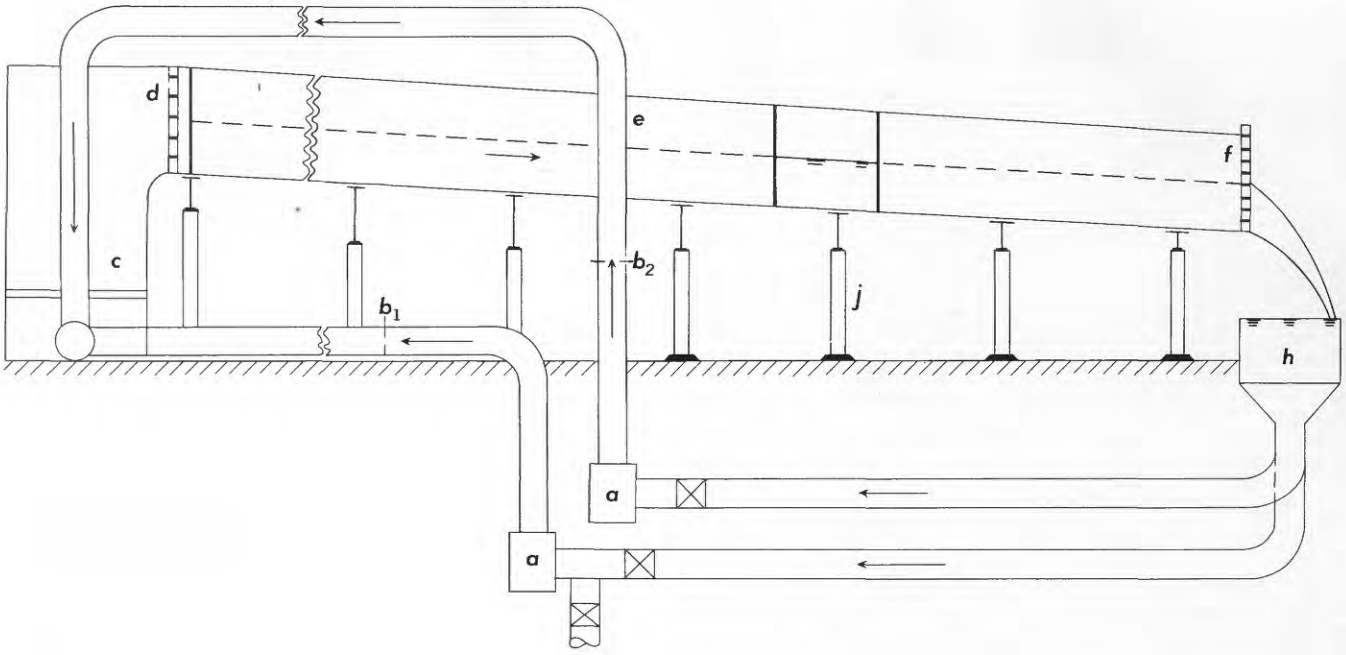

FIGURE 1.—Schematic diagram of the flume and circulation system. a, pumping units; b_1, b_2, orifices; c, head-box and diffuser; d, baffles and screens; e, flume (8 ft × 2 ft × 150 ft); f, tailgate; h, tail-box; j, jacks supporting the flume.

7.83 feet wide by 2 feet deep. The interior of the flume was surfaced with tarred plywood except for a section of the right sidewall 40 feet long which was made of transparent plexiglass. Figure 1 shows a schematic diagram of the flume.

In order to satisfy approximately the restrictions on Elder's (1959) longitudinal dispersion theory that (1) the velocity varies only with distance above the bed and (2) the turbulence is homogeneous with respect to the x and z directions, a uniform arrangement of artificial roughness was placed on the bed of the flume. The roughness elements consisted of wooden cleats and were arranged in the pattern shown in figure 2.

HYDRAULIC DATA

Hydraulic data were obtained to provide a base of reference for the dispersion experiments. These data included water discharge, water-surface and bed slopes, depth, water temperature, and velocity profiles. A side-contracted orifice in the pipeline was used to measure water discharges. Bed- and water-surface elevations and slopes were determined using an engineer's level and rod and Lory point gages. Depths of flow were obtained by determining the difference in elevation between the mean water surface and bed profiles. No correction for the roughness cleats was applied to the bed level. However, the volume occupied by the roughness cleats, if spread evenly over the floor of the flume, would have added only 0.004 foot to the bed level. Water temperatures were measured with a standard laboratory mercury thermometer. Because a period of two or three days each was required for completion of many of the runs, temperature fluctuations of up to 2°C occurred during several runs. Point velocity measurements were obtained with a 15 mm-diameter Delft propellor meter and the electronic pulse-shaping and counting system shown in figure 3.

Uniform flow conditions for all runs were established by manipulating the setting of the vertical-slat tailgate until the water-surface slope was parallel to the bed slope. This could be done quite accurately by intentionally setting the tailgate to obtain slight M_1 and M_2 backwater curves and then finding the correct tailgate setting by interpolation.

Each type of dispersion experiment was performed using one or more of three different flow conditions. The hydraulic data describing these flow conditions and information characterizing the various types of dispersion experiments are listed in table 1.

Velocity profiles for each of the three flow conditions were obtained at cross sections approximately 100 feet downstream from the flume entrance. In order to check the applicability of the two-dimensional flow assumption used in the dispersion analysis, velocity profiles were obtained at several verticals across the flume. For the intermediate flow condition ($Q \approx$ 7 cfs), sets of velocity profiles were also obtained at several cross sections along the flume in order to ascertain the distance downstream from the flume entrance required for the establishment of uniform flow.

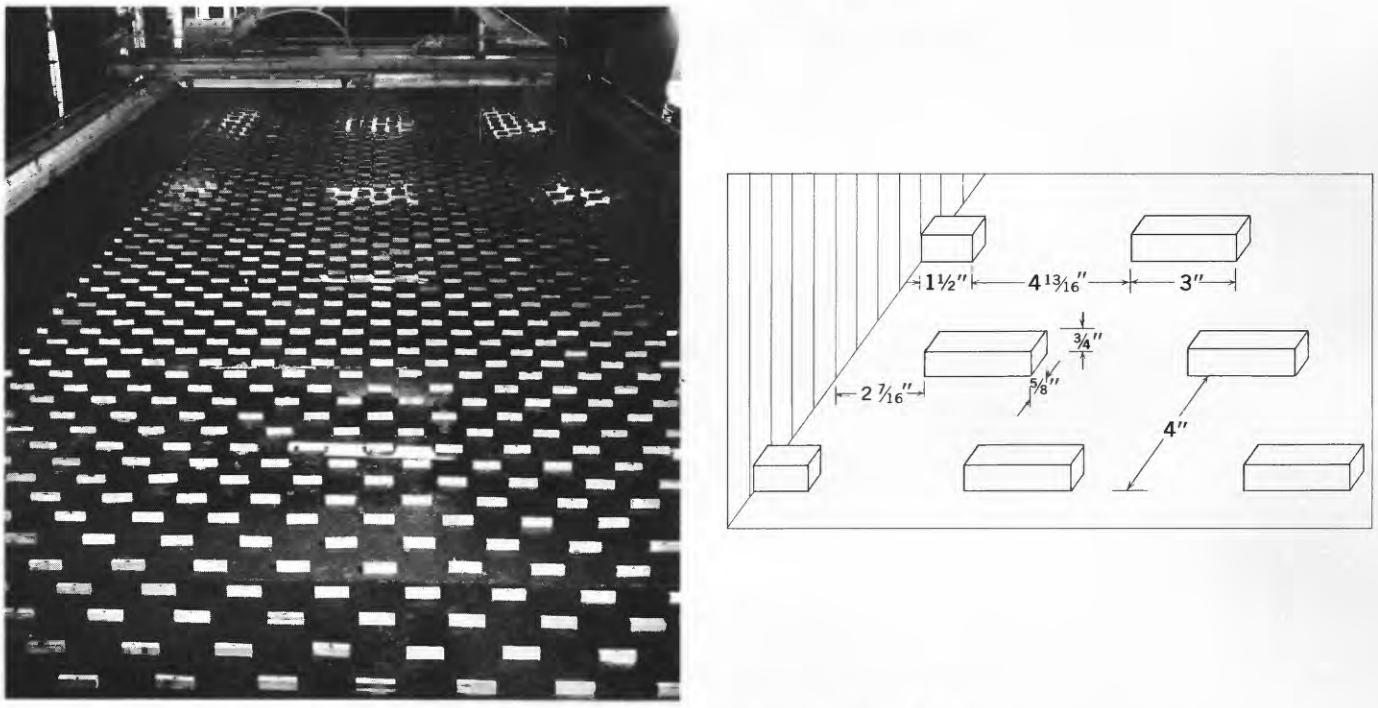

FIGURE 2.—Arrangement of roughness cleats on the bed of the flume.

These measurements indicated that a distance of 30 feet was sufficient to establish a pattern of velocity distribution which did not change very much in the x direction. The velocity measured at each point was an average during a period of 100 seconds.

LONGITUDINAL DISPERSION EXPERIMENTS

Longitudinal dispersion experiments were conducted with three different types of dispersants—fluorescent dye, suspended silt-size particles, and floating polyethylene particles. A different set of equipment and techniques was required for each type of dispersant.

In both the dye and the suspended-sediment experiments the same basic procedure was employed. The dispersant was dumped into the flume from an elevated trough which extended across the flume a short distance above the water surface in such a way that the initial distribution of dispersant approximated an instantaneous plane source with the dispersant uniformly distributed over the entire flow cross section. The concen-

TABLE 1.—*Hydraulic conditions and types of dispersion experiments*

Dispersion	Run	Q (cfs)	y_n (ft)	$\overline{U}$ (ft per sec)	S	T (°C)	Source	Dispersant
Longitudinal	LO-D-1	2.88	0.493	0.747	0.001	20	Instanteous plane source.	Rhodamine B dye.
	2	7.17	.798	1.15	.001	20		Do.
	3	14.9	1.217	1.56	.001	5		Pontacyl brilliant pink B dye.
	FS-1	2.88	.493	.747	.001	20		15–30μ natural silt.
	2	7.17	.798	1.15	.001	20		Do.
	CS-1	2.88	.493	.747	.001	20		53–62μ natural silt.
	FG-1	2.93	.486	.770	.001	7		<44μ glass beads.
	3	14.9	1.217	1.56	.001	6		Do.
	CG-1	2.93	.486	.770	.001	5		53–62μ glass beads.
	2	7.12	.814	1.12	.001	4		Do.
	3	14.9	1.217	1.56	.001	6		Do.
	P-1	2.93	.486	.770	.001	6	Intermittent point source.	Polyethylene particles.
	2	7.12	.814	1.12	.001	4		Do.
	3	14.9	1.217	1.56	.001	10		Do.
Lateral	LA-D-1	2.93	.486	.770	.001	7	Continuous point source.	Pontacyl brilliant pink B dye.
	2	7.12	.803	1.13	.001	20		Rhodamine B dye.
		7.12	.814	1.12	.001	4		Pontacyl brilliant pink B dye.
	3	14.9	1.217	1.56	.001	7		Do.
	P-1	2.93	.486	.770	.001	6	Intermittent point source.	Polyethylene particles.
	2	7.12	.803	1.13	.001	20		Do.
	3	14.9	1.217	1.56	.001	9		Do.
Vertical	V-D-1	2.93	.486	.770	.001	6	Continuous point source.	Pontacyl brilliant pink B dye.
	2	7.12	.814	1.12	.001	4		Do.
	3	14.9	1.217	1.56	.001	8		Do.

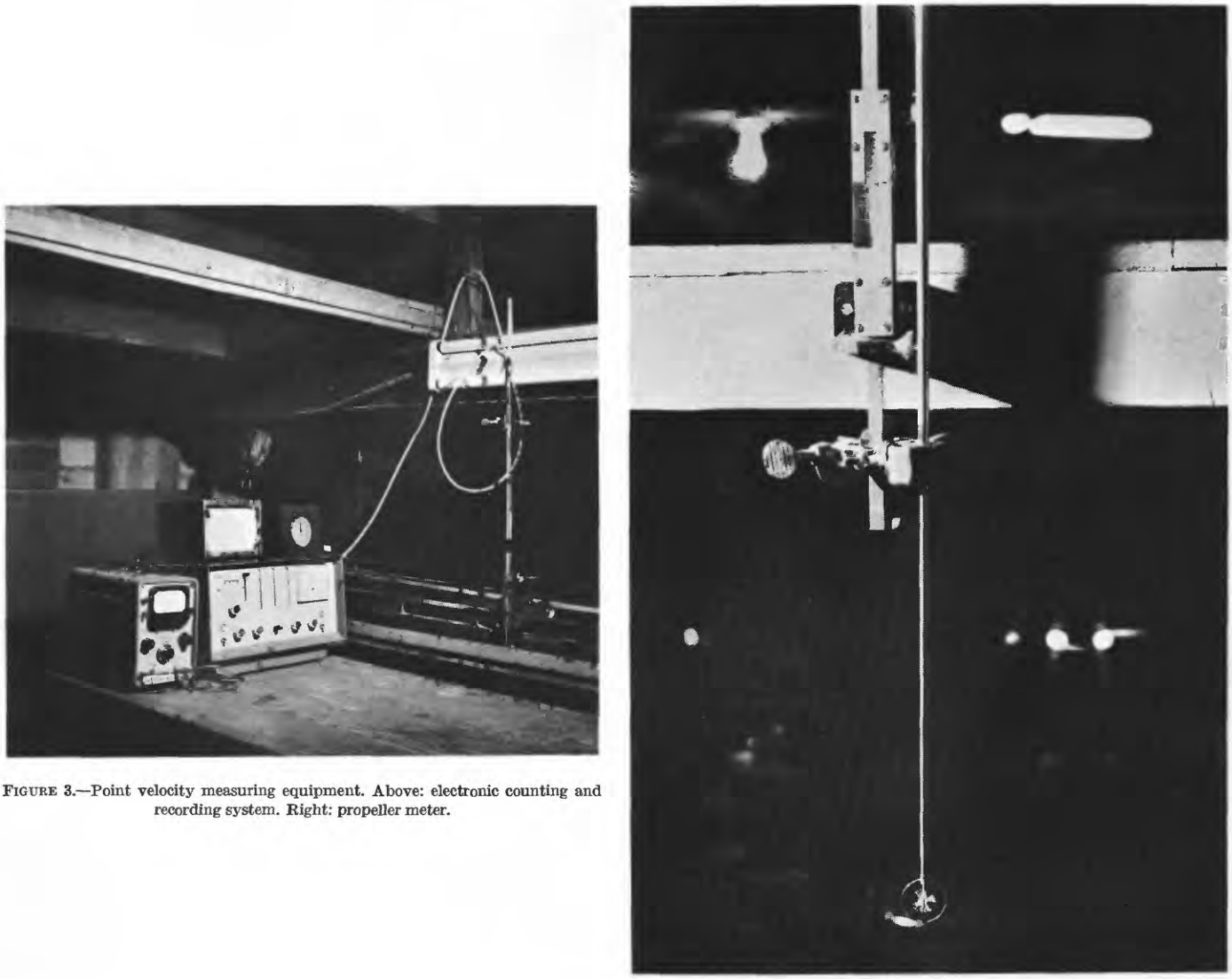

FIGURE 3.—Point velocity measuring equipment. Above: electronic counting and recording system. Right: propeller meter.

tration of dispersant was then measured as a function of time at each of four downstream sampling stations as the slug of dispersing material was carried by. The dispersion distances, defined as the distances from the source to the sampling stations, were 32.8, 65.6, 88.5, and 115.0 feet. The source was always located at least 30 feet downstream from the flume entrance.

In runs LO–D–1 and –2, LO–CG–2, and the LO–FS and –CS series of runs, a simple dumping trough was used in which mixing and suspension of sediment was done with manual stirring rods. The dispersant was introduced into the flow simply by tipping the trough on edge. Because an even distribution of dispersant across the flume was difficult to obtain with this trough, and because some of the sediment remained deposited in the trough after dumping, an improved trough, shown in figure 4, was used in the remaining experiments. The improved trough contained a rotating mechanical agitator for keeping the sediment in suspension, compartments for maintaining an even distribution of dispersant along the length of the trough, and a spring-loaded hinge mechanism which allowed one side of the trough to swing open from the top so that all of the sediment was instantaneously flushed into the flow. Visual inspection through the transparent sidewall indicated that a satisfactory distribution of dispersant throughout the depth of flow was obtained from both the troughs.

A continuous sampling and concentration-measuring system was used to measure the dye concentrations, and a discrete sampling system was used to collect suspended-sediment samples. Both systems are shown in figure 5.

The continuous system consisted of a ¼-inch ID sampling nozzle and polyethylene tube having a combined length of 7.3 feet feeding into a Model 111

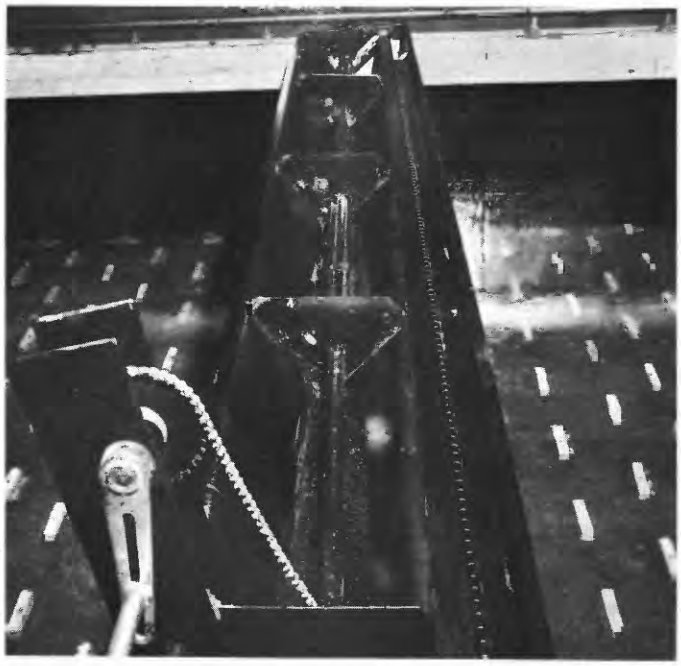

FIGURE 4.—Improved dumping trough for dye and suspended sediment in longitudinal dispersion experiments.

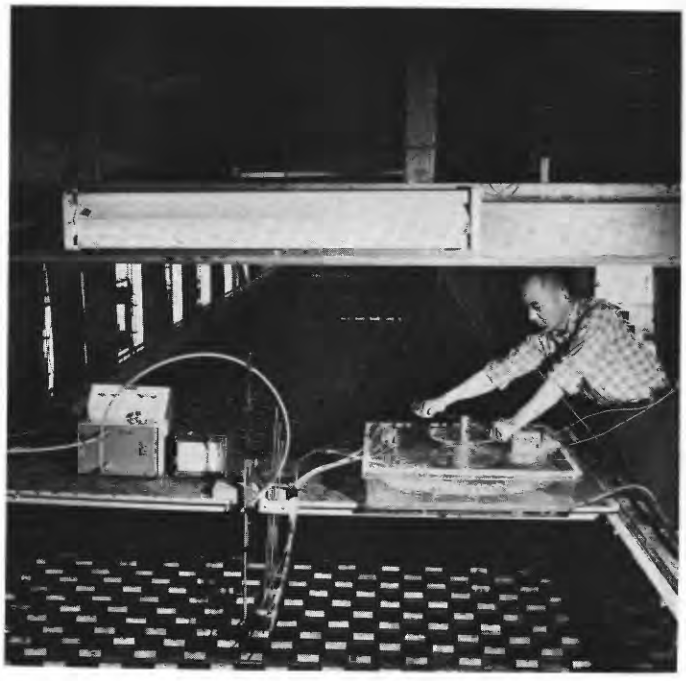

FIGURE 5.—Continuous and discrete sampling systems used for determining dye and sediment concentrations in longitudinal dispersion experiments. The continuous system is on the left, and the discrete system on the right.

Turner Fluorometer equipped with a continuous-flow door having a 5-cc continuous-flow square cuvette and ⅜-inch I.P.S. fittings. The response speed of the fluorometer was increased by installing a lamp adaptor with a green T–5 envelope lamp. In some of the experiments the response was improved further by removing the fine mesh wire screen from the lamp adaptor. A strip-chart recorder connected to the fluorometer gave a continuous record of dye concentration in the solution flowing through the fluorometer. The sampling nozzle was positioned at middepth on the centerline of the flume. The velocity in the sampling nozzle and feed tube was maintained at approximately 2.5 feet per second for all runs. The response characteristics of this system are discussed in the section on experimental evaluation beginning on page E65.

The Turner Fluorometer is capable of measuring concentrations of fluoroescent dyes such as Rhodamine B and Pontacyl Brilliant Pink B which are as small as 0.1 ppb. The theory and practice of fluorometry as applied to dispersion measurements in surface waters has been reviewed by Feuerstein and Selleck (1963).

Because there was only one continuous sampling system, it was necessary to repeat the dumping and the concentration-measurement operation for each dispersion distance. Sufficient time between successive dumpings was allowed to permit the dye to become uniformly distributed throughout the circulation system.

The discrete sampling system used in the sediment-dispersion experiments consisted of four separate sampling units with one unit serving each dispersion distance. Each unit consisted of three ¼-inch ID sampling nozzles feeding continuously through 4-foot lengths of ¼-inch ID mayon tubing into an enclosed plexiglass box in which negative pressure was maintained by means of a siphon. Inside the sampling box there was a rotatable circular rack with spaces for holding 25-cc glass vials at equal intervals around the perimeters of three concentric circles. There were 60 spaces on each circle. The three sampling nozzles were positioned on the centerline of the flume at depths beneath the water surface of one-fourth, one-half and three-fourths of the flow depth. Each feed tube terminated at a point on top of the box immediately above a point on the circumference of one of the three circles, so that by rotating the rack the vials could be filled in rapid sequence. Thus, a sequence of 60 discrete samples from each sampling nozzle could be obtained during a single revolution of the rack. A ratchet-operated microswitch and an event recorder automatically provided a record of the times at which each group of three vials was being filled. In the experiments, the rack was rotated manually by means of a handle on top of the box according to a predetermined time schedule so that the elapsed time between the first and the last samples would be longer than the time required for the dispersing sediment cloud to pass the

sampling station. The sampling velocity in the nozzles and feed tubes was maintained at 1.35 feet per second in all of the sediment-dispersion experiments. As explained in the section beginning on page E65, the response characteristics of the sampling system would have been improved considerably if the velocity in the feed tubes had been increased to about 2.5 feet per second.

After the samples had been collected, the concentration of sediment in each sample was determined by using the Turner Model 111 Fluorometer as a nephelometer—an instrument which measures the amount of light scattered by dilute suspensions. For this operation the fluorometer was equipped with a standard cuvette door. Of the various light-filter combinations which were tried, a color spec. No. 2A–12 primary filter together with a color spec. ND 1 percent secondary filter seemed to be the most satisfactory. With this arrangement, a linear calibration of fluorometer readings as functions of sediment concentration was obtained, and concentrations of silt-size particles down to less than 10 ppm could be measured. Each concentration measurement entailed transferring a part of the sample into a 5-cc square cuvette, placing the cuvette in the fluorometer, and reading the fluorometer dial. Owing to the high sensitivity of the fluorometer to any one of a number of possible sources of contamination, considerable care had to be observed with respect to cleanliness of hands and glassware. However, with a reasonable degree of care and practice, concentration measurements of different portions from the same sample could usually be repeated with deviations not exceeding about 5 percent.

In the sediment-dispersion experiments, since the discrete sampling systems at each of the four sampling stations could be operated simultaneously, only one dumping was required for each run. In addition, the continuous system was operated at one of the four stations during each run, which provided a direct comparison between the two systems.

Four kinds of silt-size particles were used in the sediment-dispersion experiments. These were natural silt in the 15–30μ size range, natural silt in the 53–62μ size range, glass beads in the $<44\mu$ size range, and glass beads in the 53–62μ size range. The natural silt particles had a specific gravity of about 2.65 and were irregular in shape. The glass beads had a specific gravity of about 2.6 and were approximately spherical. Fall-velocity distribution curves for the four kinds of particles are shown in figure 6.

In the floating polyethylene particle experiments, the particles were released intermittently from a point source located on the centerline of the flume, and the travel time of each particle to each of four timing stations along the flume was measured. The stations were located at distances of 16.4, 32.8, 49.2, and 65.6 feet downstream from the source. The particles were disk shaped, having a diameter of one-eighth inch and a thickness of one-sixteenth inch, and had a specific gravity of about 0.96. The particles were the same kind as were used in lateral dispersion experiments by Sayre and Chamberlain (1964) and similar to those used by Orlob (1958, 1961). The source, which is shown in figure 7, consisted of a manually operated particle dispenser and a funnel, with a $\frac{3}{16}$-inch-diameter tip, positioned just above the water surface. Each timing station consisted of a string stretched across the flume immediately above the water surface and a unit consisting of a telegraph key and one or more flashlight batteries connected to a strip-chart recorder as shown in figure 8.

The release time of each particle was marked on the recorder chart by the event-marking pen, and the arrival time of a particle at each station was marked by a pulse on the recorder chart caused by depressing the telegraph key. The station at which a particular arrival had occurred was identified by the pulse height which was proportional to the number of batteries in the branch of the circuit for that station. With a chart speed of 8 inches per minute, the traveltime of each particle could be estimated to the nearest 0.1 second by measuring the distance on the chart between release and arrival pulses.

For each flow condition two sets of data were obtained. They differed only in the time interval between particle releases. For each set of data at least 100 particles were released in sequence.

LATERAL DISPERSION EXPERIMENTS

Lateral dispersion experiments were conducted with both fluorescent dye and floating polyethylene particles as dispersants. In both kinds of experiments the dispersant was released from a point source in the center of the flume and the distribution of dispersant across the flume at each of four or more stations downstream from the source was determined. The four primary stations were located at dispersion distances of 16.4, 32.8, 49.2, and 65.6 feet from the source. In some of the experiments lateral distributions were obtained at dispersion distances of 88.5 and 115.0 feet also.

In the dye experiments a concentrated dye solution was released continuously at a constant rate from a $\frac{1}{8}$-inch brass tube. The horizontal leg at the discharge end of the tube was oriented in the direction of flow, and the rate of release of dye solution was set so that the discharge velocity from the tip was equal to the

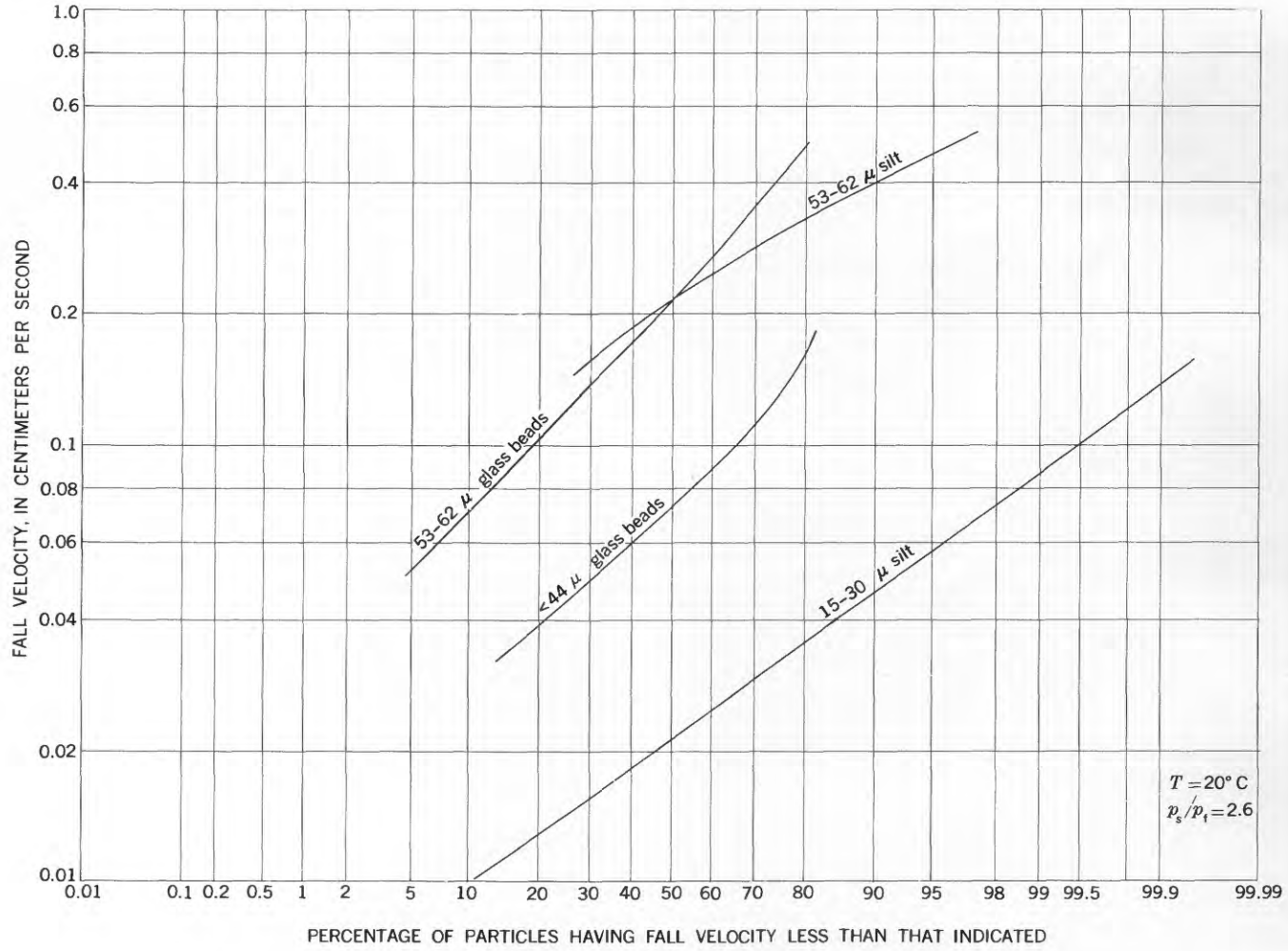

FIGURE 6.—Fall-velocity distribution curves for the sediments used in longitudinal dispersion experiments.

local ambient flow velocity. The source arrangement is shown in figure 9.

Lateral dye concentration profiles were obtained by slowly moving the sampling nozzle of the continuous-sampling system, which was described in the previous section, across the flume. The traversing mechanism, shown with the continuous sampling system in figure 10, was mounted on the flume carriage. It consisted principally of a chain drive operated by a hand crank and a series of regularly spaced electrical contacts, which, together with the recorder event-marking system, recorded the lateral position of the sampling nozzle as it was being moved across the flume. Approximately 2–3 minutes was required for each traverse. As with the longitudinal dye dispersion experiments sufficient time between traverses was allowed to permit the dye to become uniformly distributed throughout the flume circulation system. At each dispersion distance three traverses were made, with both the source and the sampling nozzle positioned respectively at one fourth, one-half, and three-fourths of the flow depth.

The equipment and techniques employed in the lateral dispersion experiments with floating polyethylene particles were virtually the same as those described by Orlob (1958, 1961) and Sayre and Chamberlain (1964). The intermittent point source arrangement was the same as that used in the longitudinal dispersion experiments. At a given dispersion distance the particles were caught in a sieve having 1-centimeter-wide compartments. The sieve was placed across the flume as shown in figure 11. The lateral distribution of particle paths was determined by counting and recording the number of particles trapped in each compartment. This operation was repeated with lots of 100 particles at each dispersion distance for time intervals between particle releases of 1, 2, and 5 seconds.

VERTICAL DISPERSION EXPERIMENTS

The vertical dispersion experiments with fluorescent dye were performed with the limited objective of determining the dispersion distance required in order to obtain a uniform vertical distribution of dye solution

FIGURE 7.—Point source used in polyethylene-particle dispersion experiments.

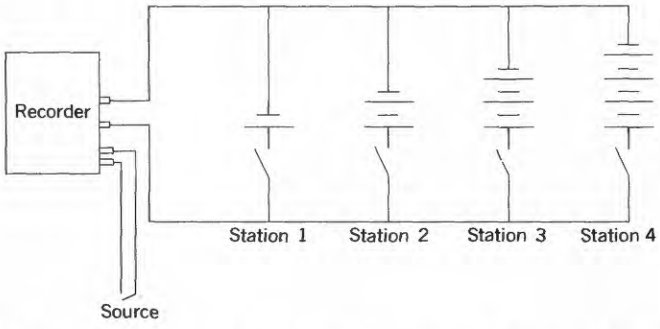

FIGURE 8.—Circuit diagram of time-measuring system used to determine travel-times of polyethylene particles.

originating from a continuous point source positioned at middepth on the centerline of the flume. No attempt was made to define the vertical dispersion pattern. The source and sampling systems were the same as those used in the lateral dye dispersion experiments. Beginning at a dispersion distance of about 3 feet, several vertical concentration profiles were taken along the centerline of the flume at increasing dispersion distances until the concentration in the vertical was found to be essentially uniform. A concentration profile was obtained by slowly moving the sampling nozzle, which was mounted on a point gage assembly, from the bed

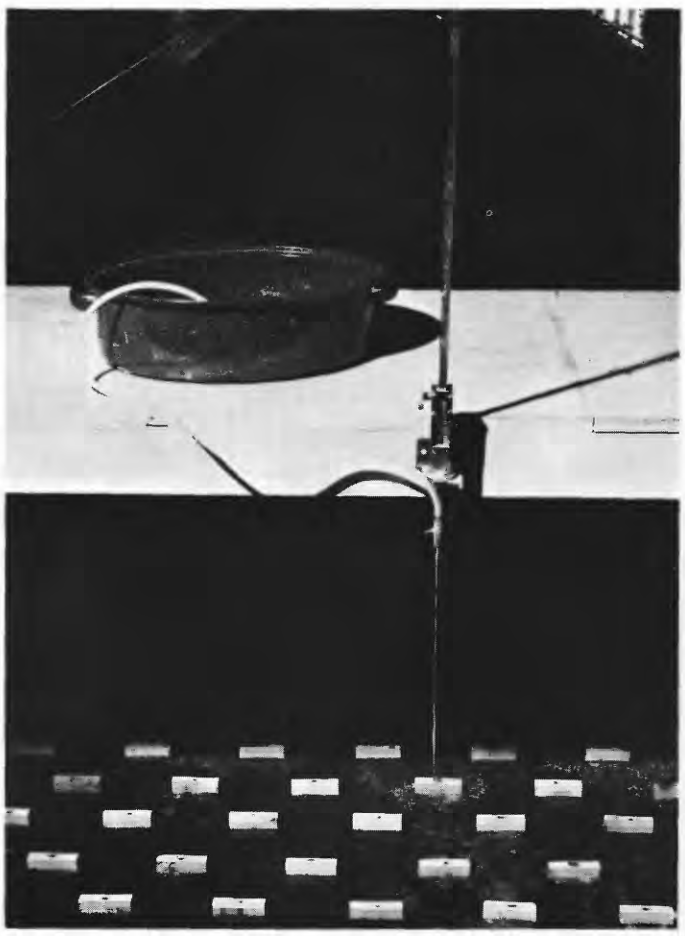

FIGURE 9.—Point-source arrangement used in lateral dispersion experiments with fluorescent dye.

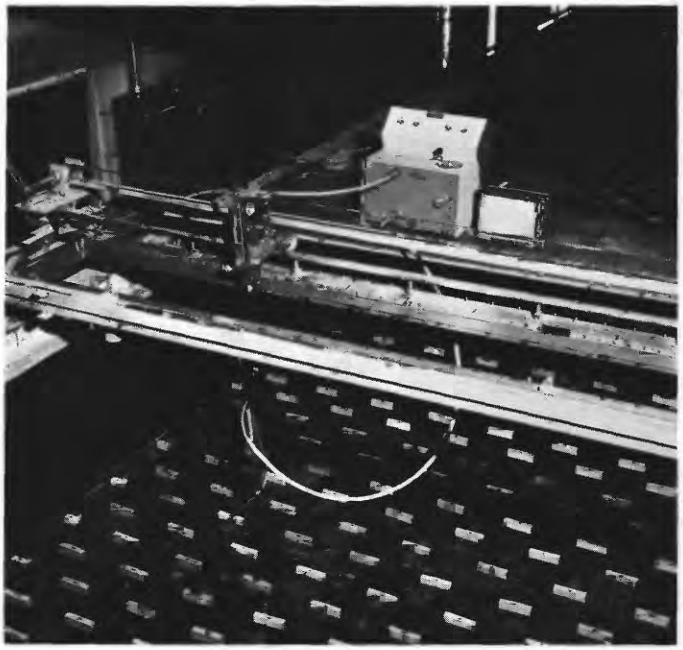

FIGURE 10.—Continuous-sampling system and traversing mechanism used in lateral dispersion experiments with fluorescent dye.

FIGURE 11.—Compartmented sieve collector used in lateral dispersion experiments with floating polyethylene particles.

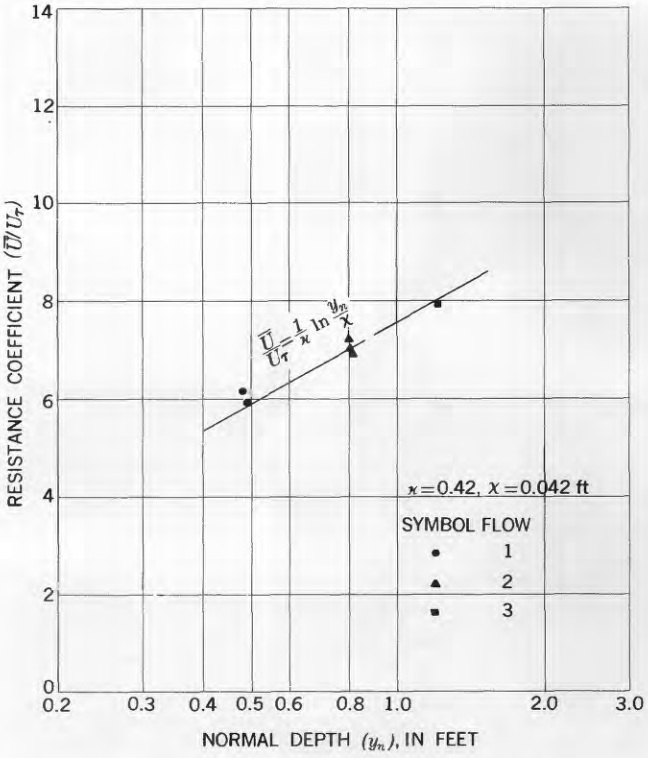

FIGURE 12.—Variation of resistance function with depth of flow.

to the water surface or vice versa. The time span for each vertical profile was about 2–4 minutes.

PRESENTATION AND ANALYSIS OF DATA

HYDRAULIC DATA

The characteristics of the flows in which the dispersion experiments were conducted are defined by the hydraulic data. The mean flow characteristics of discharge, depth, velocity, slope, and temperature are listed in table 1. In figure 12 the resistance coefficient, $\overline{U}/U_\tau$, is shown as a function of the normal depth, y_n. The data follows the trend of the von Karman–Prandtl resistance law for turbulent flow in a wide channel with a rough bottom,

$$\frac{\overline{U}}{U_\tau}=\frac{1}{\kappa}\ln\frac{y_n}{\chi}. \tag{46}$$

In figure 13 the measured velocity profiles are seen to compare well with the von Karman–Prandtl law for velocity distribution near a rough boundary,

$$\frac{U}{U_\tau}=\frac{1}{\kappa}\left[\ln\frac{y}{\chi}+1\right]. \tag{47}$$

For the curves in both figures 12 and 13, the values of the von Karman turbulence coefficient and the roughness measure are respectively $\kappa=0.42$ and $\chi=0.042$ foot. The application of equations 46 and 47 in rough-boundary open-channel flow has been discussed in detail by Sayre and Albertson (1963).

The velocity distribution measurements, which were obtained at several verticals across the width of the flume, indicated that there was no significant variation of velocity with respect to lateral position except in the immediate vicinity of the sidewalls. The thickness of the boundary layer within which the velocity distribution was influenced by the proximity of the sidewalls was not greater than 0.5–1.0 foot. Thus, the condition of two-dimensional flow was essentially satisfied.

The mean flow data in table 1 and figure 12 show some scatter. For some undetermined reason the conditions of flows 1 and 2 sometimes could not be duplicated. This tended to occur when a period of several weeks or months was allowed to elapse between different sets of runs for the same flow condition. The most likely explanation is that alternate periods of wetting and drying, coupled with loading changes, caused the plywood bed of the flume to assume slightly different configurations which could not be duplicated.

LONGITUDINAL DISPERSION

DYE

The basic data in the LO–D series of experiments consisted of sets of distribution curves in which fluorometer readings were recorded on strip charts as a continuous function of time. For convenience in analyzing the data, each distribution curve was normalized by

dividing the fluorometer readings by the area under the curve, which gave all the normalized distribution curves an area of 1. The normalized distribution curves are shown as the dashline curves in figures 14, 15, and 16 for flows 1, 2, and 3 respectively. The time base for these curves was corrected for response lag in the concentration-measuring system, using the appropriate $\bar{\tau}$ values from table 11 in the section beginning on page E5. The

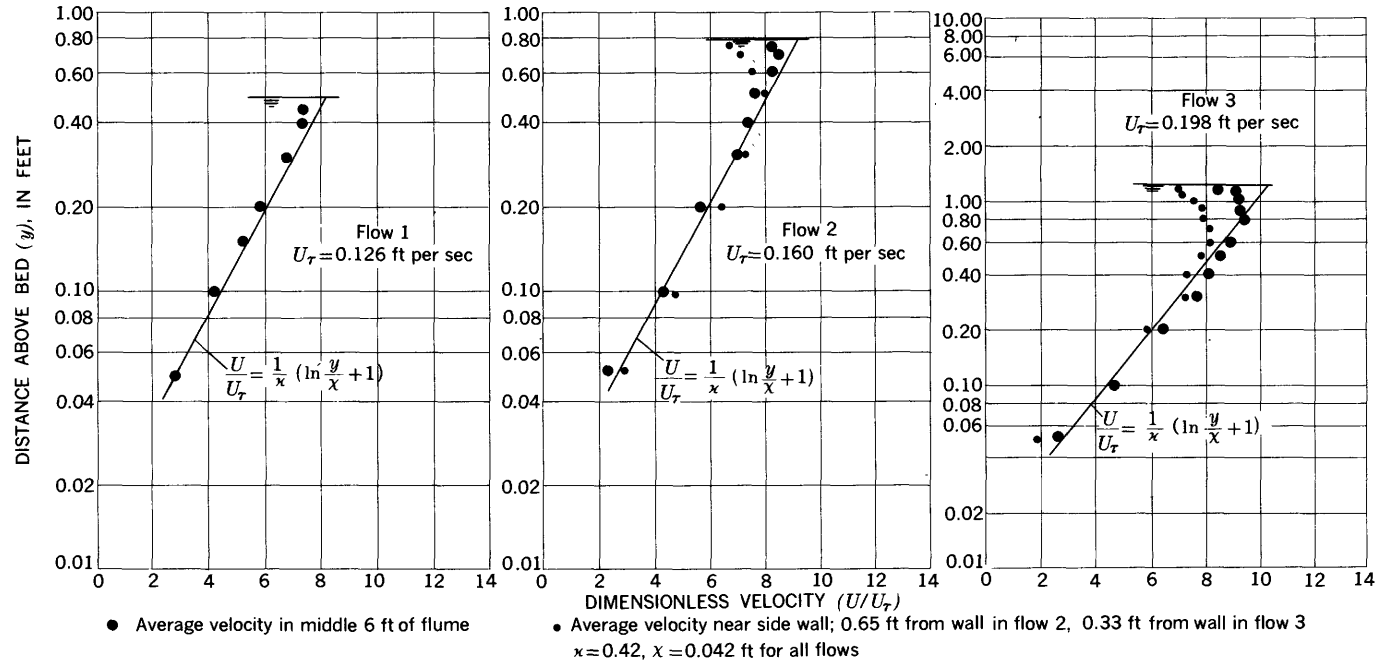

FIGURE 13.—Velocity profiles for flow conditions in dispersion experiments.

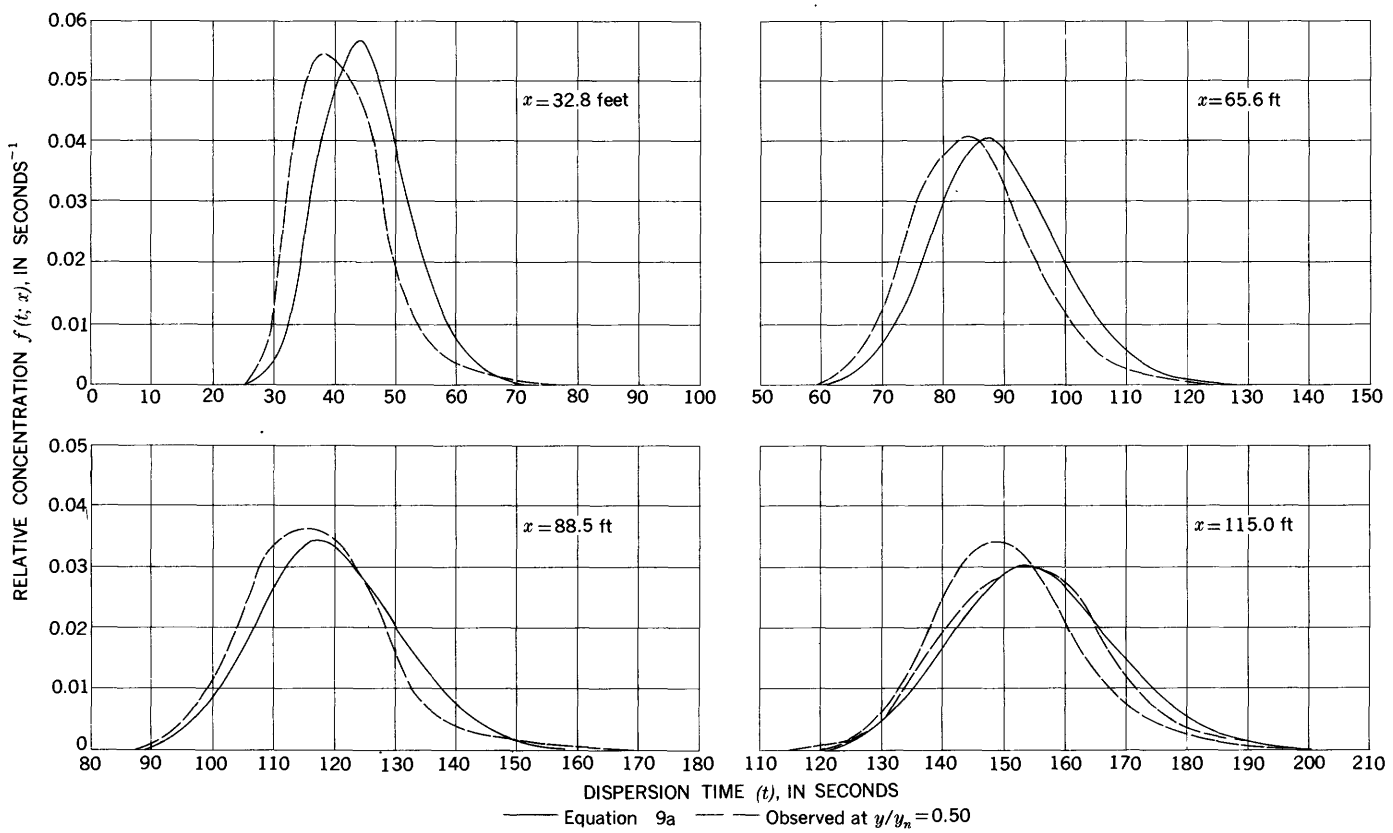

FIGURE 14.—Relative concentration of dye as a function of time at various dispersion distances in run LO-D-1.

281-661 O - 68 - 4

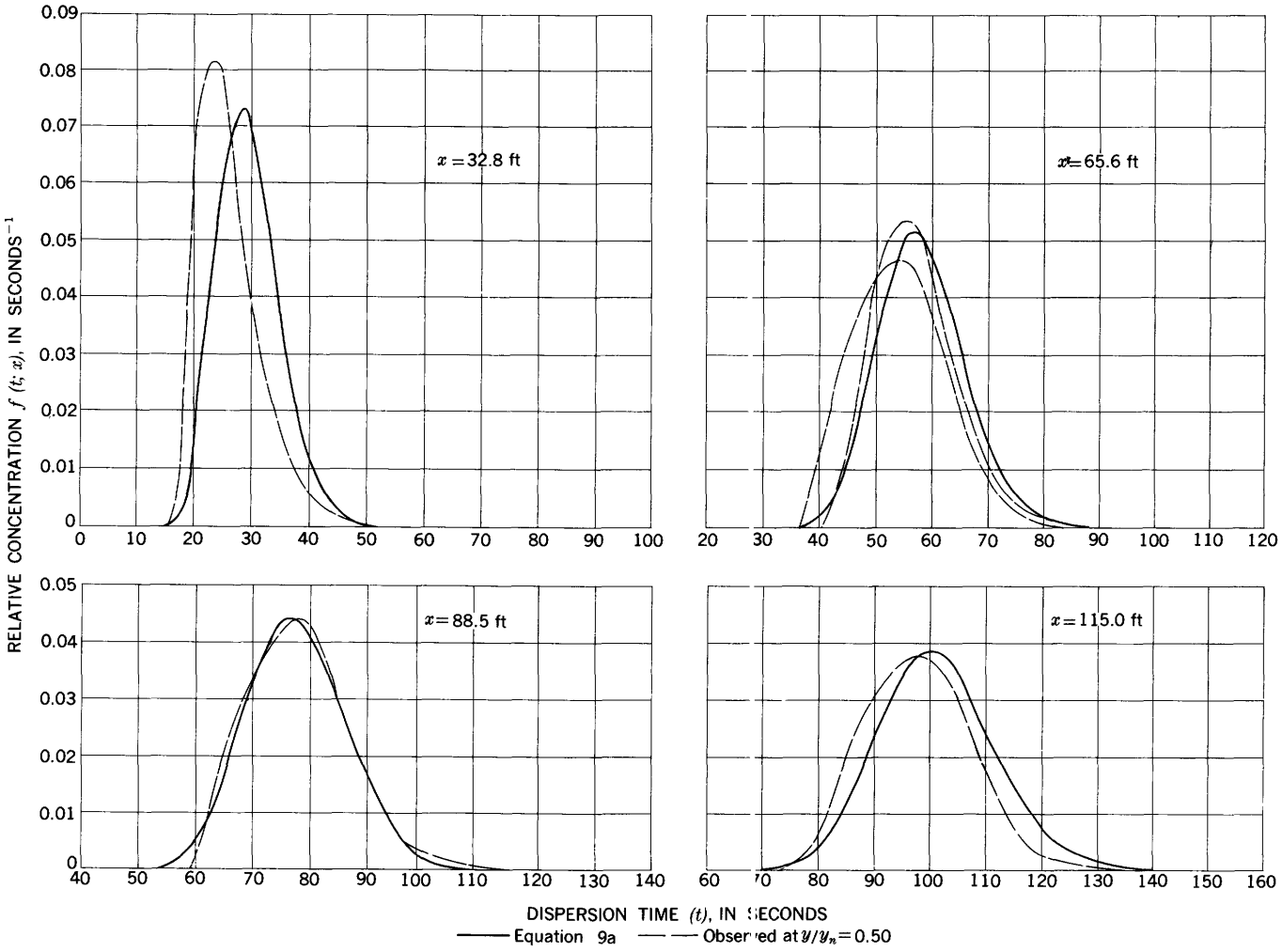

FIGURE 15.—Relative concentration of dye as a function of time at various dispersion distances in run LO-D-2.

solid-line curves which were obtained from equation 9a, using K_x values determined from the data, provide a comparison between the experimental distribution curves and theoretical curves given by the one-dimensional Fickian diffusion model. Characteristically, the experimental curves tend to have a steeper rising limb and a somewhat longer tail on the receding limb than do the theoretical curves. However, the shape of the experimental curves tends to approach the form of the more symmetrical theoretical curves as the dispersion distance increases, which suggests that equation 9a is valid as an asymptotic limit. Even at relatively short dispersion distances there is fairly good agreement between the theoretical and experimental curves. The differences between individual realizations of the experimental curves, when repeated, are in several cases as great as the differences between the experimental and theoretical curves. This is an indication of the randomness of the dispersion process. Irregularities in the experimental curves such as the kinks in figure 16 were presumably caused by large eddies. As a rule, such irregularities tended to even out with increasing dispersion time.

Mean traveltimes, calculated from the experimental distribution curves by the method of moments using the formula

$$\bar{t} = \sum_{i=1}^{\infty} t_i f(t_i; x) \Delta t_i, \tag{48}$$

are shown as a function of dispersion distance in figure 17. In equation 48 the width of the increments Δt_i was varied between 1 and 4 seconds, depending on the rate of change of concentration with time; t_i is the dispersion time at the midpoint of the increment, and $f(t_i; x)$ is the average value of the relative concentration in the increment. For comparison, the relationship between mean traveltime and dispersion distance according to the Fickian theory (eq 10) is also shown. Except for a 3-second displacement, agreement between the experimental and theoretical relationships is good. The reciprocal of the slopes of the curves, which indicates the mean rate of movement of the dye, is equal to the

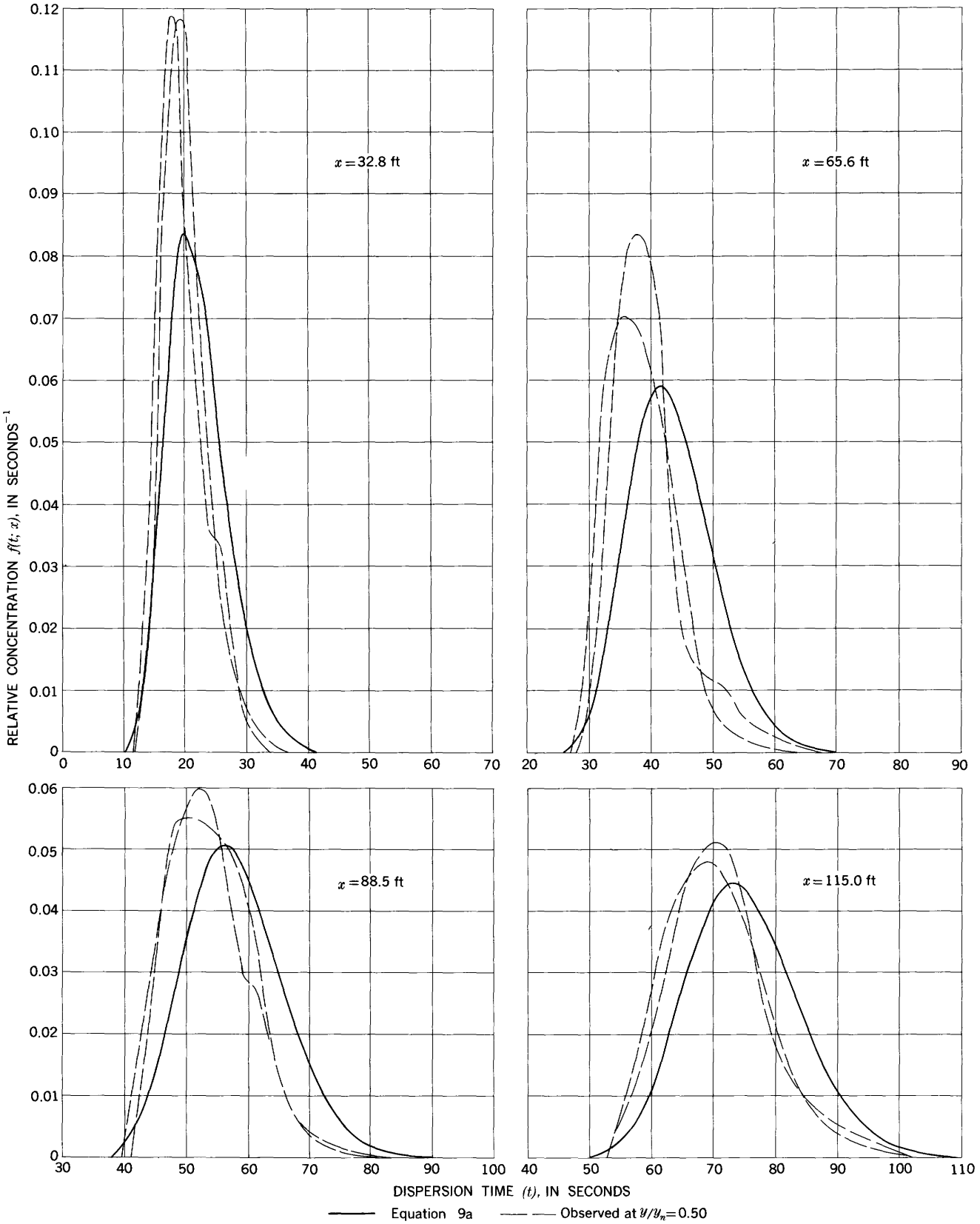

FIGURE 16.—Relative concentration of dye as a function of time at various dispersion distances in run LO-D-3.

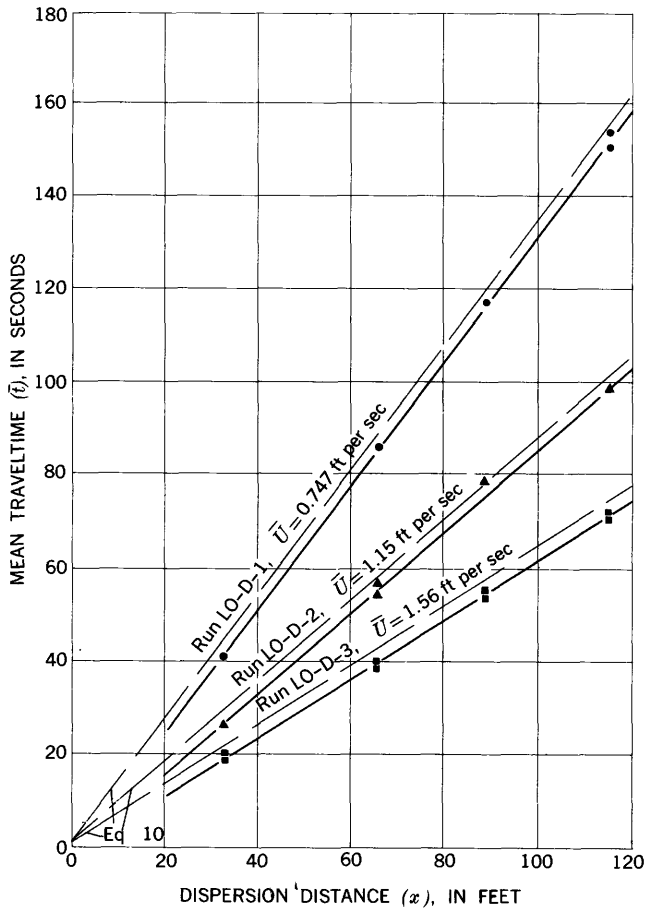

FIGURE 17.—Mean traveltime as a function of dispersion distance, longitudinal dispersion of dye.

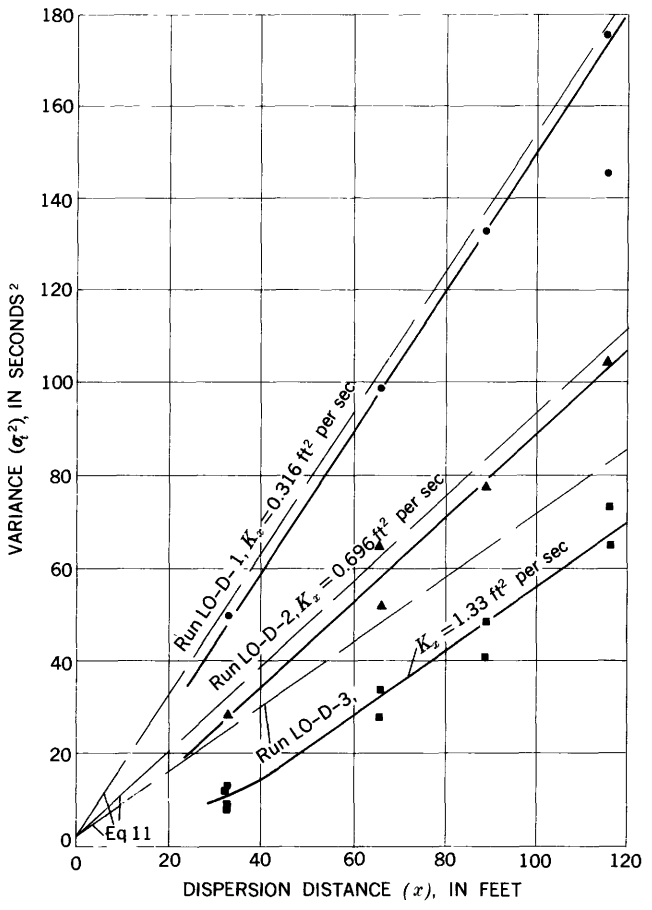

FIGURE 18.—Variance of traveltime as a function of dispersion distance, longitudinal dispersion of dye.

average flow velocities determined from the hydraulic measurements, as required by the Fickian theory. The 3-second displacement could have been caused either by an initial vertical distribution of dye which was weighted toward the water surface or an overcorrection for response lag.

Variances of the experimental distribution curves were calculated, also by the method of moments, using the formula

$$\sigma_t^2=\sum_{i=1}^{\infty} t_i^2 f(t_i; x)\Delta t_i-\bar{t}^2. \tag{49}$$

These variances, like the time base, were corrected for system-response lag by subtracting the appropriate σ_R^2 values taken from table 11 in the section beginning on page E65. The corrected variances are shown as a function of dispersion distance in figure 18. With the exception of the region near the origin or at short dispersion distances, the data show that the relationship between the variance and the dispersion distance is linear. The linearity of this relationship, which is implicit in the Fickian diffusion theory, permits the longitudinal dispersion coefficient, K_x, to be determined from the relationship

$$K_x=\frac{\bar{U}^3}{2}\operatorname*{Lim}_{x\to\infty}\frac{d\sigma_t^2}{dx}. \tag{50}$$

Equation 50 was used for evaluating K_x from the data.

The fact that the experimentally determined σ_t^2 versus x curves fall consistently below the curves given by equation 11 indicates that the dispersion rate during the initial phase of the dispersion process was somewhat less than that specified by the one-dimensional Fickian theory. Going from flow 1 to flow 3, the differences between the actual and theoretical initial dispersion rates tends to increase. This suggests that the duration of the initial phase within which the Fickian theory does not apply is a function of the flow conditions.

In figure 19 the peak relative concentrations of the experimental distribution curves are shown as a function of the dimensionless distance. Comparison of the data with the maxima given by equation 9a indicates that the rate of attenuation of the observed peak con-

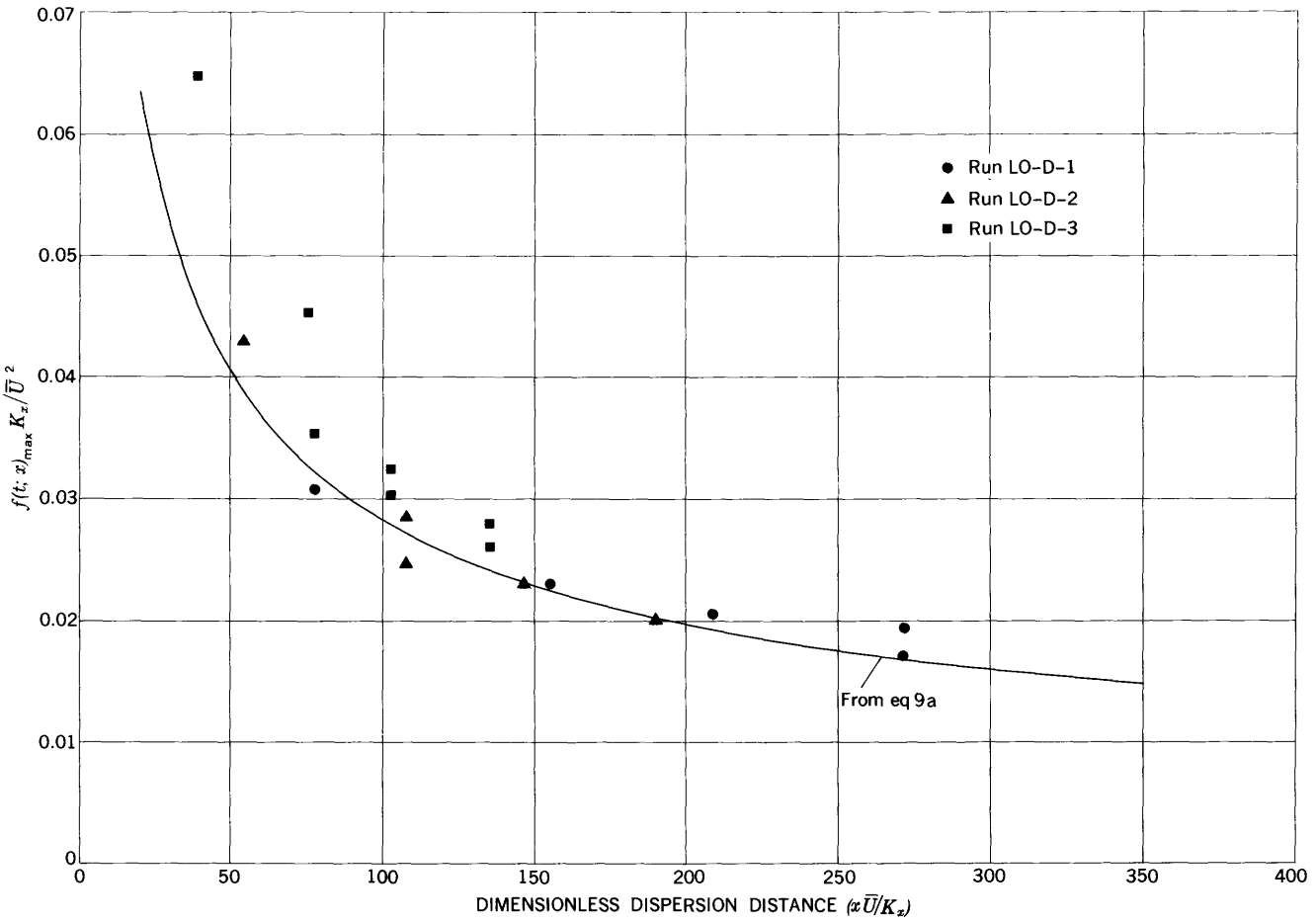

FIGURE 19.—Dimensionless peak relative concentration as a function of dimensionless dispersion distance, longitudinal dispersion of dye.

centrations with increasing dispersion distance is in reasonably close accord with that given by the Fickian theory. The fact that the experimentally determined peak concentrations tend to exceed the theoretical concentrations at small dispersion distances is consistent with the previous observation that actual initial dispersion rates tend to be less rapid than the rates specified by the theory.

In figure 20 the recovery ratio, A_m/A_t, for each of the distribution curves is plotted against dispersion distance. The recovery ratio is an index of the amount of dispersant actually recovered by the sampling apparatus relative to that which would be recovered if the sampling were truly representative and the calibration perfect. It is conveniently defined as the ratio of the area, A_m, under the experimental distribution curve to the area, A_t, under the theoretical distribution curve. Numerically,

$$\frac{A_m}{A_t}=\frac{A'_m/F}{35{,}300W/Q}, \tag{51}$$

where A'_m is the area under the experimental curve in fluorometer unit-seconds, F is the sensitivity of the fluorometer, determined by calibration, in fluorometer units per parts per billion of dye, and W is the weight of dye, in grams, used in the experiment. The numerical conversion factor changes the units of A_t from gram-seconds per cubic foot to parts per billion-seconds.

The data in figure 20 show considerable scatter. Probably the most significant factor contributing to the scatter was that the concentration of dye at the sampling point was not representative of the mean concentration in the cross section. This would be consistent with the randomness of the dispersion process which is apparently more pronounced in the initial phases. In addition, some of the more likely sources of scatter are errors in the operations of weighing, pipetting, and dilution in the preparation of the dosing and calibration solutions.

The information obtained from the longitu dinal dispersion experiments with dye is summarized in table 2.

POLYETHYLENE PARTICLES

The basic data from the LO–P series of experiments consisted of traveltime for known distances of single floating polyethylene particles. The particles were released sequentially in lots of approximately 100, with

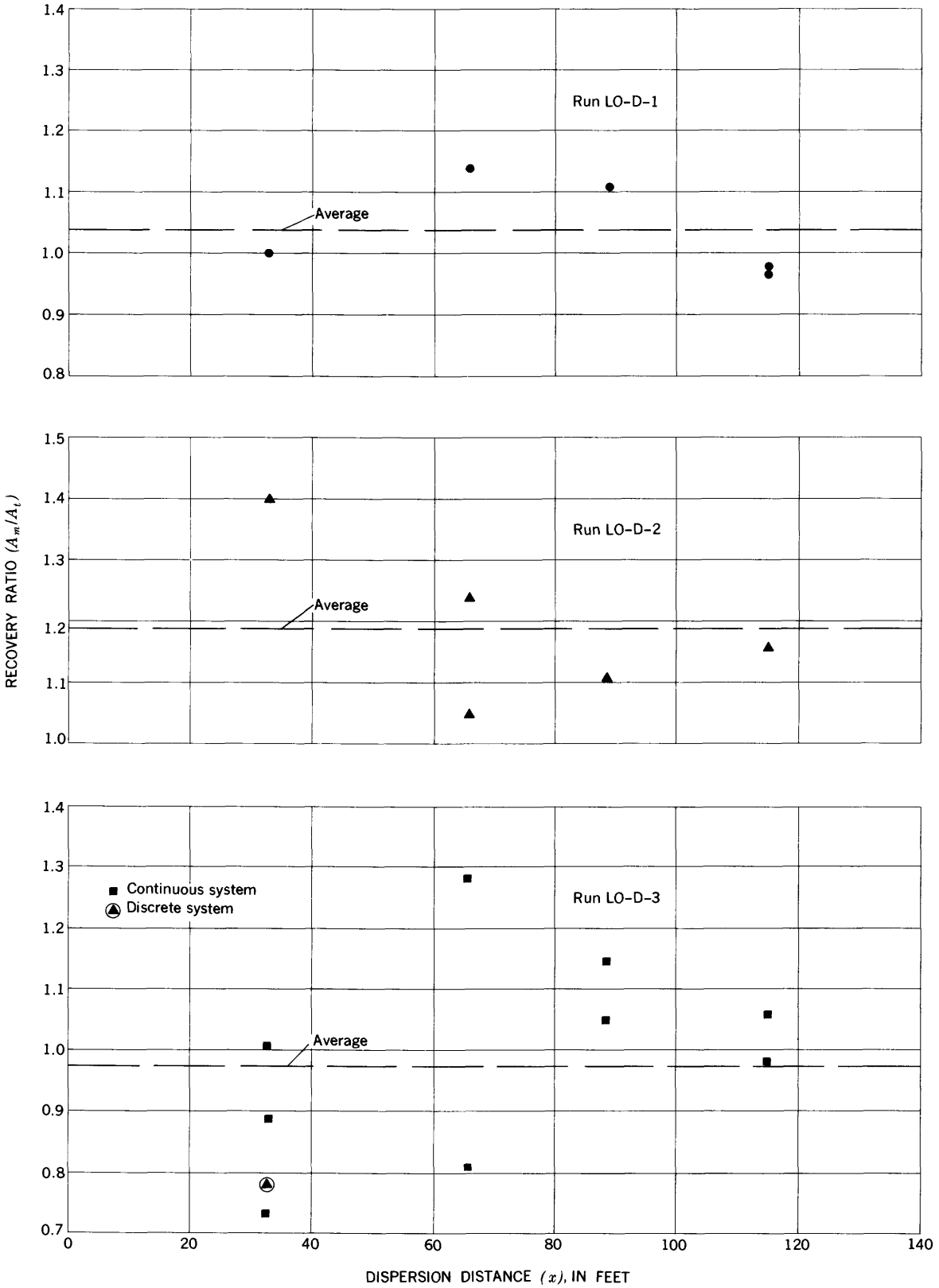

FIGURE 20.—Recovery ratio for area under concentration versus time curves as a function of dispersion distance, longitudinal dispersion of dye.

TABLE 2.—*Longitudinal dispersion of dye: summary of data*

Run (LO-D-)	x (ft)	W (gm)	F (fluorometer units per ppb)	A_t (ppb-sec)	A_m (ppb-sec)	$\bar{t}$ (sec)	σ_t^2 (sec^2)	$f(t;x)_{max}$ (sec^{-1})
1	32.8	0.0330	2.96	405	405	41.1	47	0.0545
	65.6	.0495	2.72	607	691	85.5	96	.0408
	88.5	.0667	2.80	819	907	116.9	133	.0365
	115.0	.0667	2.88	819	792	153.6	174	.0303
		.0667	2.84	819	803	150.4	144	.0343
2	32.8	.0525	2.76	258	362	26.5	28	.0820
	65.6	.110	2.64	542	675	54.2	66	.0470
		.110	2.72	542	566	56.9	52	.0545
	88.5	.110	2.72	542	599	78.1	77	.0440
	115.0	.110	2.68	542	627	98.6	104	.0382
3	32.8	.0515	6.75	122	123	19.9	11.8	.119
		.0412	6.80	97.5	86.6	19.4	12.6	.118
	65.6	.0590	6.85	140	114	39.6	34	.0835
		.0758	6.80	177	227	38.3	28	.0705
	88.5	.0706	6.80	167	192	54.1	41	.0552
		.0706	6.80	167	176	53.5	48	.0601
	115.0	.0808	6.70	191	202	70.2	65	.0480
		.101	6.80	237	234	71.2	74	.0515
	32.8	.0412	6.75	97.5	76.5	19.1	8.0	.132
(1)	32.8	.0412	4.84	97.5	71.3	20.6	9.1	.163

[1] Discrete system.

a time interval, Δt, between successive releases. In analyzing the data it was assumed that the flow velocity at the water surface was a statistically stationary function of time so that the statistical characteristics of the distribution of traveltimes would be the same as if the entire lot of particles had been released simultaneously.

A typical set of traveltime distribution data is shown in the form of a histogram in figure 21. The ordinate of the histogram, which represents the relative frequency with which the time required for a particle to travel from 0 to x is in the range $t_j-\frac{\Delta t_j}{2}\leq t_j<t_j+\frac{\Delta t_j}{2}$, is

$$f(t_j;\, x)=\frac{n_j}{N\Delta t_j}. \tag{52}$$

In equation 52,

t_j = time at the midpoint of the j'th time interval,

Δt_j = 0.3 sec = duration of the j'th time interval,

n_j = number of particles counted in the j'th time interval, and

N = total number of particles counted.

For comparison, the curve representing equation 9a with $\overline{U}=\overline{U}_s$ and $K_x=K_{x_s}$ evaluated from the data is also shown in figure 21. The subscript s denotes

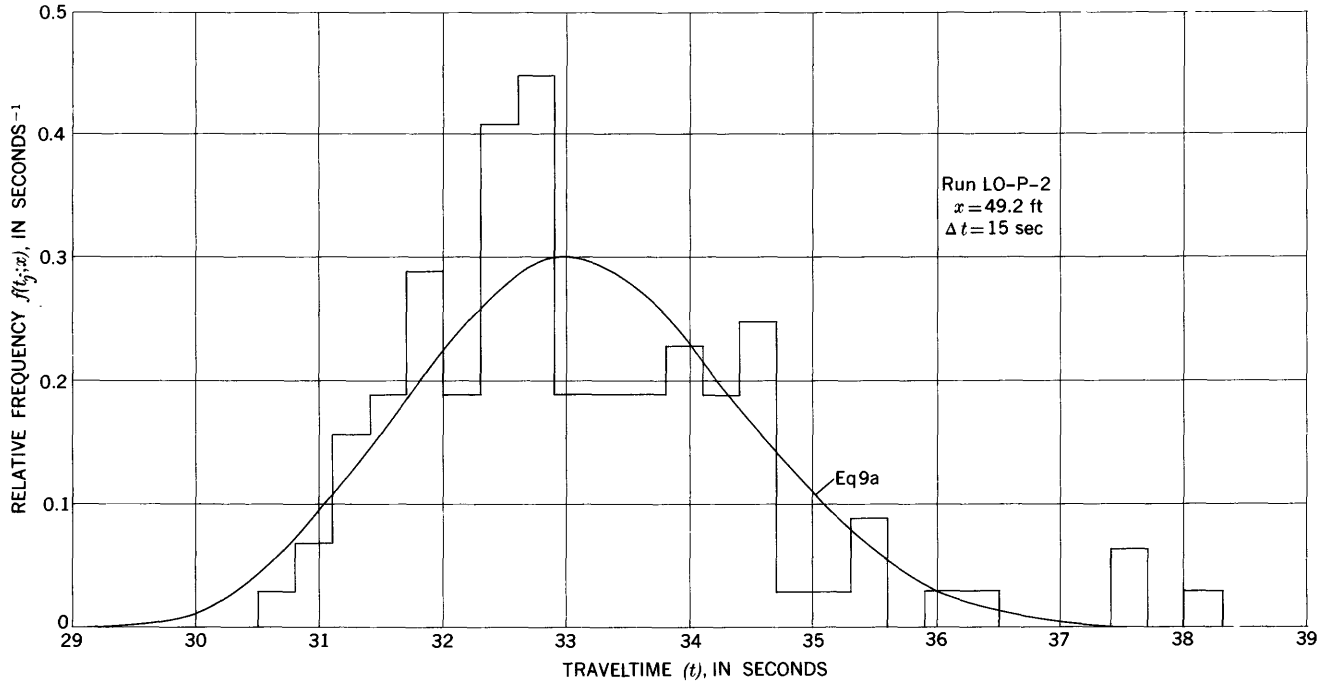

FIGURE 21.—Typical traveltime distribution, longitudinal dispersion of polyethylene particles.

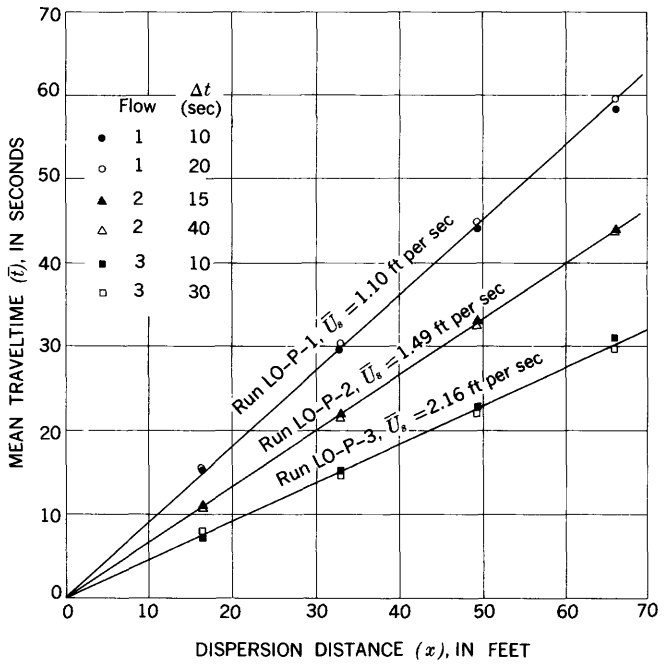

FIGURE 22.—Mean traveltime as a function of dispersion distance, longitudinal dispersion of polyethylene particles.

reference to the water surface. The irregularity of the histogram, which was typical of all sets of data, indicates that the number of particles in each lot, $N \approx 100$, was too small to permit a detailed comparison between the shapes of the histograms and the distribution curves generated by equation 9a. However, N was sufficiently large to permit reliable estimates to be made of the mean and variance of the traveltimes.

In figure 22 the mean traveltime

$$\bar{t} = \frac{1}{N} \sum_{i=1}^{N} t_i, \tag{53}$$

where t_i is the traveltime of the i'th particle, is shown as a function of dispersion distance. The average velocities of the particles, indicated by the slopes $\frac{dx}{d\bar{t}}$, are $\overline{U}_s = 1.10$, 1.49, and 2.16 feet per second. These agree closely with the water-surface velocities of 1.03, 1.53, and 2.06 feet per second calculated by equation 47 for the flow conditions in runs LO–P–1, LO–P–2, and LO–P–3. Changing the time interval, Δt, between particle releases had no apparent effect on the mean traveltimes.

In figure 23 the unbiased estimate of the variance of the traveltimes, calculated according to the formula

$$\sigma_t^2 = \frac{1}{N-1} \sum_{i=1}^{N} (t_i - \bar{t})^2, \tag{54}$$

is shown as a function of dispersion distance. Longitudinal dispersion coefficients, K_{x_s}, for the particles were evaluated from this data using equation 50 with $\overline{U}$ replaced by $\overline{U}_s$. The results for flow 3 differ markedly from those for flows 1 and 2 in two important respects. The first difference is the apparent dependence of the σ_t^2 versus x relationship on Δt in run LO–P–3. No satisfactory explanation for this has been found. The argument that the periodicity of the turbulence was sufficient to produce so pronounced an effect is inconsistent with the notion that turbulence is basically a random phenomenon. The second difference is the obvious nonlinearity of the σ_t^2 versus x relationships in run LO–P–3 for $x \lesssim 20$ feet. The results from run LO–D–3 in figure 18 are similar in this respect. The initial nonlinearity may be associated with a Lagrangian velocity correlation as suggested by the theory of diffusion by continuous movements. However, the existence in flow 3 of a scale of turbulence sufficiently large to indicate a persistence of correlation over a distance of 20 feet would be somewhat surprising. It is quite possible that for small x the relationship between σ_t^2 and x would be nonlinear for flows 1 and 2 also, but that the region of nonlinearity does not extend to sufficiently large x to be apparent from the data in figure 23.

A summary of the longitudinal dispersion data obtained in the polyethylene particle experiments is given in table 3.

SUSPENDED SILT-SIZE PARTICLES

In contrast to the dye dispersion experiments where the basic data for the concentration-distribution curves consisted of continuous recordings of the fluorometer reading, the basic data for most of the concentration-distribution curves in the silt dispersion experiments consisted of a set of discrete fluorometer readings for a group of 25–30 small water-sediment samples. These samples were obtained in rapid sequence as the silt cloud passed the sampling station. Also, whereas sampling was restricted to one point at middepth in the dye dispersion experiments, samples were collected simultaneously from three sampling depths ($y/y_n = 0.25$, 0.50, and 0.75, where y is the distance above the flume bed) in the silt dispersion experiments.

The distribution data shown in figure 24, where each plotted point represents the fluorometer reading and dispersion time for a single sample, is quite typical. Figure 24 illustrates quite well the degree of definition which is obtainable by nephelometric tracing techniques. The degree of definition is limited not only by sample reading techniques, which are complicated by the tendency of the particles to settle while a reading is being made, but also by sampling statistics as related to the number of particles contained in the sample.

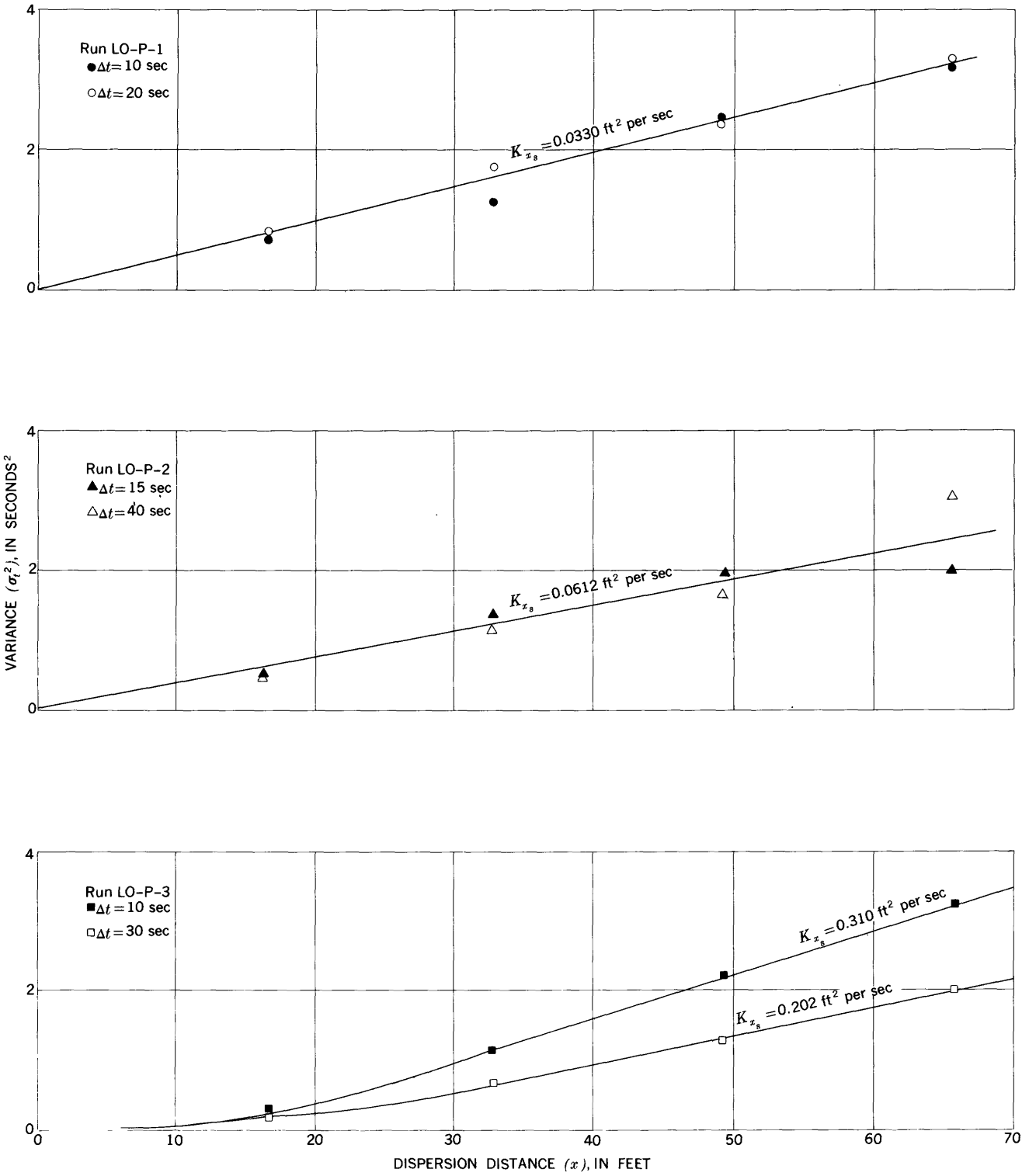

FIGURE 23.—Variance of traveltime as a function of dispersion distance, longitudinal dispersion of polyethylene particles.

Both of these restrictions tend to become stronger with increasing particle size.

The data for all the experiments were plotted in the manner shown in figure 24. Smooth curves were drawn by eye through the data and a line representing the background fluorometer reading was drawn. The time base was corrected for response lag using the appropriate $\bar{\tau}$ values from table 11 in the section beginning on page E65. The curves were normalized by dividing the net fluorometer readings (fluorometer reading minus

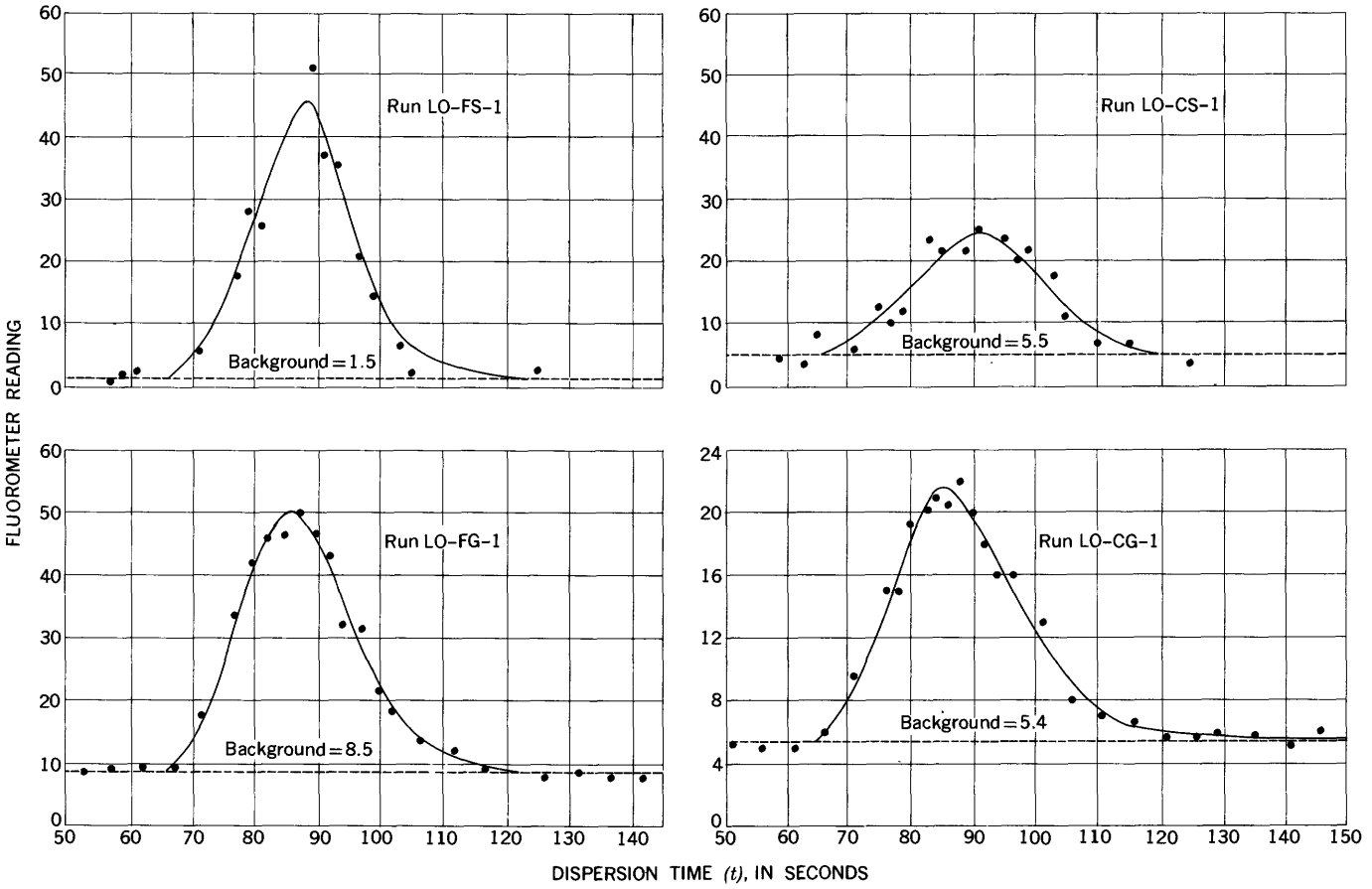

FIGURE 24.—Typical traveltime distribution data, longitudinal dispersion of natural silt and glass beads, flow 1, x=65.6 feet, y/y_n=0.50.

TABLE 3.—*Longitudinal dispersion of floating polyethylene particles: summary of data*

Run (LO-P-)	Δt (sec)	x (ft)	Number of particles released	Number of particles counted [1]	$\bar{t}$ (sec)	σ_t^2 (sec^2)
1	10	16.4	116	105	15.1	0.74
		32.8		99	29.9	1.28
		49.2		93	44.8	2.48
		65.6		99	58.8	3.19
	20	16.4	115	111	15.4	.75
		32.8		114	30.2	1.71
		49.2		110	45.0	2.39
		65.6		109	59.9	3.27
2	15	16.4	130	118	11.1	.45
		32.8		96	22.1	1.35
		49.2		105	33.2	1.97
		65.6		112	44.1	2.00
	40	16.4	98	97	10.9	.42
		32.8		97	21.5	1.14
		49.2		95	32.8	1.64
		65.6		95	44.0	3.07
3	10	16.4	115	112	7.5	.27
		32.8		105	14.9	1.12
		49.2		91	22.8	2.22
		65.6		84	31.0	3.63
	30	16.4	110	110	7.6	.22
		32.8		107	14.8	.65
		49.2		105	22.4	1.29
		65.6		106	30.0	2.06

[1] Particles which were not counted were not seen by the observers.

background) by the area enclosed by the distribution curve and the background line.

In each run, one distribution curve was obtained with the continuous sampling and recording system. This data was processed to obtain normalized distribution curves in exactly the same way as the dye dispersion data.

The normalized distribution curves for all the silt dispersion experiments are shown in figures 25 through 32. Given in these figures for the indicated dispersion distances are the distribution curves obtained at each of the three sampling depths, the distribution curve (for one dispersion distance only) obtained with the continuous sampling and recording system, and, for comparison, the distribution function according to equation 9a. The different curves are identified by the symbols defined in the figures.

The values of K_x used in obtaining the curves from equation 9a are either the same as those determined from the dye dispersion experiments for the same flow conditions, or they are adjusted values of K_x, used where the flow conditions as listed in table 1 differed slightly from the conditions for the corresponding dye experiments. The adjustment was made by assuming, in accordance with equation 34, that K_x is directly proportional to $y_n U\tau$ so that K_x can be adjusted in proportion to the change in $y_n U_\tau$.

The original intent was to compare the sediment dispersion curves directly with the dye curves. However, because of the inability to repeat flow conditions more

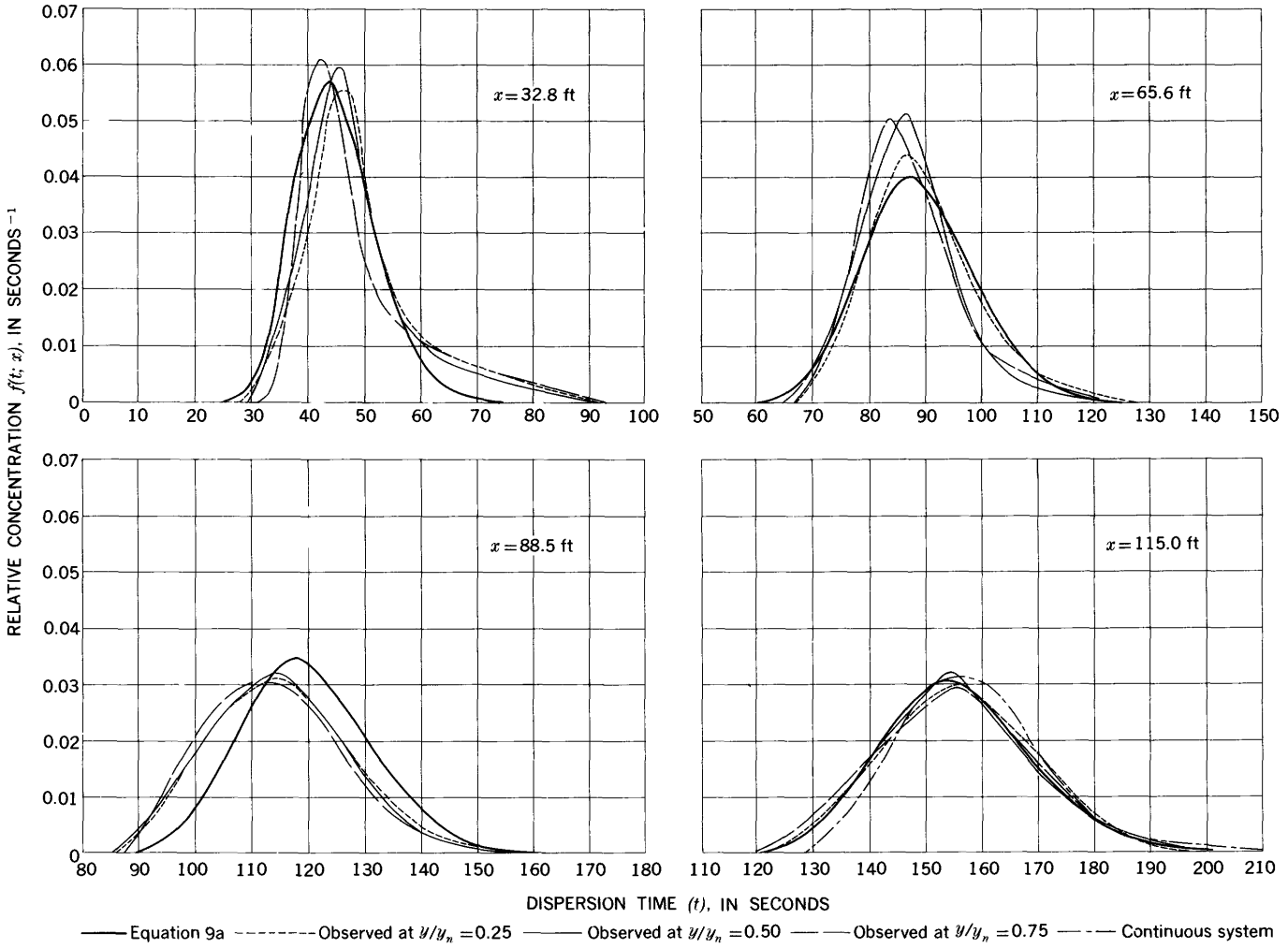

FIGURE 25.—Relative concentration of 15–30μ silt as a function of time at various depths and dispersion distances in run LO–FS–1.

closely it was considered preferable to compare both to a common standard, equation 9a.

The distribution curves for the fine particles for the most part agree fairly closely with the curves derived from equation 9a. Indeed, in several instances the fine particle curves seem to follow the theoretical curves more closely than do the dye curves. In comparison, the curves for the coarse particles characteristically tend to have lower peaks and longer tails on the receding limb. This results from the tendency of the coarse particles to settle more rapidly, which is conducive to the establishment of a concentration gradient that is more heavily weighted toward the bottom. Therefore, there is greater probability that the coarse particles will either be retarded in the slower moving region of flow near the bed or be deposited on the bed. In opposition to the settling process, however, turbulence is continually tending to redistribute the particles more uniformly in the vertical, so that some of the particles which have been temporarily retarded or deposited are reentrained in the main stream of the flow. These are the particles which contribute to the tails on the curves.

A comparison of the curves for runs LO–CG–1, LO–CG–2, and LO–CG–3 in figures 30, 31, and 32 shows that the tails tend to become progressively more pronounced going from flow 1 to flow 3. This suggests that the capacity of the turbulence to reentrain the retarded and deposited particles tends to increase with the depth and velocity of the flow. The lack of any pronounced tails in the curves for the fine particles suggests that the level of turbulence was sufficient to largely inhibit the establishment of a negative concentration gradient. These observations are consistent with the recovery ratio data in figures 39 and 40, which give an indication of the settling rates, and the mean traveltime data in figure 34, which indicates the mean velocity of the particles.

A comparison of the distribution curves obtained at the different sampling depths indicates a two-dimensional relative concentration-distribution pattern,

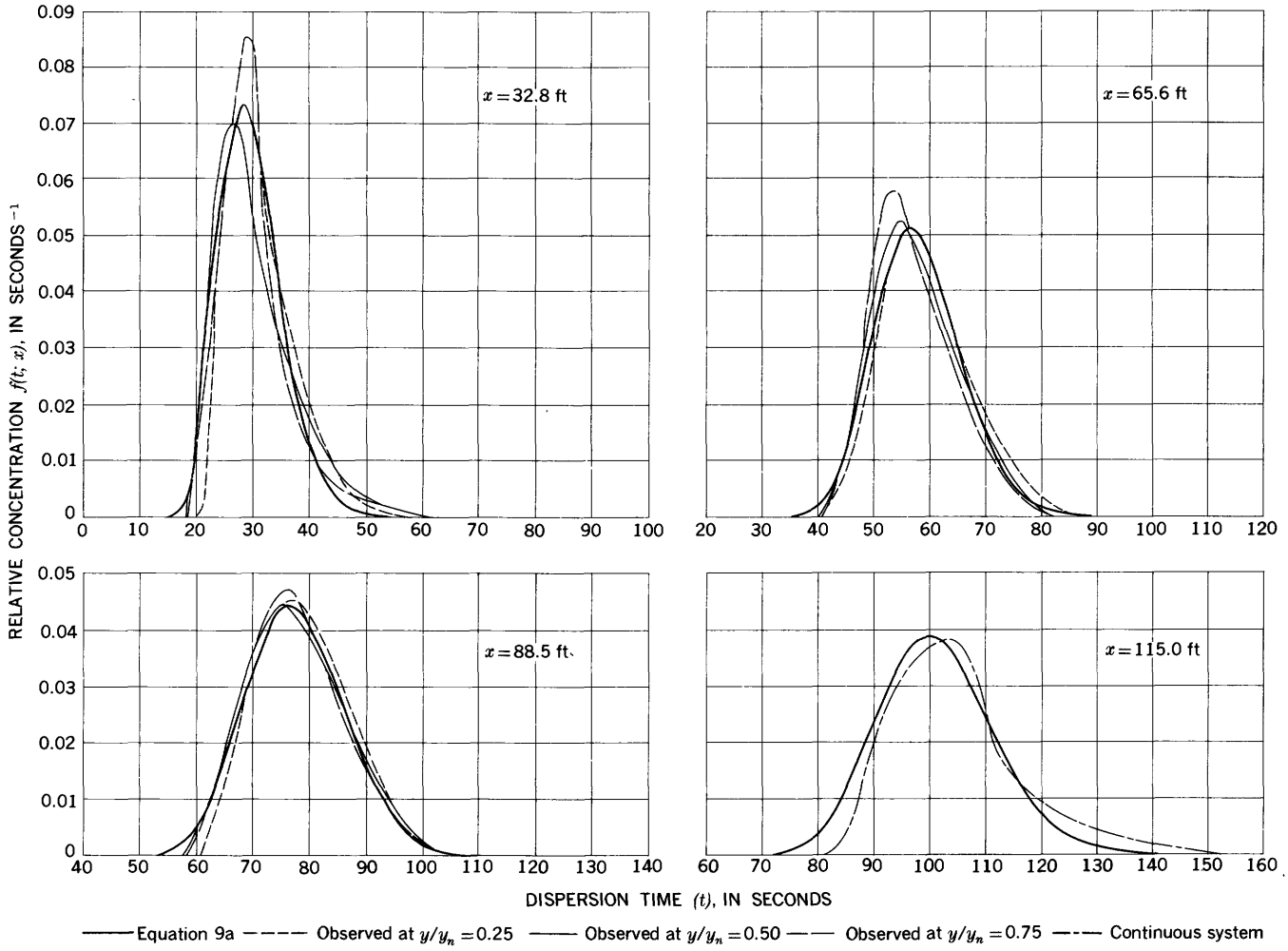

FIGURE 26.—Relative concentration of 15-30μ silt as a function of time at various depths and dispersion distances in run LO-FS-2.

$f(t, y; x)$, which is repeated quite consistently in most of the observations. As the observation level is raised from the bed toward the water surface, the position of the distribution curve, $f(t; y, x)$, is shifted slightly along the time axis in the direction of decreasing time, and the peak relative concentration tends to increase slightly, reflecting a small decrease in the degree of dispersion. This suggests that a longitudinal cross section taken through the cloud of dispersing particles would be somewhat trapezoidal in shape with both the leading and trailing ends inclined in the direction of flow, but with the leading end less inclined. This result is entirely consistent with the distribution patterns, $C(x, y, t)$, developed by Yotsukura and Fiering (1964) from their numerical solution of equation 27. The data shows, however, that the degree of dependence of $f(t; y, x)$ on y in the present experiments is quite small and for most purposes can safely be ignored.

The normalized relative concentration-distribution data for the silt-size particles were processed in exactly the same way as the data from the dye experiments to obtain the graphical relationships in which the mean traveltime, the variance of traveltime, the dimensionless peak relative concentration, and the recovery ratio are shown as functions of dispersion distance. The only difference was the substitution of parts per million for parts per billion as concentration units in calculating the recovery ratio and the consequent reduction of the constant in equation 51 by a factor of 1,000. Many of the observations pertaining to these relationships which were made for the dye data apply equally well to the sediment. Only those which differ significantly are discussed.

The data in figures 33 and 34 show that in most runs the mean velocity of the suspended particles agrees very closely with the mean flow velocity. The exceptions are runs LO–CG–2 and LO–CG–3, where the mean velocity of the particles was somewhat retarded. This was

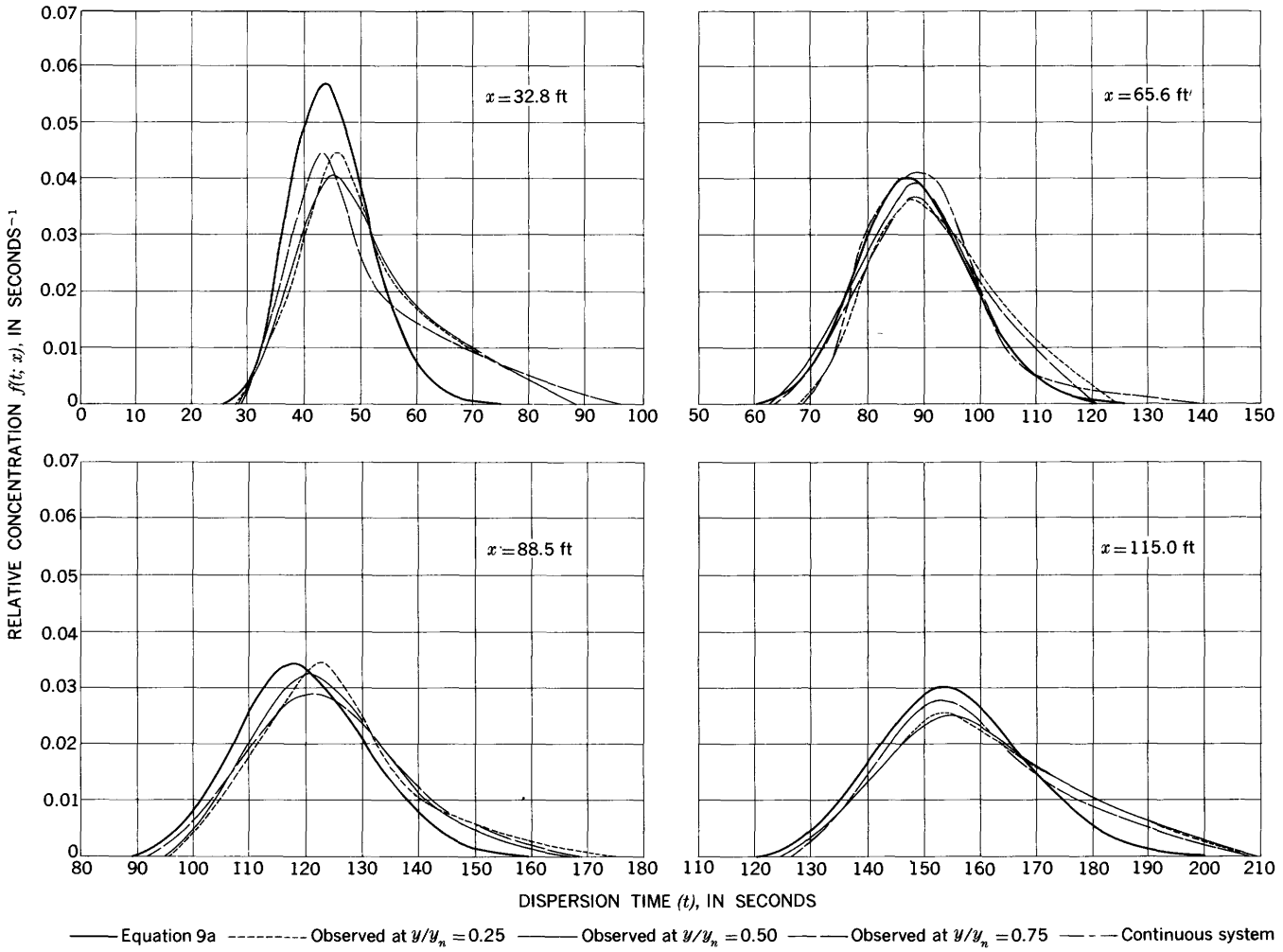

FIGURE 27.—Relative concentration of 53–62μ silt as a function of time at various depths and dispersion distances in run LO–CS–1.

probably caused by the development of a negative vertical concentration gradient and perhaps also by temporary deposition on the bed.

The relationship between σ_t^2 and x, shown in figures 35 and 36 for the fine particles, follows equation 11 quite closely. However, the relationship for the coarse particles differs markedly. In flow 1, σ_t^2 for the coarse particle data is two to three times the value given by equation 11 at $x=32.8$ feet, but as x increases the relationships tend to converge. In flows 2 and 3, the trend is exactly opposite. No satisfactory explanation for this reversal in trend has been found.

The trends of the peak relative concentration data in figures 37 and 38 are consistent with those of the variance data but are considerably less exaggerated. This is reasonable because the peak relative concentration is approximately inversely proportional to the square root of the variance.

The conclusions concerning the general properties of the two-dimensional relative concentration distribution, $f(t, y; x)$, which were inferred from a comparison of the distribution curves obtained at different sampling depths, are reinforced by the data on mean traveltime, variance, and peak relative concentration. According to the conclusions, with increasing y/y_n, values of $\bar{t}$ and σ_t^2 should occur in descending order, and values of $f(t; x)_{max}$ should occur in ascending order. Out of a total of 31 sets of observations, the expected order occurs 17 times for $\bar{t}$, 9 times for σ_t^2, and 14 times for $f(t; x)_{max}$. If all possible orders were equally likely, the expected orders would have occurred, on the average, only one out of six times.

Applying a similar analysis to the recovery ratio data in figures 39 and 40, for a concentration gradient of sediment which is weighted toward the bottom, values of A_m/A_t should occur in descending order with increasing y/y_n. For the finer particles, the expected order occurs 6 out of 15 times and for the coarser

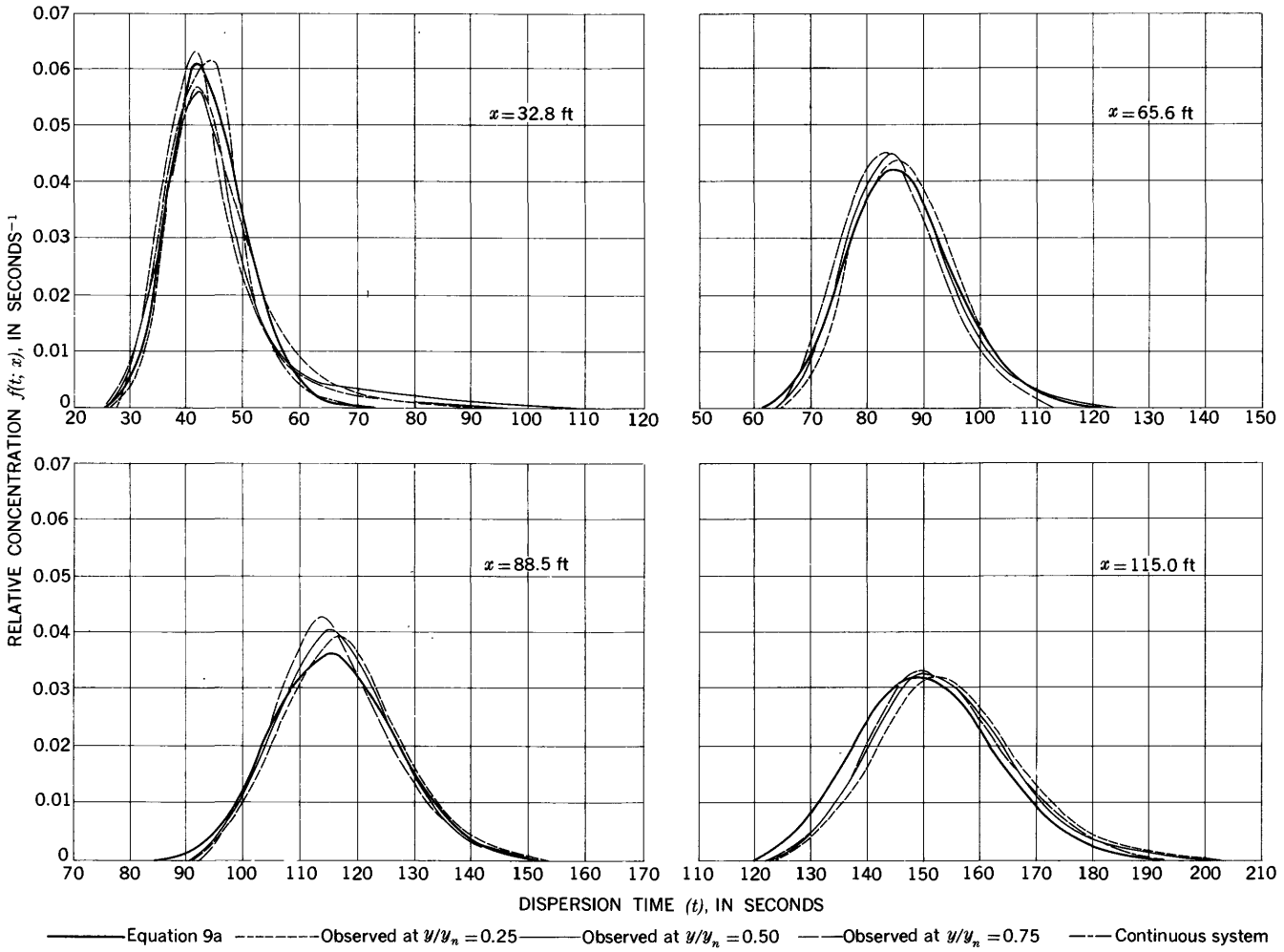

FIGURE 28.—Relative concentration of <44μ glass beads as a function of time at various depths and dispersion distances in run LO-FG-1.

particles, 8 out of 16 times. This indicates a tendency, although not a very consistent one, for the concentration gradient in the vertical to be negative, as was expected.

The recovery ratio data for the sediment differs fundamentally from the data for dye because of the tendency for the particles to settle and deposit on the bed of the flume. Since A_t is the theoretical area which would have been under the concentration-distribution curve had no settling occurred, the ratio A_m/A_t represents the relative amount of sediment remaining in suspension at the sampling level, y/y_n, integrated over the time of passage of the sediment cloud past the sampling nozzle. If A_m is averaged over the depth of flow,

$$\overline{A}_m=\frac{1}{y_n}\int_0^{y_n} A_m dy,$$

then the ratio $\overline{A}_m/A_t$ represents the relative amount of sediment in the entire vertical which remains in suspension as the cloud passes the sampling location, x. The curves in figures 39 and 40, which show $\overline{A}_m/A_t$ as a function of x, were determined from a theory given by Camp (1944, 1946) for sedimentation in settling tanks with turbulent flow. According to Camp's theory,

$$\frac{\overline{A}_m}{A_t}=72\beta^2 e^{3\beta}\sum_{i=1}^{\infty}\frac{(-1)^{i-1}\alpha_i^2 e^{-(9\beta^2+\alpha_i^2)\frac{\kappa x}{6y_n\overline{U}/U_\tau}}}{(9\beta^2+\alpha_i^2+6\beta)(9\beta^2+\alpha_i^2)^2}, \qquad (55)$$

where $\beta=V_p/\kappa U_\tau$ as in equation 42, and α_i ($i=1, 2,$

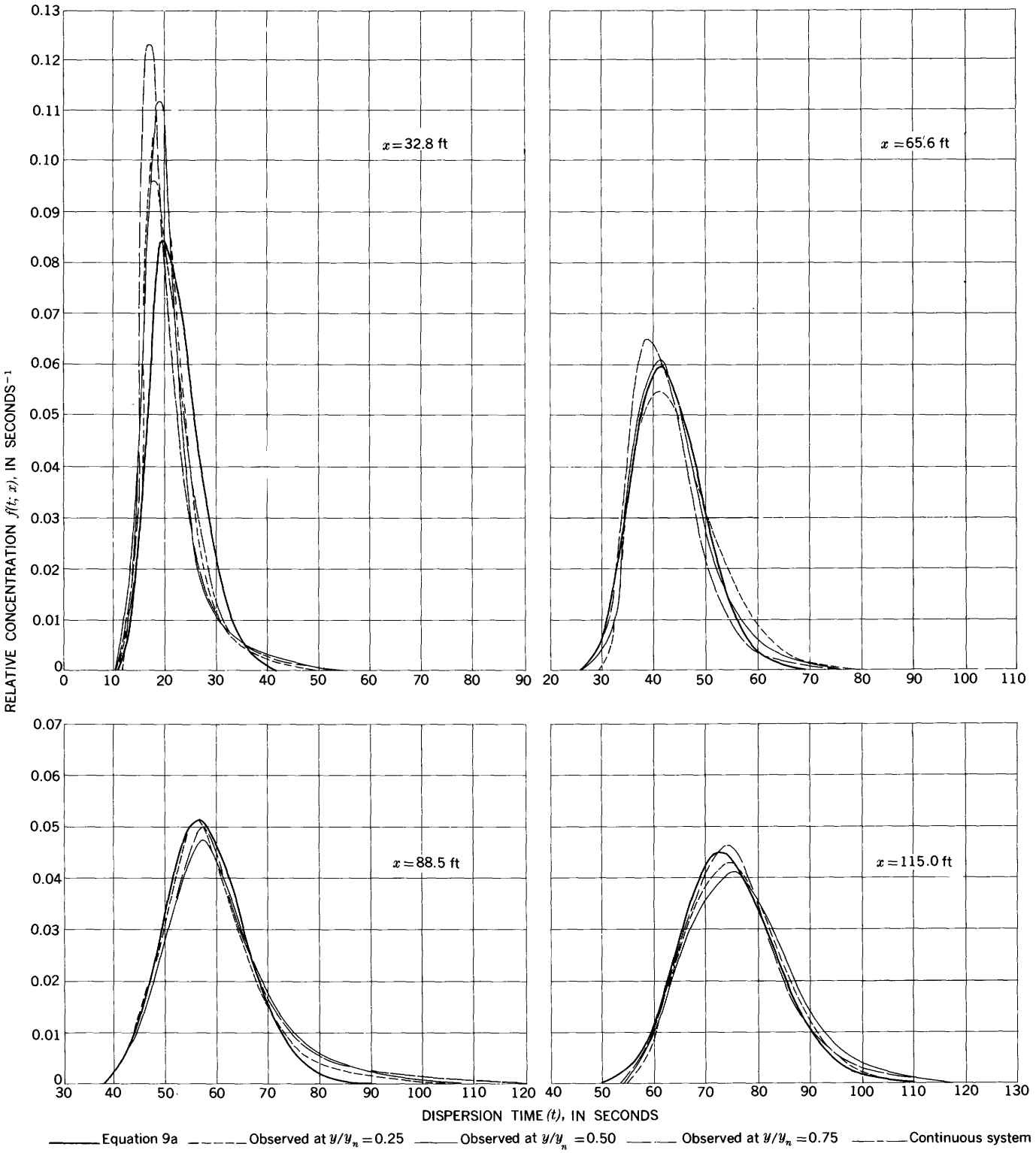

FIGURE 29.—Relative concentration of <44μ glass beads as a function of time at various depths and dispersion distances in run LO–FG–3.

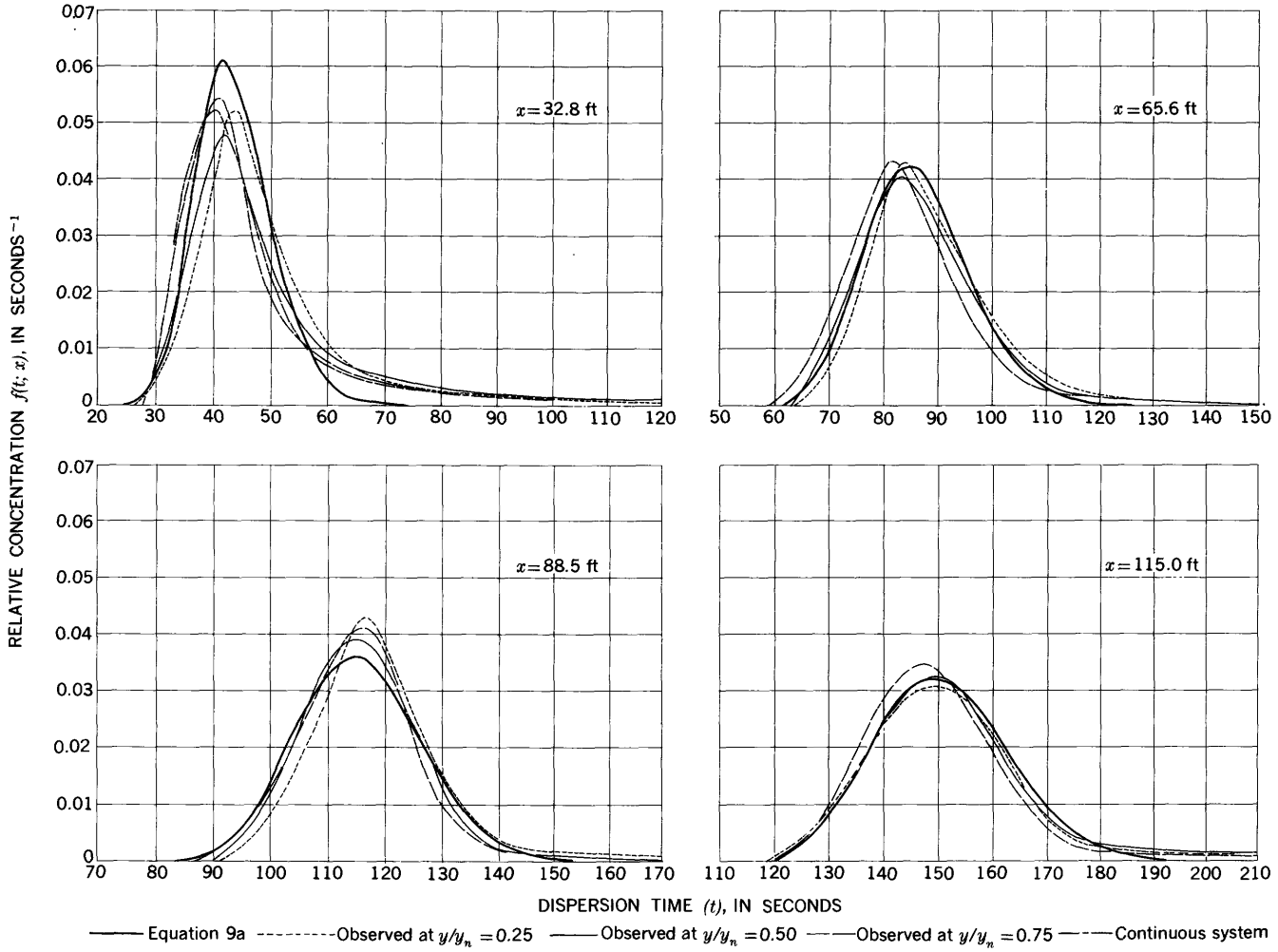

FIGURE 30.—Relative concentration of 53–62μ glass beads as a function of time at various depths and dispersion distances in run LO–CG–1.

3, . . .,) are the successive real positive roots of the transcendental equation

$$2 \cot \alpha = \frac{\alpha}{3\beta} - \frac{3\beta}{\alpha}.$$

Equation 55 is a solution of equation 41 for the initial condition of a vertically uniform distribution of sediment at the entrance of the tank, and the boundary condition of no entrainment of sediment from the bed. In order to obtain this solution it was necessary to assume that: (1) $\frac{\partial C}{\partial t} = \overline{U} \frac{\partial C}{\partial x}$, (2) the velocity distribution, $U(y)$, is parabolic so that ϵ_y is a constant, and (3) $\epsilon_{p_y} = \epsilon_y = \kappa y_n U_\tau / 6$. In performing the calculations required for plotting the $\overline{A_m}/A_t$ versus x curves, Camp's graphical representation of equation 55 was used. Also the fall-velocity distribution data given in figure 6 were corrected for temperature by means of Stoke's law. Finally, the fall-velocity distribution data were separated into five ranges, using 20-percent increments. The calculations were done separately for each range, using the average fall velocity within the range, and the final values of $\overline{A_m}/A_t$ were obtained by averaging the values obtained for the five different ranges.

The theoretical $\overline{A_m}/A_t$ versus x relationships agree reasonably well with the experimental data for all runs except for run LO–CS–1, where the data were probably subject to a large systematic error of undetermined origin. Likely sources of experimental error in the remaining runs were an uneven initial

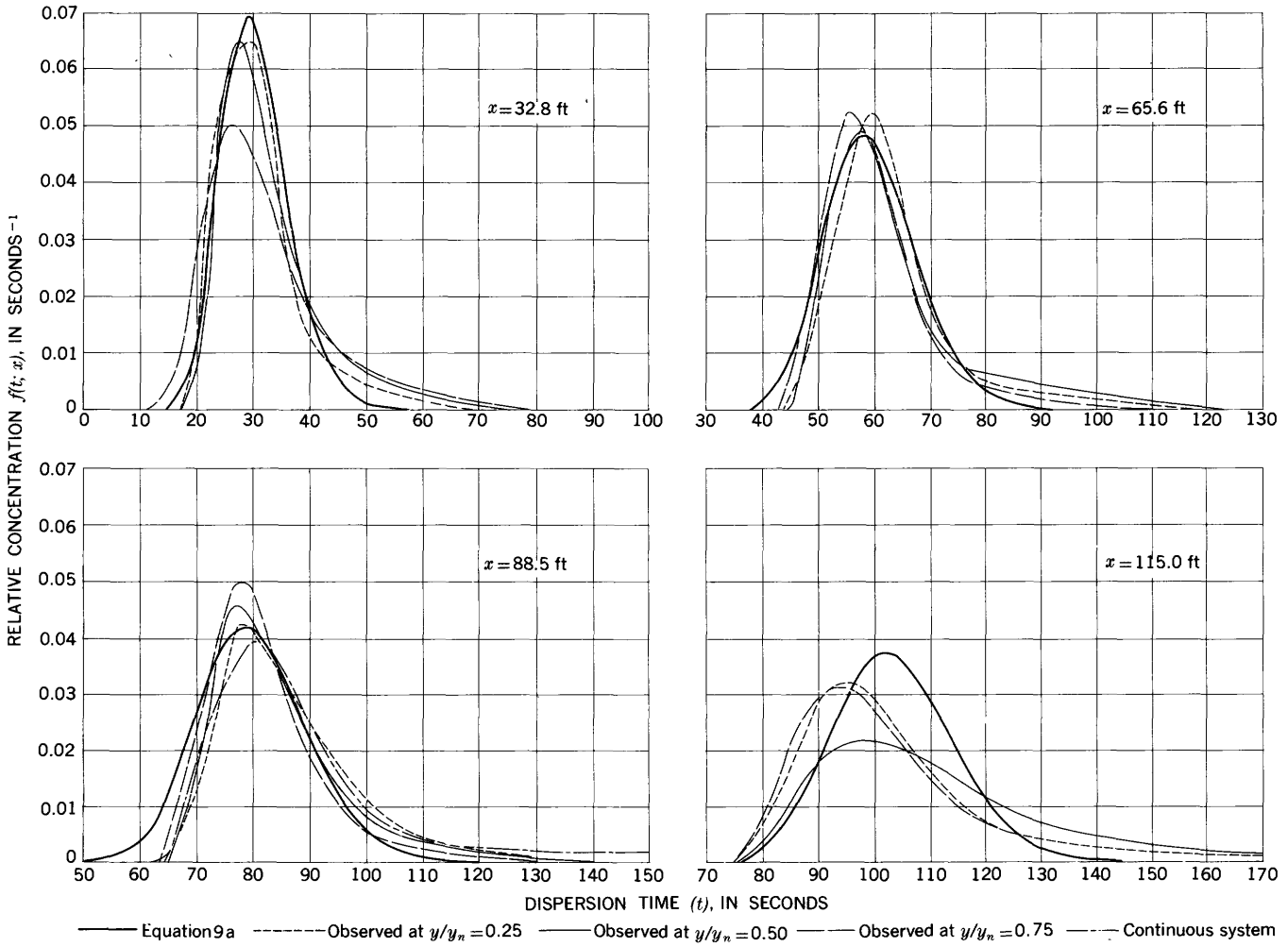

FIGURE 31.—Relative concentration of 53–62μ glass beads as a function of time at various depths and dispersion distances in run LO-CG-2.

distribution of sediment across the flume, calibration errors, and an abnormally high rate of deposition near the source when initial local concentrations of sediment exceeded the transport capacity of the flow. The initial distribution of sediment across the flume tended to be more even in those runs in which the improved dumping trough was used. Calibrating the fluorometer for sediment concentration was one of the most difficult operations in the entire experimental program. Because the calibrations required such small quantities of sediment, the extent to which the calibration samples were truly representative is open to question. Another possible source of error was a shift in the size distribution of the suspended sediment with increasing dispersion distance caused by the tendency of the coarser particles to be deposited sooner. Because the sensitivity of the fluorometer increases as particle size decreases, this would cause the fluorometer to register higher concentrations than actually existed at large dispersion distances. A spot check consisting of a visual examination with a microscope indicated that the average size of particles in a sample collected at $x=115$ feet did not differ significantly from that of a sample obtained at the source. However, spot checks with small samples can be misleading.

A summary of the data obtained in the longitudinal dispersion experiments with silt-size particles is given in table 4.

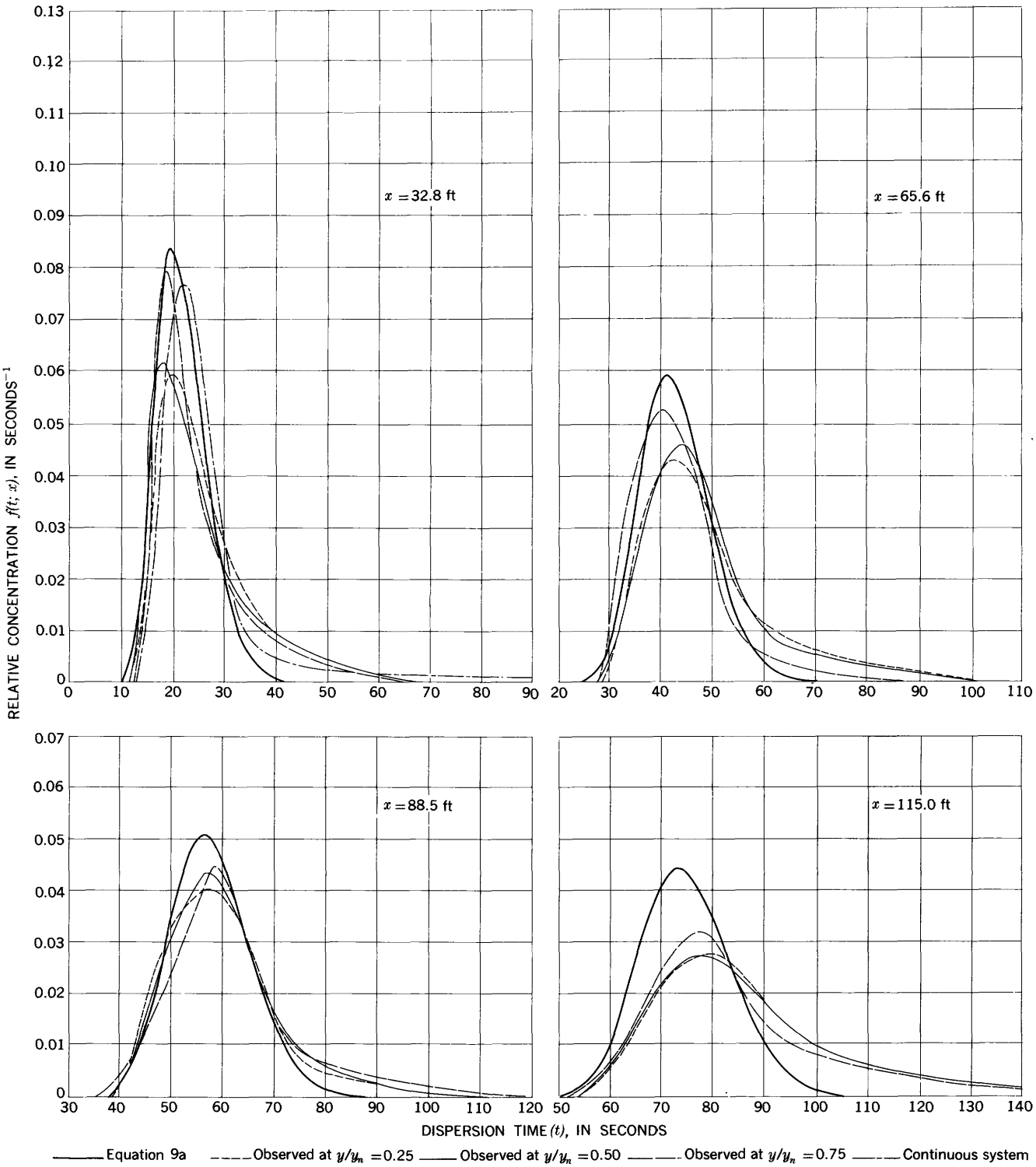

FIGURE 32.—Relative concentration of 53–62μ glass beads as a function of time at various depths and dispersion distances in run LO–CG–3.

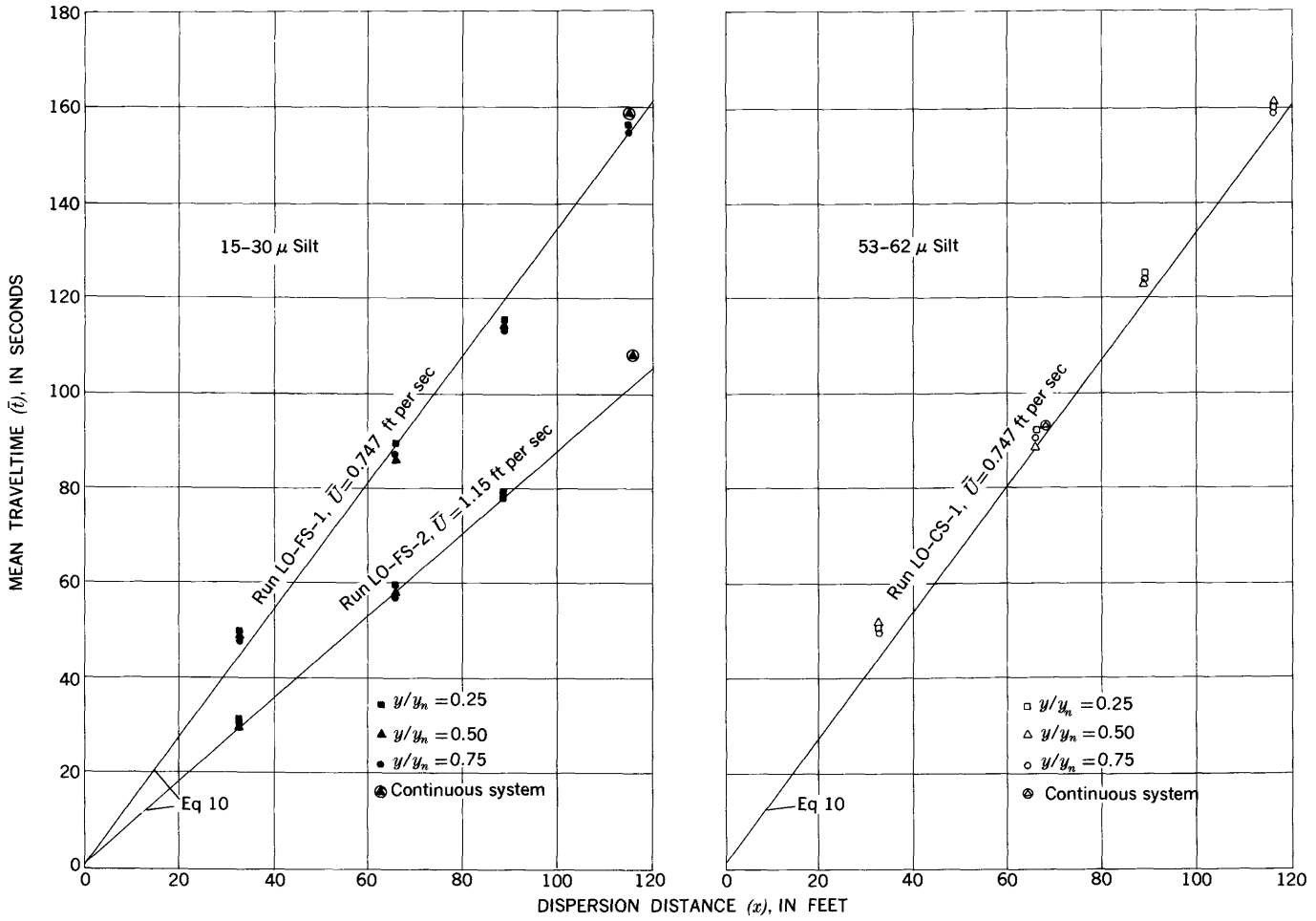

FIGURE 33.—Mean traveltime as a function of dispersion distance, longitudinal dispersion of natural silt.

LATERAL DISPERSION

DYE

The basic data in the LA–D series of experiments consisted of strip-chart recordings of fluorometer readings, which were obtained as the sampling nozzle was moved slowly across the flume. Event marks on the chart provided a record of the lateral position of the sampling nozzle. The data were corrected for the 4.8-second lag time of the sampling system, and lateral distribution curves were obtained by plotting fluorometer readings as a function of lateral displacement from the flume centerline. The traverse speed was slow enough so that no appreciable distortion of the curves was caused by mixing in the sampling tubes. The curves were smoothed somewhat to reduce the time fluctuating component of concentration, and they were normalized by dividing the ordinates by the area under the curve. The normalized lateral distribution curves are shown in figures 41, 42, and 43. Each figure shows all of the lateral dye distribution curves obtained for a particular flow condition. At each of the indicated dispersion distances, curves are given, in most cases, for the three sampling depths y/y_n=0.25, 0.50, and 0.75. The sampling depths are identified by the symbols defined in figure 41. For comparison, the theoretical lateral distribution function according to equations 14 and 18 is also shown. Use of equation 18 was necessary only when a significant amount of dye reached the flume walls and was reflected back toward the center. The values of K_z and K_x used in equation 14

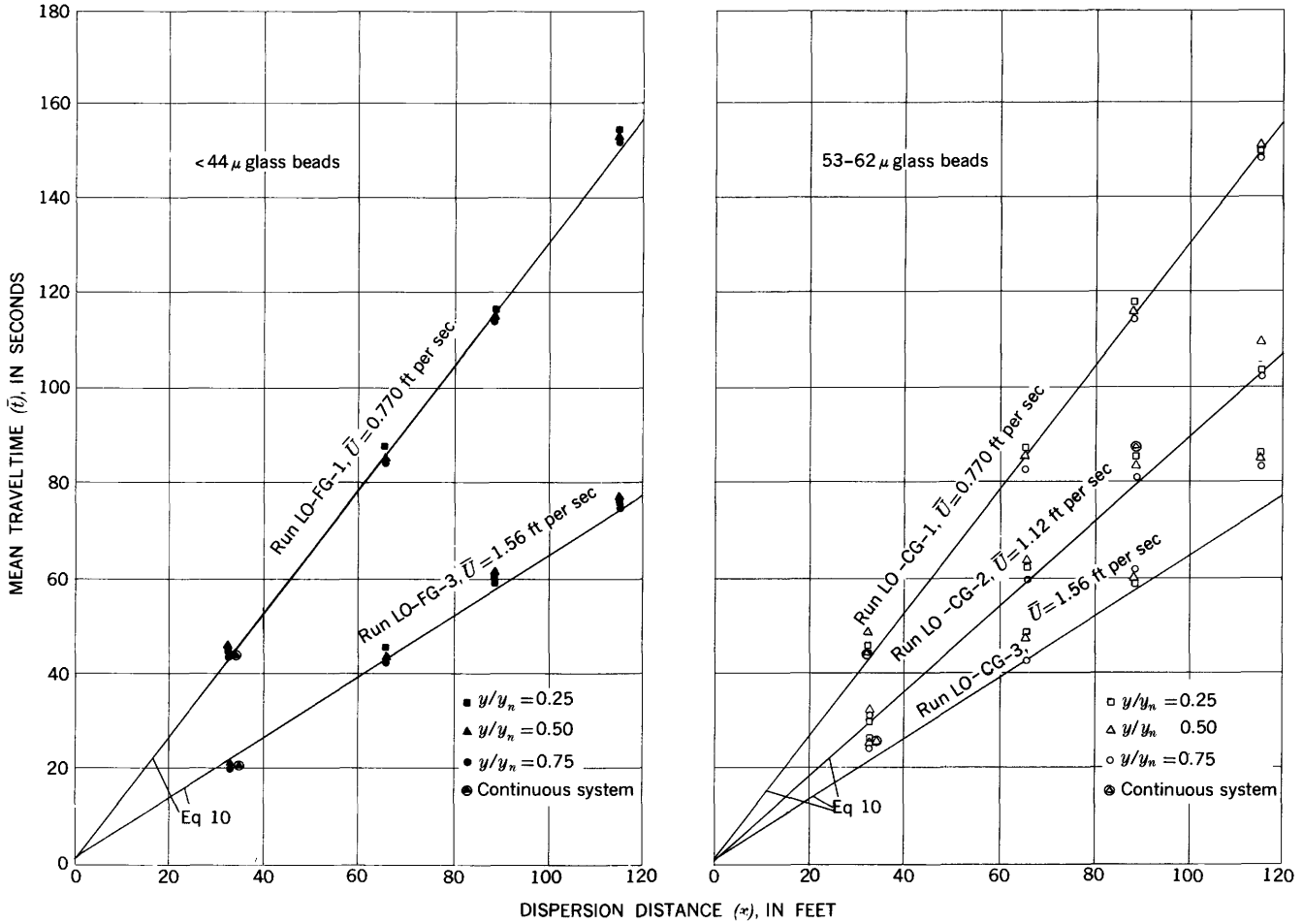

FIGURE 34.—Mean traveltime as a function of dispersion distance, longitudinal dispersion of silt-size glass beads.

were obtained respectively from the data in figure 44 and the results of the longitudinal dispersion experiments.

The data for the three sampling depths from runs LA–D–1 and LA–D–2 in general agree quite closely with one another and with equation 14, the agreement tending to improve with increasing dispersion distance. The data show that the degree of dispersion tends to increase somewhat with decreasing y/y_n. However, dispersion in the vertical direction tends to equalize the concentration in the vertical, thus largely masking the effect of variation in lateral diffusivity with depth. The data for run LA–D–3 show a consistent drift to the left at the relative depths y/y_n=0.25 and 0.50 and a drift to the right at y/y_n=0.75.

In figure 44 the estimated variances of the lateral distribution curves are shown as functions of dispersion distance. Because the main purpose for determining the variances was to evaluate the lateral dispersion coefficient, K_z, as a function of flow conditions in a two-dimensional flow field, it was necessary to determine the variances which would have occurred without the confining influence of the sidewalls. Therefore σ_z^2 was not calculated by the method of moments but from the relationship

$$\sigma_z^2=\frac{1}{2\pi[f(z;\,x)_{\max}]^2}, \tag{56}$$

which follows directly from the normal probability law. In equation 56, $f(z;\,x)_{\max}$ is the peak observed relative concentration. Whereas values of σ_z^2 computed by the method of moments are affected by the sidewalls as soon as an appreciable amount of dispersant reaches the walls, values of σ_z^2 computed by equation 56 are not affected until a significant quantity of the dispersant, which is reflected back from the walls, actually reaches the centerline.

Lateral dispersion coefficients were evaluated from the data in figure 44 by means of the relationship

$$K_z=\frac{\bar{U}}{2}\frac{d\sigma_z^2}{dx}. \tag{57}$$

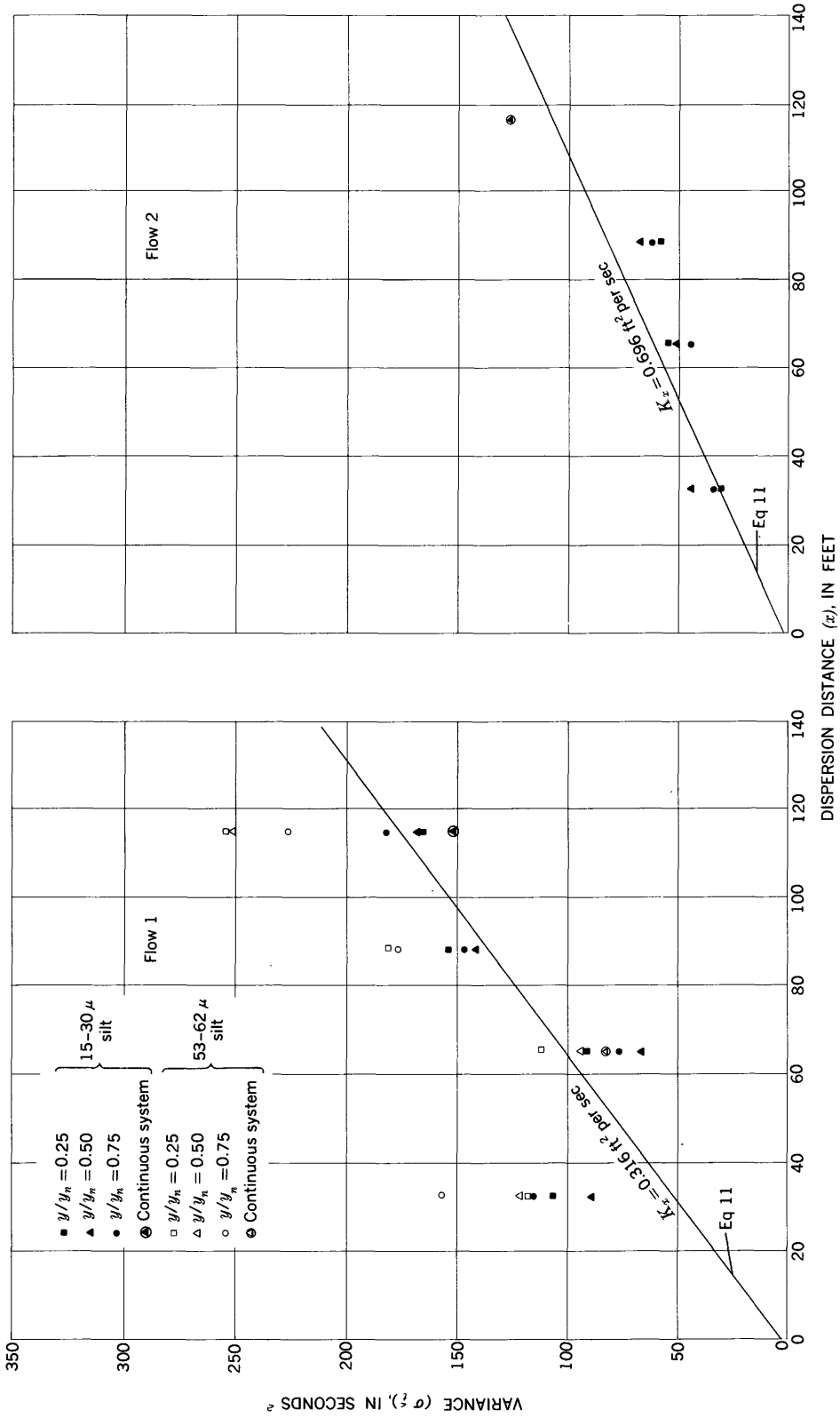

FIGURE 35.—Variance of traveltime as a function of dispersion distance, longitudinal dispersion of natural silt.

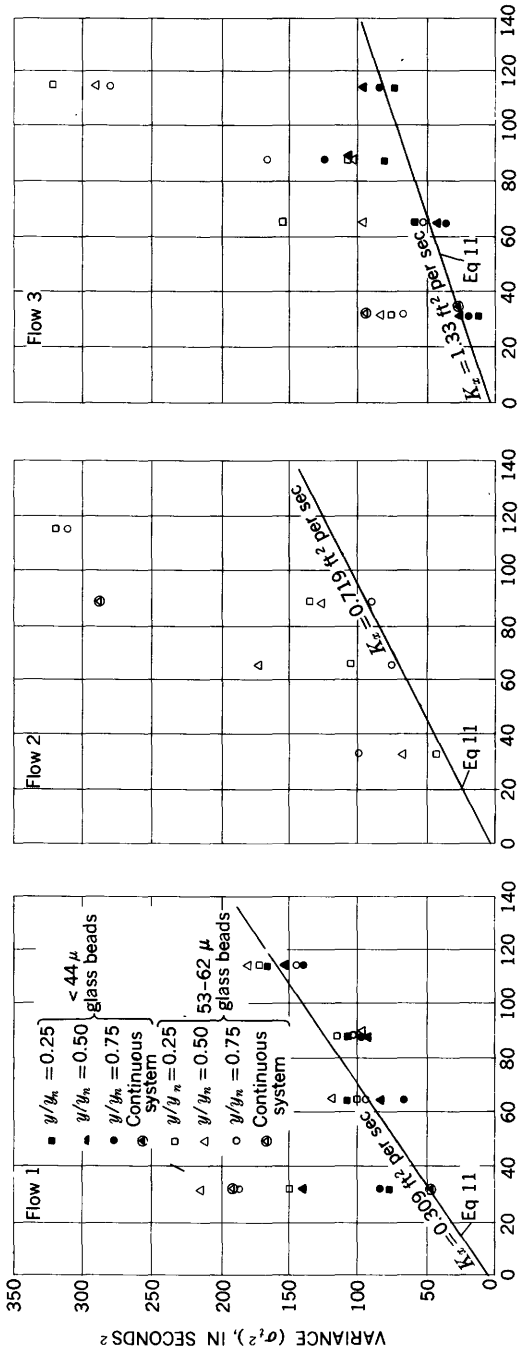

FIGURE 36.—Variance of traveltime as a function of dispersion distance, longitudinal dispersion of silt-size glass beads.

TABLE 4.—*Longitudinal dispersion of silt-size particles: summary of data*

[Boldface indicates continuous system]

Run (LO-)	x (ft)	y/y_n	W (gm)	F (fluorometer unit per ppm)	A_t (ppm-sec)	A_m (ppm-sec)	$\bar{t}$ (sec)	σ^2_t (sec^2)	$f(t;x)_{max}$ (sec^{-1})
FS-1	32.8	0.25	283	0.24	3,460	4,880	49.6	107	0.0555
		.50	283	.24	3,460	4,900	48.3	90	.0595
		.75	283	.24	3,460	4,430	48.9	116	.0610
	65.6	.25	283	.24	3,460	4,230	89.7	92	.0440
		.50	283	.24	3,460	3,570	86.8	68	.0515
		.75	283	.24	3,460	3,930	87.2	78	.0500
	88.5	.25	283	.24	3,460	3,940	115.4	154	.0310
		.50	283	.24	3,460	3,910	114.5	144	.0320
		.75	283	.24	3,460	3,760	114.1	148	.0305
	115.0	.25	283	.24	3,460	2,920	156.0	165	.0295
		.50	283	.24	3,460	3,020	155.8	168	.0320
		.75	283	.24	3,460	3,330	155.2	183	.0290
		.50	**283**	**.24**	**3,460**	**3,160**	**159.7**	**150**	**.0305**
2	32.8	.25	830	.24	4,080	4,640	31.3	31	.0730
		.50	830	.24	4,080	4,580	30.4	44	.0700
		.75	830	.24	4,080	4,940	30.2	34	.0860
	65.6	.25	830	.24	4,080	4,610	59.4	55	.0520
		.50	830	.24	4,080	4,350	57.8	50	.0530
		.75	830	.24	4,080	3,980	57.0	45	.0585
	88.5	.25	830	.24	4,080	3,910	79.1	58	.0455
		.50	830	.24	4,080	3,960	77.9	68	.0445
		.75	830	.24	4,080	3,850	77.9	63	.0475
	115.0	**.50**	**830**	**.24**	**4,080**	**4,580**	**107.5**	**125**	**.0385**
CS-1	32.8	.25	646	.069	7,920	11,400	51.1	118	.0445
		.50	646	.069	7,920	11,700	51.2	122	.0405
		.75	646	.069	7,920	10,600	50.9	156	.0445
	65.6	.25	646	.069	7,920	7,840	93.0	110	.0365
		.50	646	.069	7,920	7,390	89.1	92	.0395
		.75	646	.069	7,920	7,910	91.0	109	.0370
		.50	**646**	**.069**	**7,920**	**7,930**	**93.1**	**81**	**.0410**
	88.5	.25	646	.069	7,920	8,100	125.4	179	.0345
		.50	646	.069	7,920	7,130	123.8	147	.0325
		.75	646	.069	7,920	7,880	124.1	176	.0290
	115.0	.25	646	.069	7,920	6,200	160.5	253	.0255
		.50	646	.069	7,920	6,520	160.9	253	.0255
		.75	646	.069	7,920	6,000	159.2	226	.0280
FG-1	32.8	.25	750	.150	9,040	6,870	45.6	79	.0558
		.50	750	.150	9,040	6,470	46.3	143	.0567
		.75	750	.150	9,040	6,540	43.9	81	.0632
		.50	**750**	**.170**	**9,040**	**5,930**	**43.2**	**45**	**.0614**
	65.6	.25	750	.150	9,040	7,000	88.5	104	.0444
		.50	750	.150	9,040	6,190	86.3	83	.0447
		.75	750	.150	9,040	6,320	84.7	66	.0458
	88.5	.25	750	.150	9,040	4,860	117.5	105	.0392
		.50	750	.150	9,040	4,920	116.4	96	.0407
		.75	750	.150	9,040	5,000	116.0	95	.0427
	115.0	.25	750	.405	9,040	4,940	155.2	167	.0325
		.50	750	.405	9,040	4,940	153.7	153	.0329
		.75	750	.405	9,040	4,970	153.1	142	.0332
3	32.8	.25	2,500	.150	5,930	4,700	21.3	21	.108
		.50	2,500	.150	5,930	4,400	21.1	26	.113
		.75	2,500	.150	5,930	3,860	20.6	24	.122
		.50	**2,500**	**.170**	**5,930**	**5,270**	**20.8**	**27**	**.0977**
	65.6	.25	2,500	.150	5,930	4,526	45.4	59	.0546
		.50	2,500	.150	5,930	4,270	43.9	44	.0602
		.75	2,500	.150	5,930	4,130	42.3	38	.0646
	88.5	.25	2,500	.150	5,930	4,380	59.2	82	.0511
		.50	2,500	.150	5,930	4,470	61.0	106	.0471
		.75	2,500	.150	5,930	3,970	61.3	126	.0497
	115.0	.25	2,500	.150	5,930	4,540	76.0	76	.0426
		.50	2,500	.150	5,930	4,400	77.1	99	.0402
		.75	2,500	.150	5,930	4,200	75.9	85	.0452
CG-1	32.8	.25	1,533	.074	18,500	8,950	49.1	149	.0529
		.50	1,533	.074	18,500	8,610	49.1	215	.0557
		.75	1,533	.074	18,500	8,420	46.7	188	.0546
		.66	**1,533**	**.085**	**18,500**	**10,400**	**46.1**	**189**	**.0520**
	65.6	.25	1,533	.074	18,500	5,430	88.0	99	.0437
		.50	1,533	.074	18,500	5,410	86.6	115	.0404
		.75	1,533	.074	18,500	4,600	83.7	93	.0434
	88.5	.25	1,533	.174	18,500	4,070	118.7	113	.0436
		.50	1,533	.174	18,500	4,080	116.2	96	.0396
		.75	1,533	.174	18,500	4,050	115.6	103	.0418
	115.0	.25	1,533	.174	18,500	3,360	150.9	170	.0308
		.50	1,533	.174	18,500	3,310	151.3	178	.0321
		.75	1,533	.174	18,500	3,250	149.8	142	.0349
2	32.8	.25	2,070	.059	10,300	11,100	31.0	43	.0650
		.50	2,070	.059	10,300	13,700	33.0	67	.0650
		.75	2,070	.059	10,300	10,700	32.2	99	.0500
	65.6	.25	2,070	.059	10,300	5,430	63.1	106	.0530
		.50	2,070	.059	10,300	5,660	64.1	173	.0495
		.75	2,070	.059	10,300	5,700	60.5	75	.0530
	88.5	.25	2,070	.205	10,300	5,630	86.3	135	.0425
		.50	2,070	.205	10,300	5,170	84.6	128	.0460
		.75	2,070	.205	10,300	5,000	81.9	92	.0500
		.50	**2,070**	**.082**	**10,300**	**7,030**	**88.4**	**286**	**.0390**
	115.0	.25	2,070	.205	10,300	6,540	104.4	320	.0325
		.50	2,070	.205	10,300	6,550	111.0	404	.0215
		.75	2,070	.205	10,300	6,380	103.3	313	.0315

See footnote at end of table.

TABLE 4.—*Longitudinal dispersion of silt-size particles: summary of data*—Continued

Run (LO–)	x (ft)	y/y_n	W (gm)	F (fluorometer unit per ppm)	A_t (ppm-sec)	A_m (ppm-sec)	$\bar{t}$ (sec)	σ^2_t (sec²)	$f(t;x)_{max}$ (sec⁻¹)
CG-3	32.8	0.25	5,000	0.074	11,850	12,700	26.5	79	0.0595
		.50	5,000	.074	11,850	8,970	25.8	84	.0617
		.75	5,000	.074	11,850	6,980	25.0	68	.0813
		.50	5,000	.085	11,850	12,600	26.3	96	.0766
	65.6	.25	5,000	.074	11,850	11,400	49.4	155	.0427
		.50	5,000	.074	11,850	8,830	48.0	98	.0459
		.75	5,000	.074	11,850	8,490	43.2	55	.0525
	88.5	.25	5,000	.074	11,850	9,080	59.9	106	.0402
		.50	5,000	.074	11,850	8,210	60.4	105	.0437
		.75	5,000	.074	11,850	6,890	62.6	167	.0442
	115.0	.25	5,000	.174	11,850	10,700	87.0	321	.0279
		.50	5,000	.174	11,850	10,600	86.1	290	.0276
		.75	5,000	.174	11,850	10,400	84.1	281	.0318

[1] Continuous system.

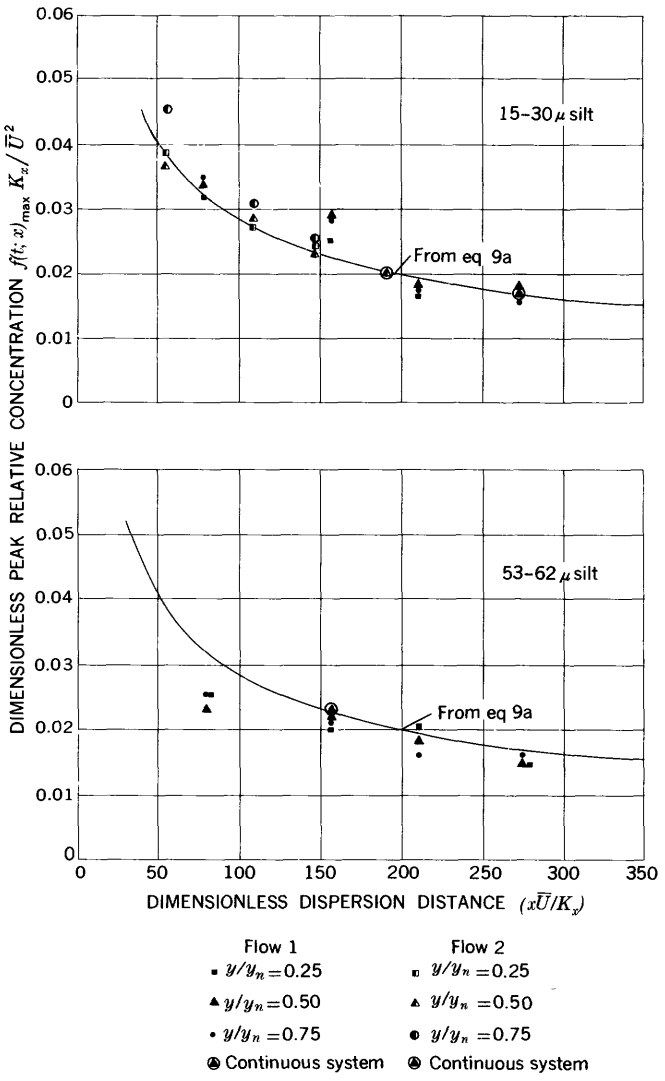

FIGURE 37.—Dimensionless peak relative concentration as a function of dimensionless dispersion distance, longitudinal dispersion of natural silt.

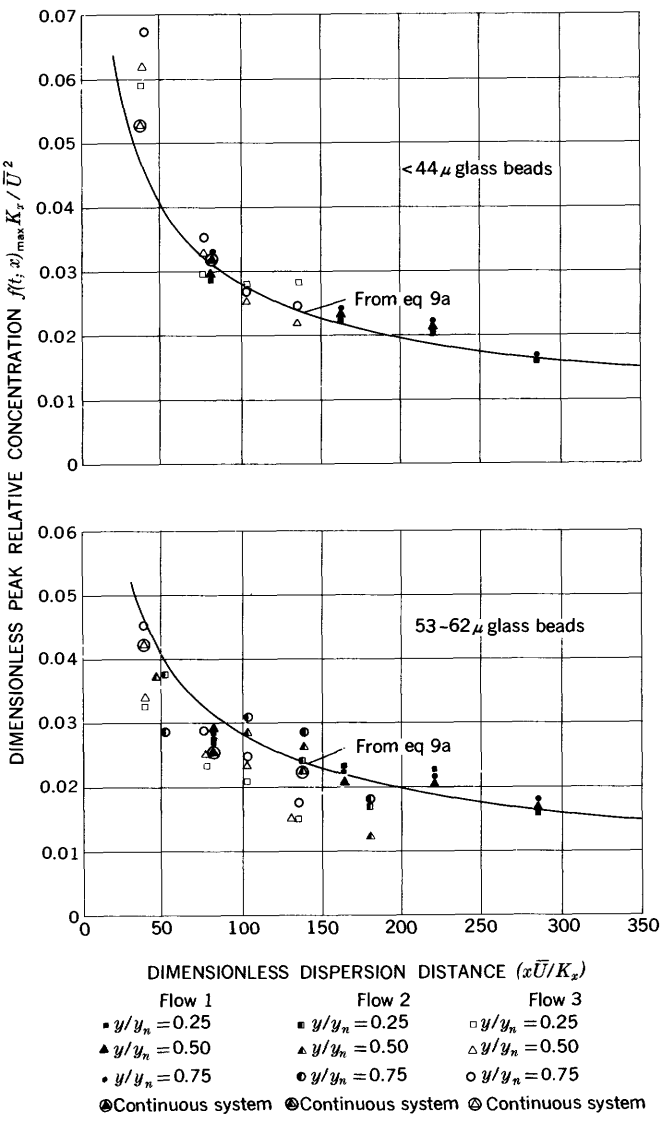

FIGURE 38.—Dimensionless peak relative concentration as a function of dimensionless dispersion distance, longitudinal dispersion of silt-size glass beads.

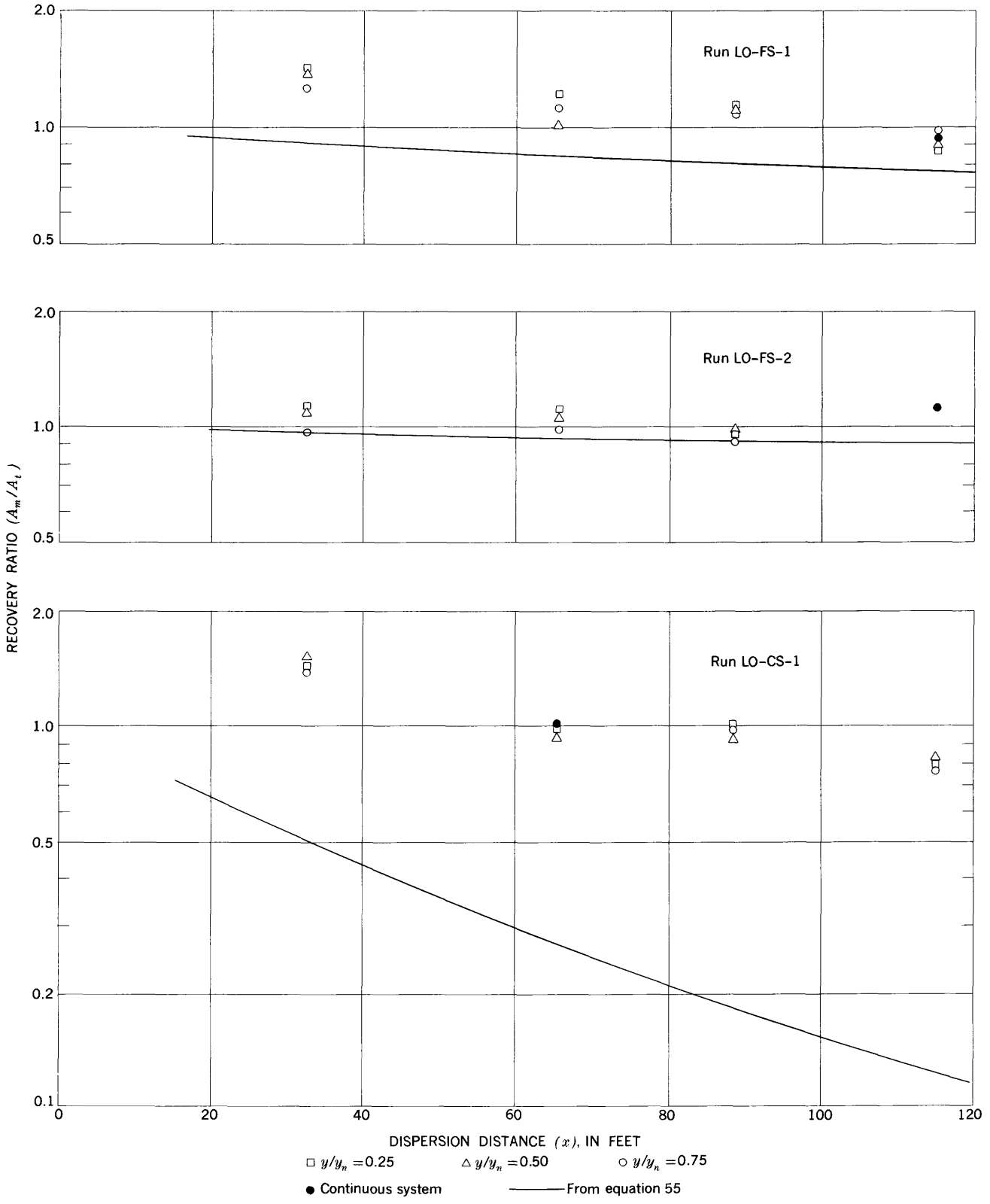

FIGURE 39.—Recovery ratio for area under concentration versus time curves as a function of dispersion distance, longitudinal dispersion of natural silt.

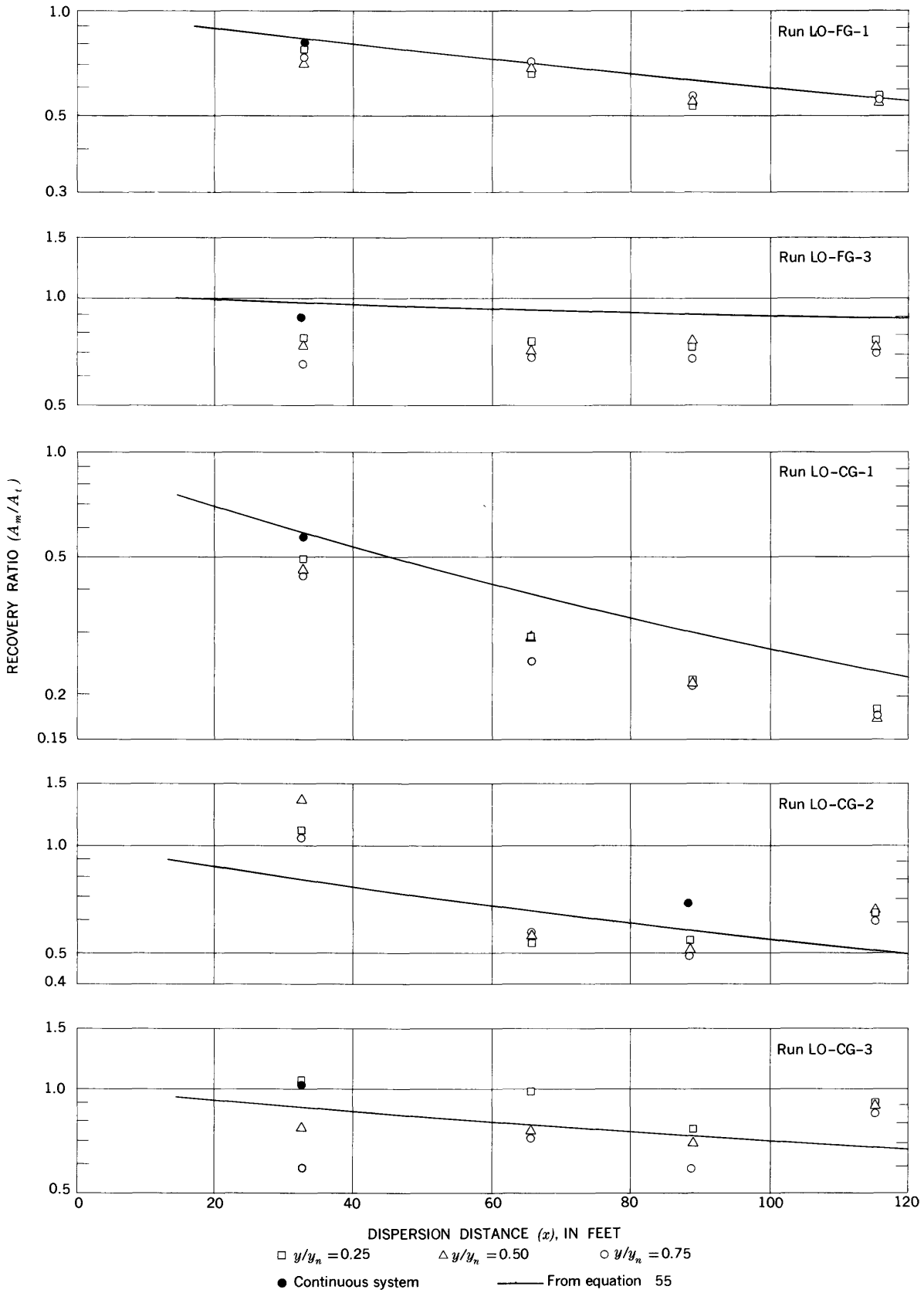

FIGURE 40.—Recovery ratio for area under concentration versus time curves as a function of dispersion distance, longitudinal dispersion of silt-size glass beads.

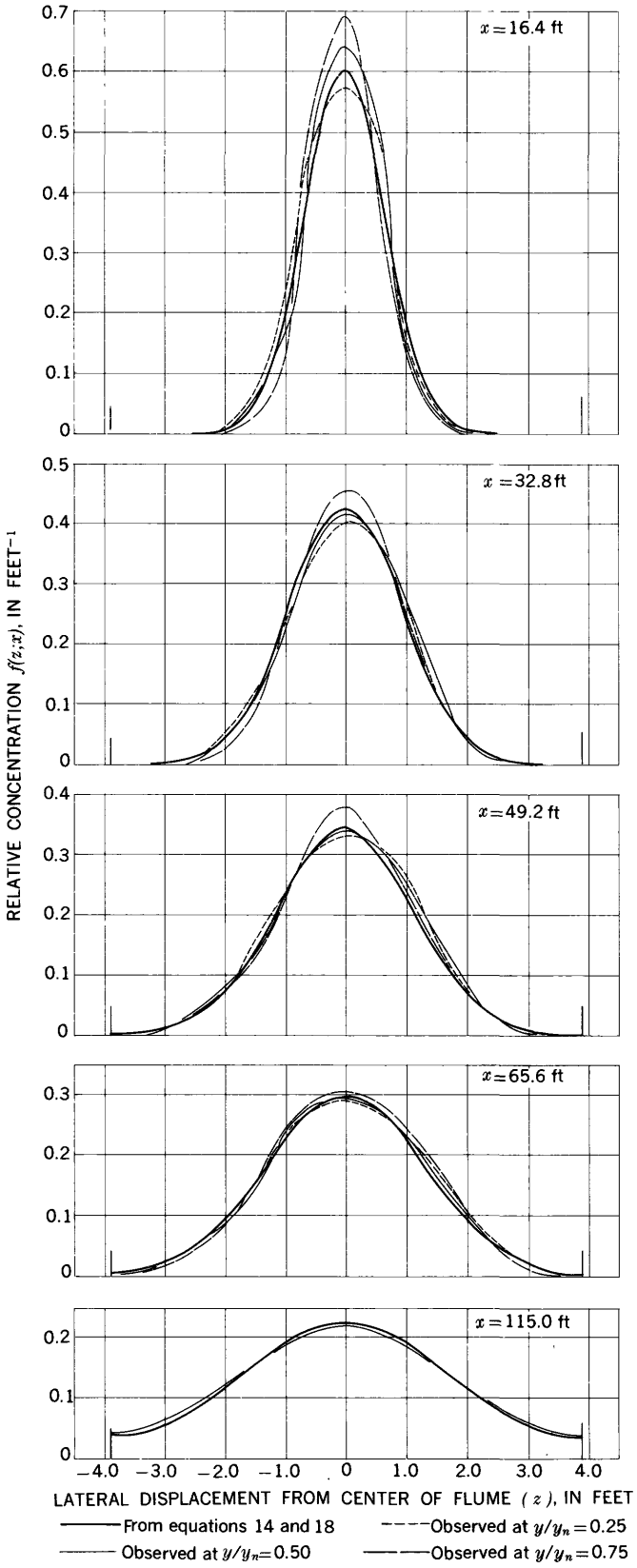

FIGURE 41.—Lateral distribution of dye at various depths and dispersion distances in run LA-D-1.

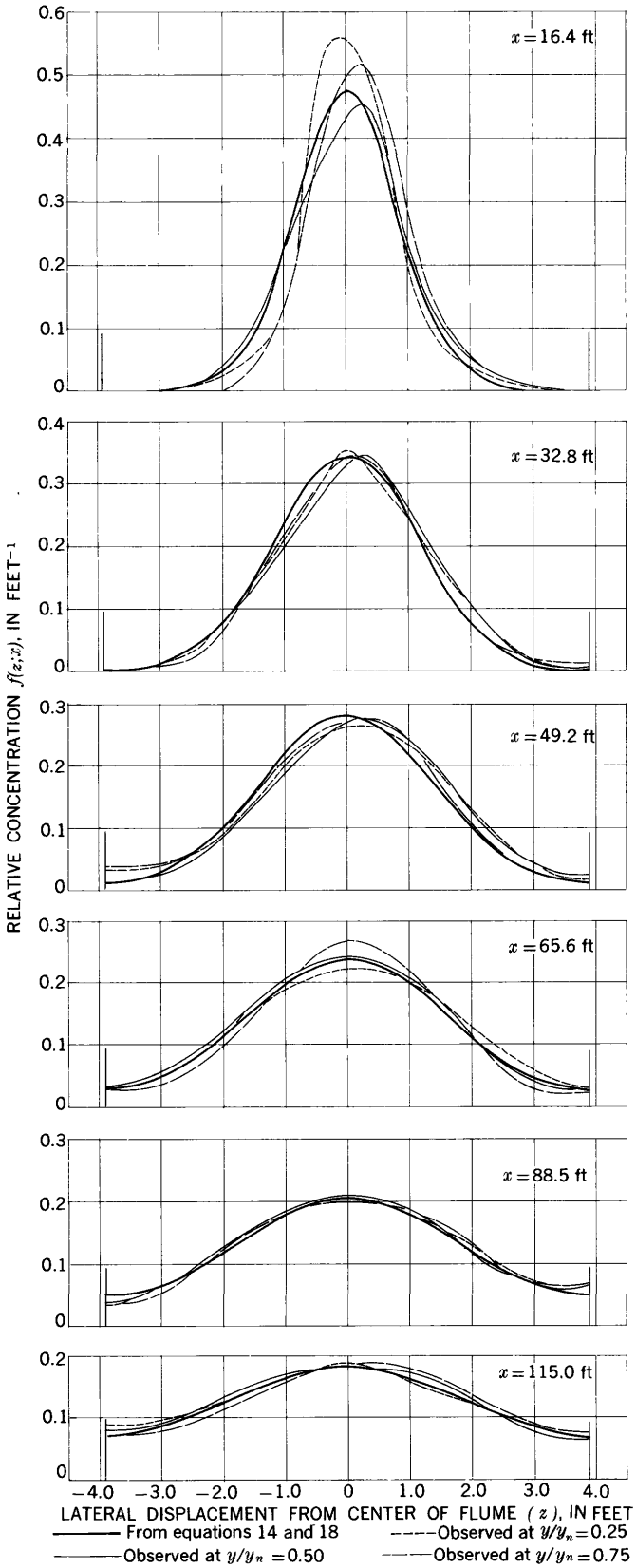

FIGURE 42.—Lateral distribution of dye at various depths and dispersion distances in run LA-D-2.

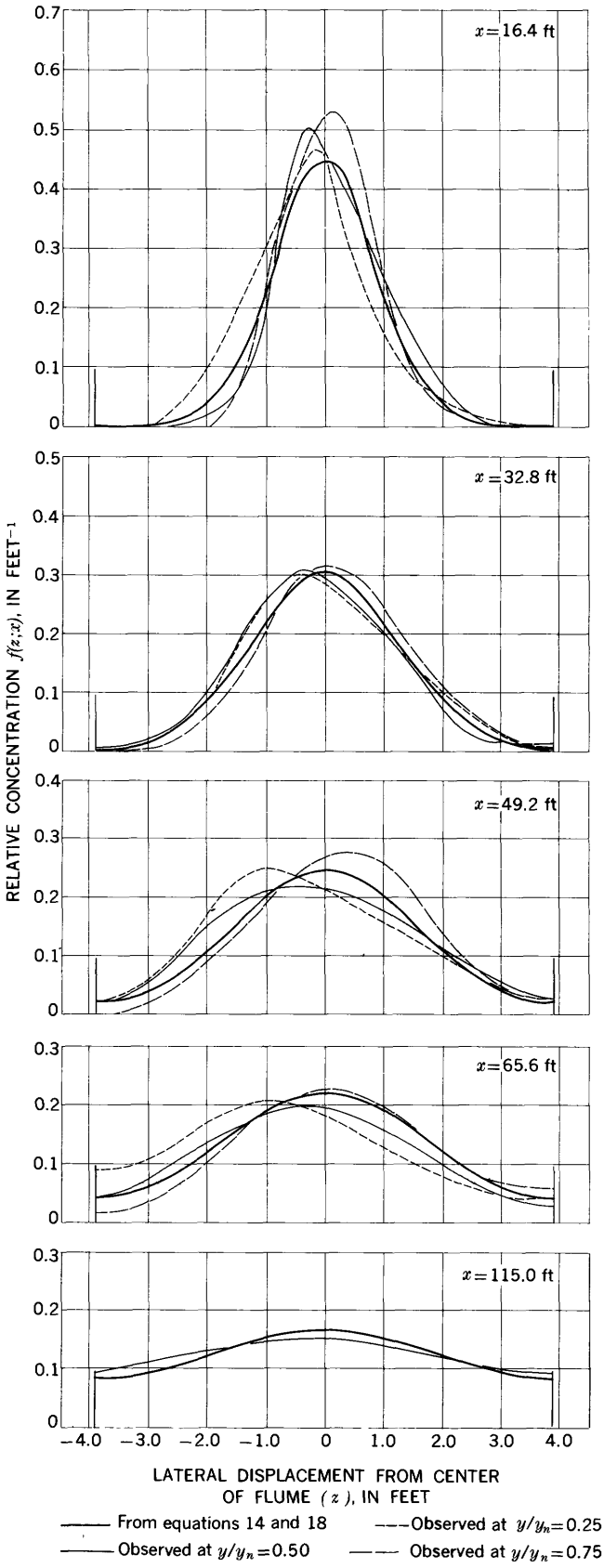

FIGURE 43.—Lateral distribution of dye at various depths and dispersion distances in run LA-D-3.

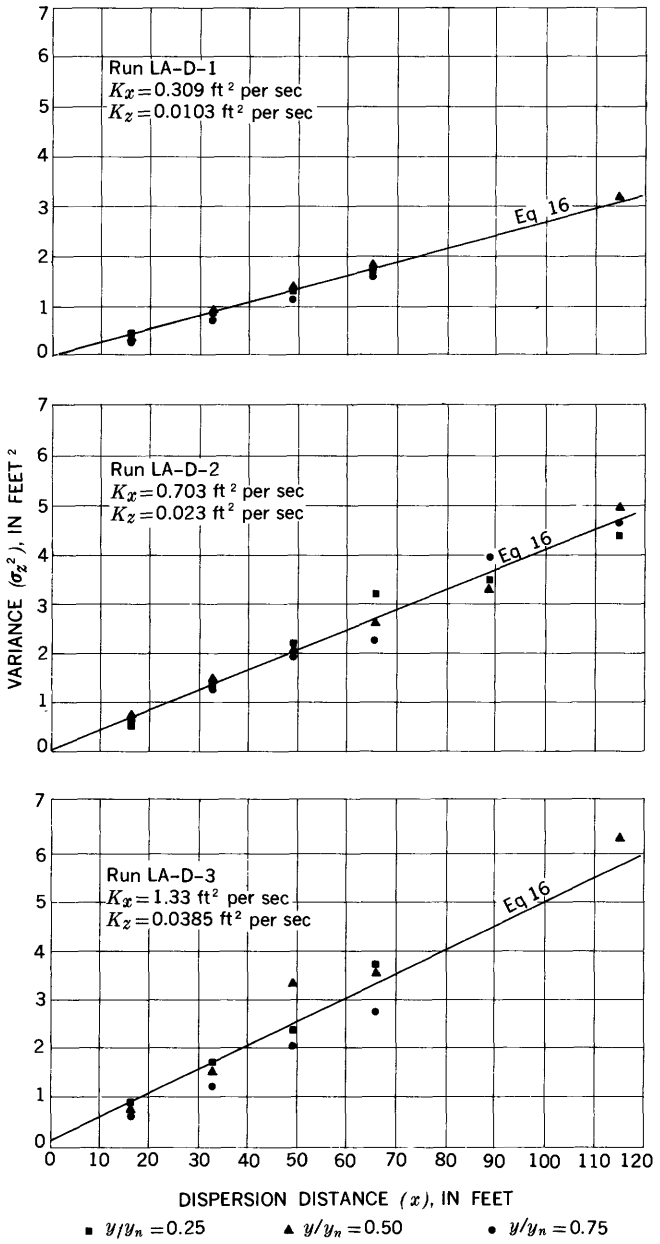

FIGURE 44.—Estimated variance of lateral displacement as a function of dispersion distance, lateral dispersion of dye.

The range of x within which equation 57 gives the desired lateral dispersion coefficient is limited at the lower end by the distance required to obtain uniform vertical distribution and at the upper end by the distance at which reflections from the channel sides begin to have an appreciable effect. The σ_z^2 versus x relationships are quite well represented by equation 16 from Fickian diffusion theory for the indicated values of K_z and K_x. As with the silt dispersion experiments, values of K_x were adjusted where necessary to compensate for the slight differences in $y_n U_\tau$ that existed between the

flow conditions for the lateral dispersion experiments and the corresponding longitudinal dispersion experiments.

The fact that the linearity of the σ_z^2 versus x relationship, as defined by the data, extends nearly back to the source indicates that convergence of the lateral dispersion process to the Fickian model is very rapid. This means that the region within which the process depends on the Lagrangian correlation coefficient is confined to very short dispersion distances.

Although equation 16 applies reasonably well to the data obtained at all three sampling depths, the data in figure 44 indicate a correlation between σ_z^2 and y/y_n that is consistent with the observations made in discussing the characteristics of the lateral distribution curves. According to these observations, the values of σ_z^2 obtained at a particular dispersion distance should be arranged in descending order with increasing y/y_n. The anticipated order occurs six times out of 14 sets of observations, whereas with random ordering it would occur only one out of six times.

Recovery ratio data for the lateral dispersion experiments is given in figure 45. For lateral dispersion from a continuous point source the recovery ratio is

$$\frac{A_m}{A_t}=\frac{(A_m'/F)\alpha}{35.3BC_0q/Q} \tag{58}$$

where B is the width of the flume, in feet, q is the discharge rate of dye at the source, in milliliters per second, C_0 is the initial concentration of dye at the source, in grams per liter, α is a correction factor for nonuniform distribution of flow across the channel, and the other variables are as defined in equation 51. The correction factor α is given by the formula

$$\alpha=\frac{1}{\bar{C}Q}\int_{-B/2}^{B/2}C(z)q(z)dz$$

where $C(z)$ is the local concentration, $\bar{C}$ is the average concentration across the width of the channel, and $q(z)$ is the local water discharge per unit of channel width. From the velocity distribution measurements it was determined that α should have remained within the range $1\leq\alpha\leq1.03$ in the experiments. In the calculations for figure 45 the correction was neglected, and it was assumed that $\alpha=1$.

In addition to the random error in figure 45, there appears to be a systematic error of approximately plus 10 percent. The systematic error is almost certainly due to a temperature difference between the dye solution flowing from the source and the flume water which was used for establishing the discharge rate of the source prior to each run. The temperature of the dye solution, which was not recorded, varied from that of the flume water up to room temperature, depending on how long the dye solution was permitted to stand before use. In most of the experiments the room temperature was on the order of 10°C higher than that of the flume water. Because the flow in the tube leading from the dye reservoir to the source was laminar, the temperature difference was sufficient to cause a significant increase in the actual discharge rate of the dye solution over the discharge rate of the flume water which had been used for measuring q. Therefore, the values of q used in equation 58 were too low. Inclusion of the correction factor α, for nonuniform distribution of flow, would have tended to increase the values of A_m/A_t still more.

In order to verify further the applicability of the reflecting barrier concept, two experimental lateral distribution curves were obtained with the source displaced 2 feet to the right of the centerline. These are shown as the dashed curves in figure 46. The solid curves, which are shown for comparison, were determined from the reflecting barrier equation (18) together with equation 14.

The data from the lateral dispersion experiments with dye are summarized in table 5.

POLYETHYLENE PARTICLES

The lateral dispersion data for polyethylene particles was analyzed in much the same manner, and with essentially the same assumptions, as the longitudinal dispersion data for polyethylene particles. The width of the flume was divided into 9-centimeter increments; the number of particles in each increment was counted, and the relative frequency of occupancy,

$$f(z_j;x)=\frac{n_j}{N\Delta z_j}, \tag{59}$$

was calculated for each increment. Equation 59 is entirely analagous to equation 52. The relative frequencies were plotted in the form of histograms as shown in the example given in figure 47. Also shown in figure 47 for comparison is the lateral distribution function according to equations 14 and 18 with the values of K_z and K_x taken from the results of the dye dispersion experiments for the same flow condition.

The example given in figure 47 is quite typical in that the dispersion pattern of the polyethylene particles is only very roughly approximated by the theoretical function. Also, the multimodal pattern of the histogram is fairly typical as is the tendency of the particles to keep away from the sidewalls. Both these characteristics suggest the existence of the multicellular type of secondary circulation described by Nemenyi (1946), in which there are one or more vortex pairs with longitudinal axes distributed across the channel. The members

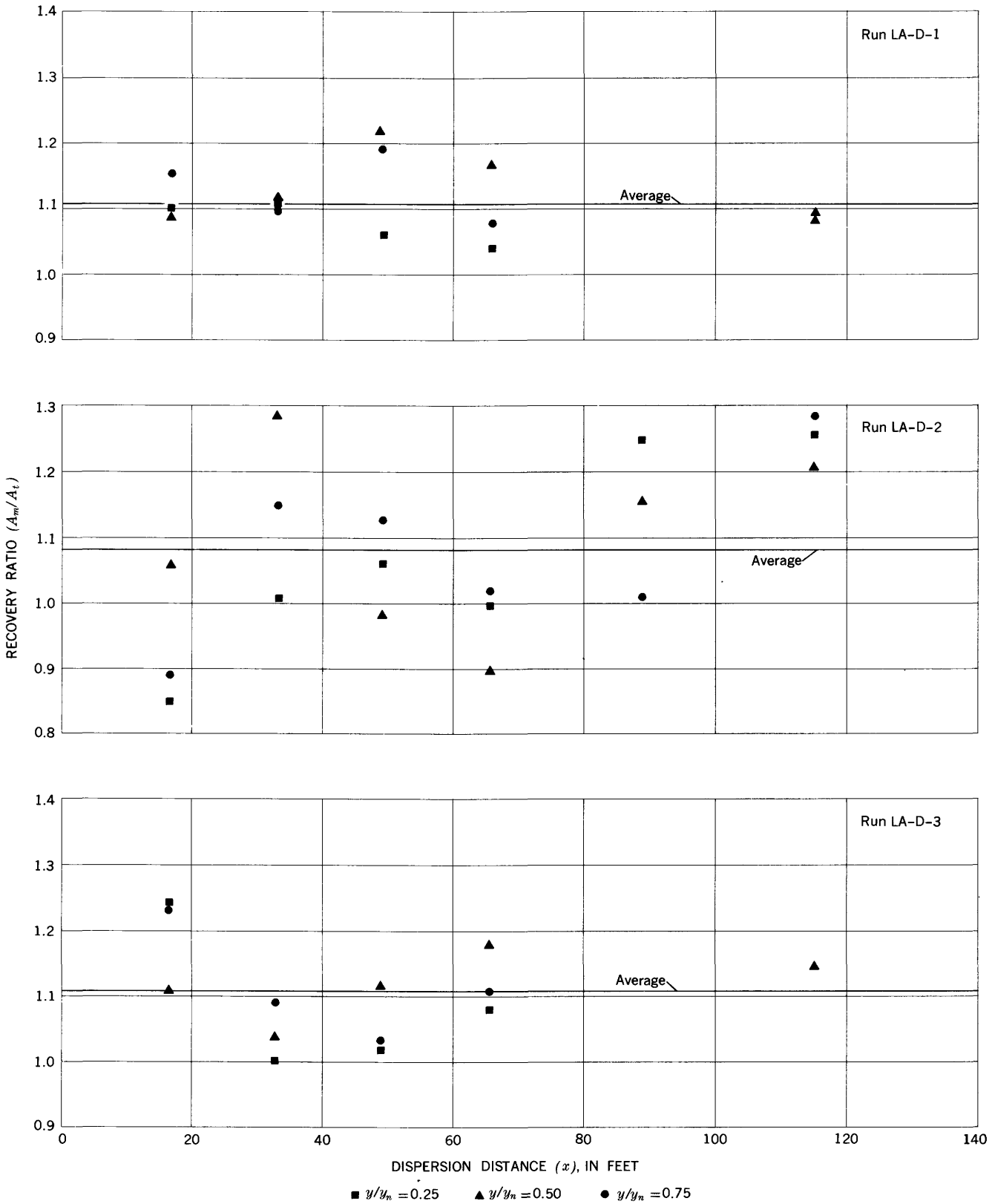

FIGURE 45.—Recovery ratio for area under lateral-distribution curves as a function of dispersion distance, lateral dispersion of dye.

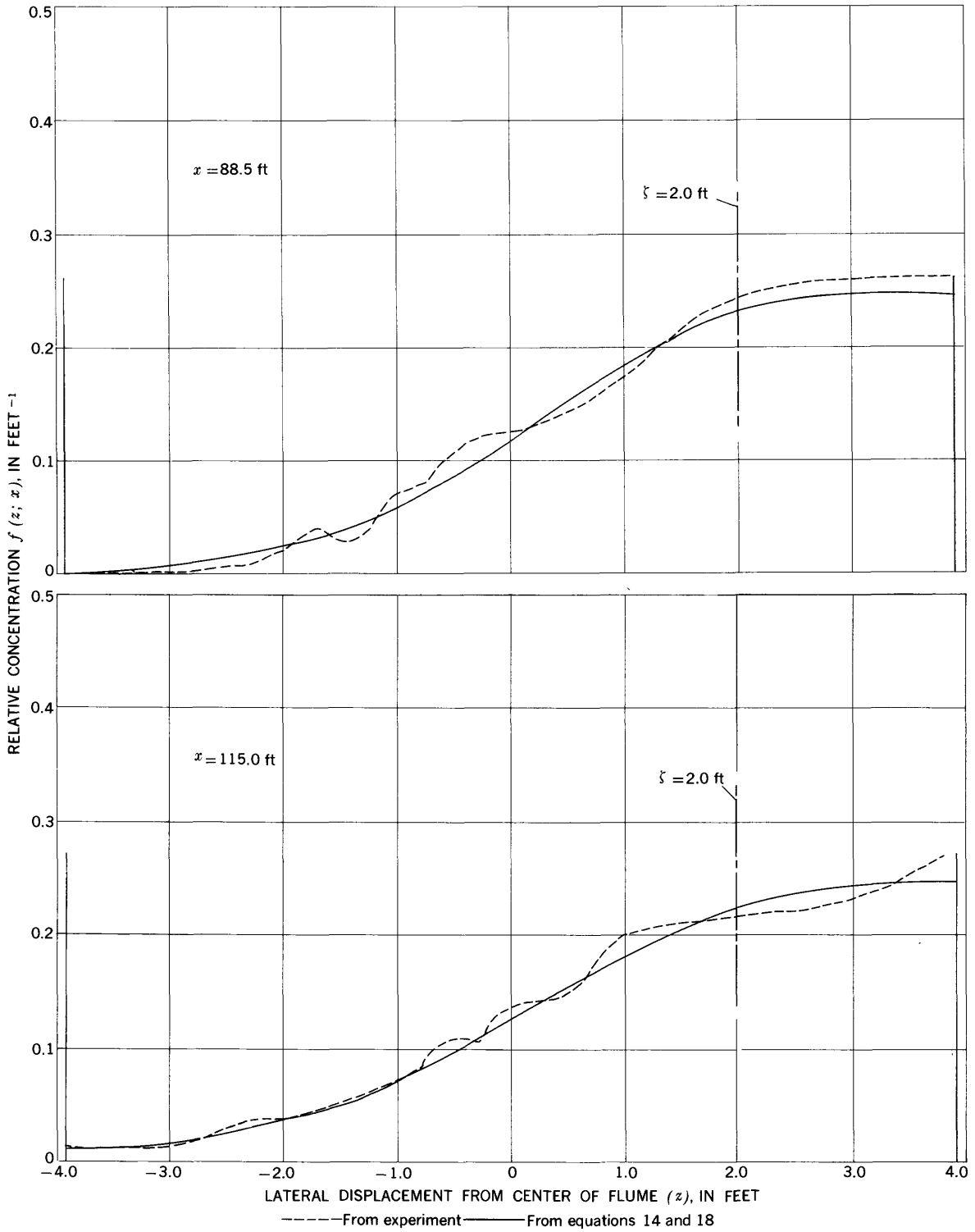

FIGURE 46.—Lateral distribution of dye for eccentrically located source. Run LA-D-2, K_z=0.719 ft^2 per sec, K_x=0.023 ft^2 per sec.

TABLE 5.—*Lateral dispersion of dye: summary of data*

Run (LA-D-)	x (ft)	y/y_n	C_0 (gm per liter)	q (ml per sec)	F (fluorometer units per ppb)	A_t (ppb-ft)	A_m (ppb-ft)	$f(z;x)_{max}$ (ft^{-1})	σ^2_z (ft^2)
1	16.4	0.25	0.10	1.31	6.60	12.4	13.6	0.575	0.47
		.50	.10	1.91	6.60	18.0	19.6	.642	.37
		.75	.10	1.91	6.60	18.0	20.7	.692	.34
	32.8	.25	.10	1.31	6.50	12.4	13.8	.404	.85
		.50	.10	1.91	6.65	18.0	20.2	.415	.91
		.75	.10	1.91	6.65	18.0	19.6	.455	.72
	49.2	.25	.15	1.44	6.50	20.4	21.6	.330	1.32
		.50	.15	1.93	6.45	27.3	33.2	.339	1.37
		.75	.15	2.03	6.60	28.6	35.2	.382	1.12
	65.6	.25	.15	1.44	6.55	20.3	21.1	.289	1.75
		.50	.15	1.93	6.55	27.3	32.0	.295	1.80
		.75	.15	2.03	6.80	28.6	32.1	.304	1.72
	115.0	.50	.25	2.29	6.75	53.8	60.2	.222	3.05
		.50	.25	1.95	6.85	45.8	51.5	.229	3.16
2 [1]	16.4	.25	.66	2.30	2.80	58.9	50.0	.560	.52
		.50	.38	3.02	2.68	44.8	47.4	.455	.77
		.75	.38	3.44	2.68	50.8	45.2	.520	.51
(1)	32.8	.25	.90	2.30	2.74	80.3	81.3	.354	1.39
		.50	.57	3.02	2.66	66.6	86.0	.347	1.52
		.75	.57	3.44	2.64	76.2	87.5	.346	1.36
(1)	49.2	.25	.90	2.30	2.68	80.6	85.5	.267	2.22
		.50	.67	3.02	2.56	78.1	76.2	.276	2.06
		.75	.67	3.44	2.68	89.2	101.2	.277	1.94
(1)	65.6	.25	1.30	2.30	2.76	116.0	115.6	.225	3.23
		.50	.67	3.02	2.60	78.5	70.8	.245	2.64
		.75	.67	3.44	2.72	89.0	91.0	.270	2.28
(2)	88.5	.25	.333	2.40	7.90	31.1	38.8	.202	3.50
		.50	.333	3.05	8.20	39.6	46.0	.209	3.34
		.75	.333	3.35	8.50	43.5	44.1	.200	3.99
(2)	115.0	.25	.333	2.40	7.80	31.1	39.2	.188	4.43
		.50	.333	3.05	8.40	39.6	48.1	.182	4.98
		.75	.333	3.35	8.10	43.5	56.0	.187	4.66
3	16.4	.25	.250	3.21	6.60	14.8	18.3	.467	.87
		.50	.250	4.13	6.55	19.1	21.2	.505	.71
		.75	.250	4.60	6.75	21.3	26.2	.532	.64
	32.8	.25	.350	3.24	6.50	20.9	22.1	.302	1.67
		.50	.350	4.11	6.70	26.7	27.8	.310	1.55
		.75	.350	4.61	6.95	29.8	32.6	.317	1.21
	49.2	.25	.500	3.24	6.95	30.0	30.5	.250	2.38
		.50	.500	4.11	6.80	38.2	42.6	.218	3.33
		.75	.500	4.50	6.70	41.7	43.1	.275	2.02
	65.6	.25	.600	3.10	6.80	34.4	37.3	.207	3.70
		.50	.600	4.08	6.85	45.4	53.4	.199	3.55
		.75	.600	4.60	6.75	51.2	56.7	.227	2.76
	115.0	.50	.500	4.15	6.90	38.6	44.4	.155	6.35

[1] y_n=0.803 ft.
[2] y_n=0.814 ft.

of each pair rotate in opposite directions. The sense of rotation is such that the direction of secondary flow is away from the sidewalls at the water surface. At those regions across the channel toward which the secondary flows converge at the water surface, the particles tend to become concentrated, accounting for the multiple modes. No doubt this type of secondary circulation existed also in the lateral dye dispersion experiments; however, its effects would have been masked by the mass exchange, due to turbulence, occurring between different levels in the flow field.

The variances of the lateral distributions of particles are plotted as a function of dispersion distance in figure 48. Because of the irregularity of the distribution histograms, the variances were calculated by the method of moments rather than by the peak relative concentration method used in analyzing the results of the lateral dispersion experiments with dye or the cumulative probability paper method introduced by Orlob (1958) for polyethylene particles. The time intervals between successive particle releases for each set of data are identified by the symbols as defined in figure 48. No consistent effect of time interval duration is detectable. Shown for the sake of comparison with the data are the theoretical σ^2_z versus x relationships corresponding to the lateral distribution functions, with and without sidewall effects, for the values of the dispersion coefficients obtained from the dye dispersion experiments. The dashed curves were taken directly from figure 44. The solid curves were determined by calculating the variances of the theoretical lateral distribution curves in figures 41, 42, and 43 that had been corrected for sidewall effect. Since the values of σ^2_z determined from the data were calculated by the method of moments, which is immediately sensitive to sidewall effect, they tend to follow the solid curve. It is significant that the lateral dispersion at the water surface, as indicated by the variances of the polyethylene particle distributions, tends to follow quite closely the pattern within the flow as established from the dye experiments. The tendency of the particle data to lie slightly below the curve may be due to a tendency for the effect of the Lagrangian correlation coefficient at the surface to persist over a longer distance. The

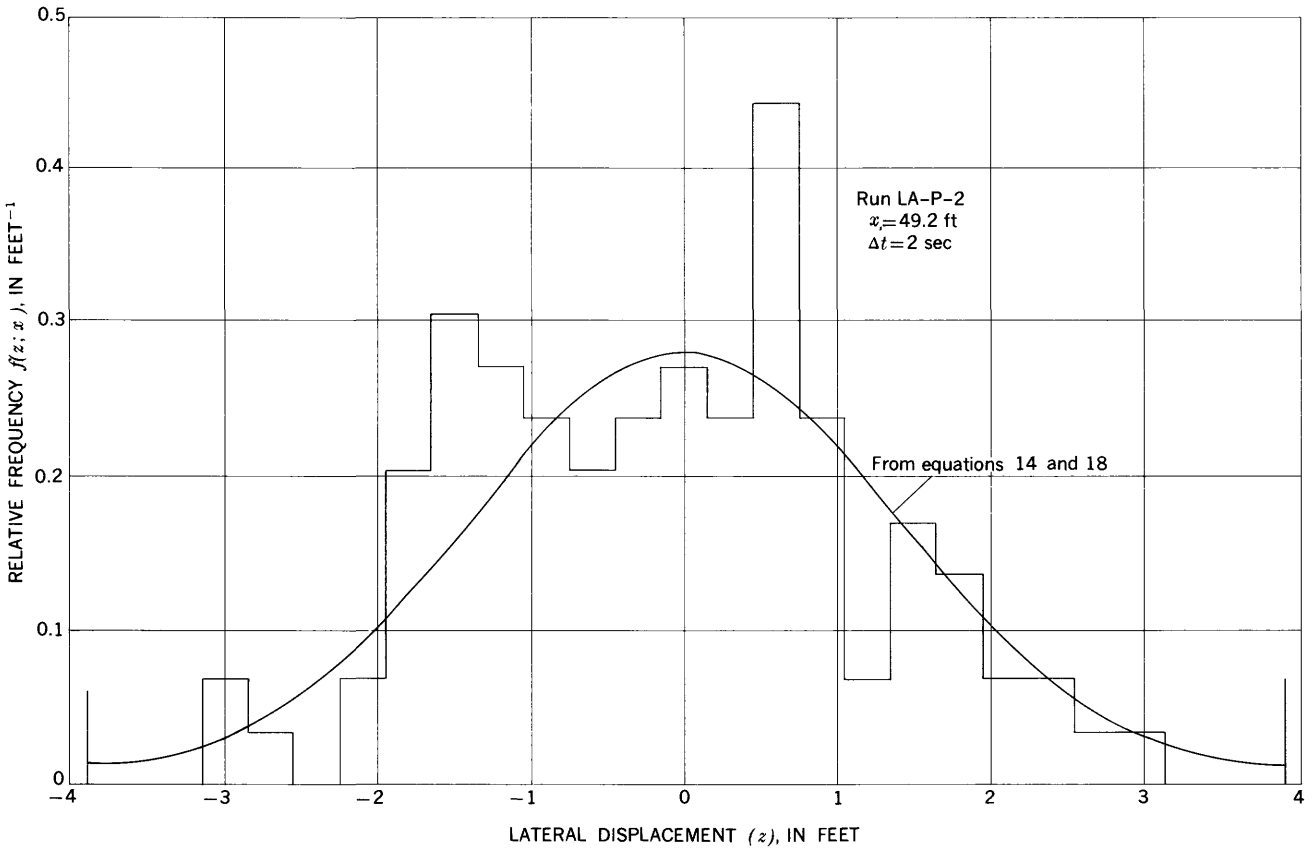

FIGURE 47.—Typical lateral distribution of polyethylene particles.

fact that the particle data lies still further below the curve at large dispersion distances is probably due to the effect of secondary circulation tending to keep the particles away from the sidewalls.

The results of the lateral dispersion experiments with polyethylene particles are summarized in table 6.

VERTICAL DISPERSION

The vertical dispersion experiments were performed to obtain an estimate of the dispersion distance required for dye released continuously from a point source at middepth to become uniformly mixed throughout the depth of flow. Because the concentration profiles were obtained close to the source and only a short period of time was allowed for each, they contained a relatively large component which fluctuated randomly with time. For this reason, the observed concentration profiles did not provide a suitable basis for determining the time-averaged concentration distribution in the vertical. An indication of the uniformity of the concentration in the vertical was obtained, however, by calculating for each profile the coefficient of variation

$$C_v=\frac{\sigma_c}{\bar{C}}, \tag{60}$$

where

$$\sigma_c^2=\frac{1}{n-1}\sum_{i=1}^{n}(C_i-\bar{C})^2,$$

in which C_i is the average concentration in the i'th increment of depth, and

$$\bar{C}=\frac{1}{n}\sum_{i=1}^{n}C_i$$

is the average concentration in the vertical. In figure 49, C_v is shown as a function of x/y_n, the relative dispersion distance at which the profiles were obtained. The data indicate that for the conditions of the experiments a dispersion distance of $x=20y_n$ is sufficient to achieve a virtually uniform vertical concentration distribution.

DISCUSSION OF RESULTS

APPLICABILITY OF FICKIAN DIFFUSION THEORY

In the analysis of the data the Fickian diffusion theory was assumed to be applicable. No particular justification was given for this assumption other than that it seemed to work. Fischer (1966) has shown that equation 7, which describes longitudinal dispersion as a one-dimensional diffusion process, is applicable when the concentration of dispersant in the cross section is nearly uniform. In terms of the notation used in deriving equation 29, a sufficient, although perhaps not necessary, condition is that $C_2(y) << C_1(\xi)$, where $C_1(\xi)$ is understood to be the mean concentration in

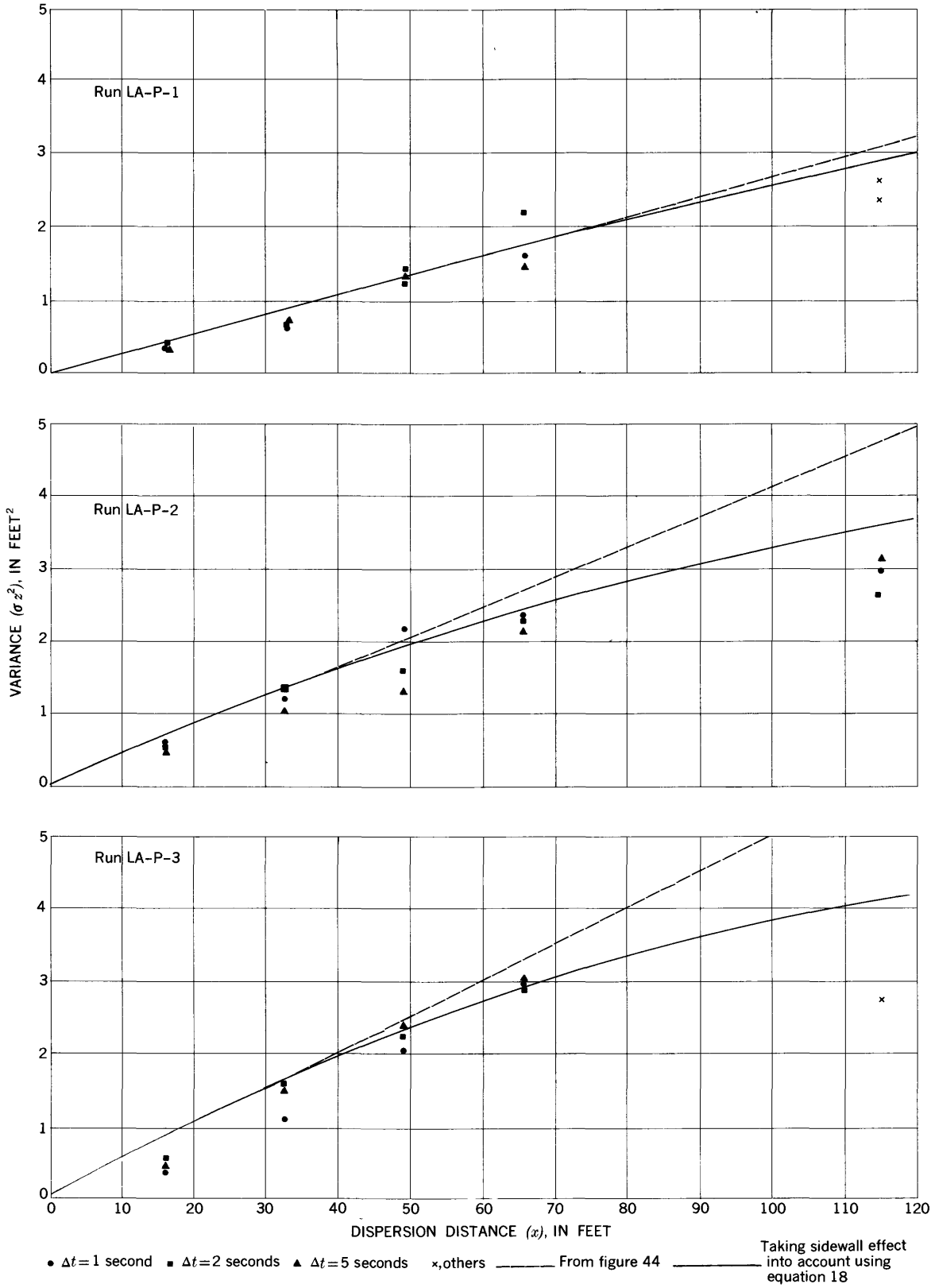

FIGURE 48.—Variance of lateral displacement as a function of dispersion distance, lateral dispersion of polyethylene particles.

TABLE 6.—*Lateral dispersion of floating polyethylene particles: summary of data*

[Minus sign indicates left of centerline of flume]

Run (LA-P-)	Δt (sec)	x (ft)	Number of particles counted	$\bar{z}$ (ft)	σ_z^2 (ft^2)
1	1	16.4	101	0.03	0.36
		32.8	102	0	.64
		49.2	105	.26	1.26
		65.6	99	.13	1.65
	2	16.4	103	.06	.41
		32.8	99	.13	.66
		49.2	100	.23	1.45
		65.6	98	.11	2.24
	5	16.4	107	.10	.36
		32.8	100	.13	.73
		49.2	99	.40	1.39
		65.6	100	.05	1.45
	10	115.0	[1] 119	.02	2.64
	20	115.0	[1] 122	.32	2.39
2	1	16.4	97	−.10	.63
		32.8	100	−.16	1.23
		49.2	94	−.30	2.22
		65.6	100	.04	2.35
		115.0	120	.34	2.97
	2	16.4	97	−.11	.58
		32.8	104	−.15	1.38
		49.2	100	−.11	1.62
		65.6	99	−.30	2.32
		115.0	130	−.26	2.65
	5	16.4	100	−.01	.56
		32.8	99	−.16	1.07
		49.2	101	−.12	1.35
		65.6	102	−.19	2.15
		115.0	124	.06	3.08
3	1	16.4	100	.09	.41
		32.8	101	.58	1.14
		49.2	100	.03	2.08
		65.6	100	−.10	3.00
	2	16.4	103	.28	.59
		32.8	100	.14	1.62
		49.2	99	−.08	2.24
		65.6	100	−.23	2.94
	5	16.4	101	.13	.44
		32.8	100	.11	1.54
		49.2	100	−.06	2.44
		65.6	102	−.24	3.02
	10 or 30	115.0	[2] 256	−.32	2.72

[1] Collected during run LO-P-1.
[2] Collected during run LO-P-3.

the cross section. Considering longitudinal dispersion in a two-dimensional flow with a logarithmic velocity gradient for the initial condition of a uniformly distributed plane source, it is apparent that the initial uniformity is immediately destroyed by the convective effect of the velocity gradient. Thus, at first, the distribution of dispersant in the flow assumes the general shape of the mean velocity profile producing the highly skewed longitudinal concentration distribution characteristically associated with short dispersion times.

Turbulence, however, tends to promote mixing in the vertical direction, leading to an eventual recovery of the condition of nearly uniform concentration of dispersant with respect to depth over most of the length of the dispersing cloud, at which time the Fickian model becomes applicable. Dispersant which is initially located near either the bed or the water surface does not become uniformly mixed over the depth of flow as rapidly as dispersant which is initially located near middepth. It is, therefore, logical to suppose that the length of the initial increment of dispersion distance

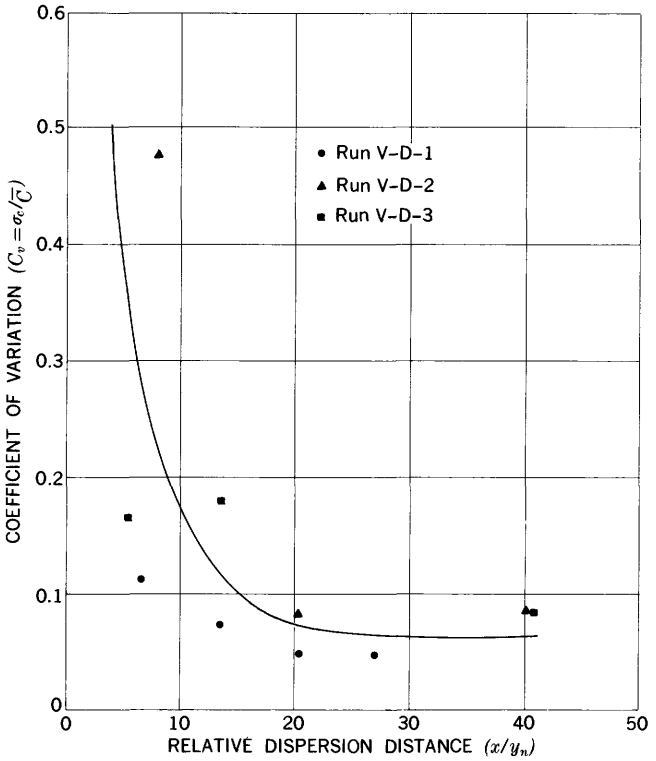

FIGURE 49.—Coefficient of variation for vertical distribution of dye as a function of relative dispersion distance.

in which the one-dimensional Fickian model does not necessarily apply, is the same as the dispersion distance required for the dispersant released from a continuous cross-channel line source located either at the bed or the water surface to become uniformly distributed with respect to depth.

The required distance can be estimated if it is assumed that the coefficient of vertical diffusion can be approximated by its average value, given in equation 33, and that the bed and water surface can be considered as reflecting barriers. With these assumptions, and the substitution of y for z, equation 18 can be used to calculate the concentration distribution in the vertical. Let it be supposed that a sufficient condition for the applicability of the one-dimensional diffusion model is that

$$\left|\frac{C(x,y)-\overline{C}(x)}{\overline{C}(x)}\right| \leq 0.1.$$

The further assumption that the vertical dispersion process follows the normal probability law with variance $\sigma_y^2=2\bar{\epsilon}_y x/\overline{U}$ then leads to the realization of this condition when $\sigma_y=y_n/1.3$, for which the required length of the initial increment is

$$L_m=0.30\,\frac{\overline{U}y_n^2}{\bar{\epsilon}_y}=1.8\,\frac{y_n}{\kappa}\,\frac{\overline{U}}{U_\tau}. \qquad (61)$$

The assumptions leading to equation 61 are indeed somewhat rough; however, the functional relationship which states that the length of the initial increment is directly proportional to depth and velocity and inversely proportional to the shear velocity and the degree of uniformity of the velocity distribution seems quite reasonable.

Equation 61, although it was developed for longitudinal dispersion from an instantaneous plane source, should apply equally well to lateral dispersion from a continuous point source located either at the water surface or the bed. For a source located at middepth, the criterion corresponding to equation 61 gives

$$L_m=0.075\frac{Uy_n^2}{\overline{\epsilon}_y}=0.45\frac{y_n}{\kappa}\frac{U}{U_\tau} \tag{62}$$

as the length of the initial increment of dispersion distance downstream from which the one-dimensional Fickian model for lateral dispersion should apply. For other initial conditions where the source is located either within the upper half or the lower half of the flow, the values of the numerical coefficients lie between the extreme values specified in equations 61 and 62.

Conceptually, L_m is related to the Lagrangian integral length scale of turbulence in that it is a measure of the dispersion distance over which the influence of the initial position of a fluid particle in the cross section persists. Indeed, it would not be surprising to find that the relationship is more than superficial.

A rough experimental confirmation of the analysis leading to equations 61 and 62 can be obtained from the vertical dispersion data in figure 49. These data are replotted in figure 50 in which the coefficient of variation, C_v, is shown as a function of $\frac{x/y_n}{\overline{U}/U_\tau}$. Also given in figure 50 are two calculated curves which show C_v as a function of $\frac{x/y_n}{\overline{U}/U_\tau}$ for (1) a source located either at the bed or the water surface and (2) a source located at middepth. For sources located in intermediate positions, C_v should lie in the crosshatched area between the curves. The calculated concentration profiles used for computing C_v were determined from the normal probability law with variance $\sigma_y^2=2\overline{\epsilon}_y x/\overline{U}$, and from the assumption that the bed and water surface behave as reflecting barriers. The experimental data in figure 50 should follow the curve for the source at $y/y_n=0.5$. The fact that the experimental C_v values are substantially larger than the calculated ones is largely due to the random-in-time concentration fluctuations which contributed significantly to the experimental C_v values.

The approximate relationship

$$\left|\frac{C(x,y)-\overline{C}(x)}{\overline{C}(x)}\right|_{\max}\approx 1.5C_v, \tag{63}$$

which applies to both sets of concentration profiles on which the curves in figure 50 are based, permits figure 50 to be compared directly with equations 61 and 62. Thus, the criterion $C_v\leq 0.07$ is equivalent to the criterion

$$\left|\frac{C(x,y)-\overline{C}(x)}{\overline{C}(x)}\right|\leq 0.1$$

used in the derivations of equations 61 and 62.

The lengths of the initial increments, according to the criteria given in equations 61 and 62, are listed in table 7 for the experimental flow conditions.

TABLE 7.—*Lengths of initial increments of dispersion distance for experimental flow conditions*

Flow	Values of L_m, in feet	
	From eq 61	From eq 62
1	12.5	3.1
2	24.6	6.1
3	41.2	10.3

The dispersion distance exceeded L_m by a safe margin in all longitudinal dispersion experiments, except those for flow 3 at $x=32.8$ feet, and for all lateral dispersion experiments, except those for flows 2 and 3 at $x=16.4$ feet. It is assumed here that the appropriate values of L_m for the lateral dispersion

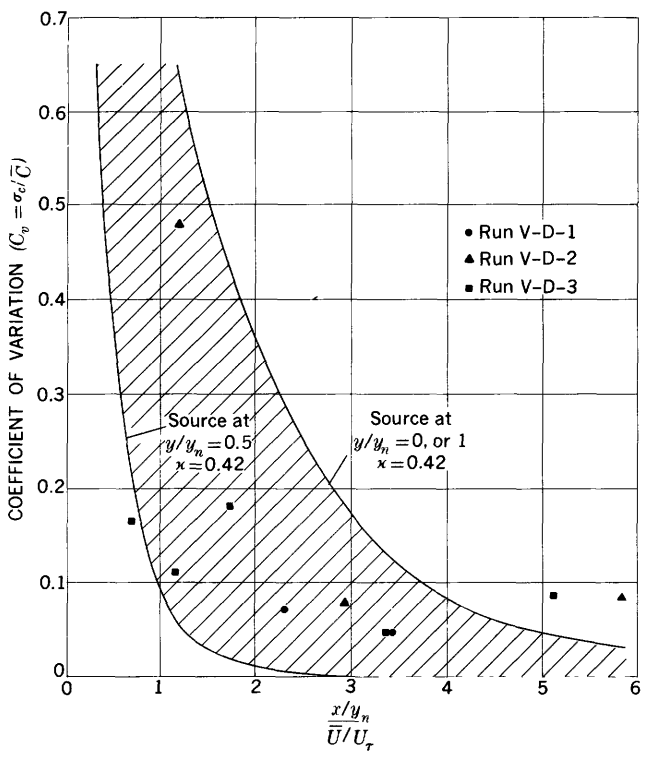

FIGURE 50.—Coefficient of variation for vertical distribution of dye as a function of relative dispersion distance divided by the resistance function.

experiments, with the source located at $y/y_n=0.25$ or 0.75, lie about halfway between the two sets of values given in table 7. Note also in figure 18 that the dispersion distance at which the experimental σ_t^2 versus x relationship for run LO–D–3 becomes linear, as is required by the Fickian model, corresponds closely to the L_m value from equation 61 given in table 7 for flow 3. It is also likely that the magnitude of the average displacements of the data in figure 18, from the curves defined by equation 11, is a function of L_m. On the basis of the analysis given here, it is concluded that use of the one-dimensional Fickian diffusion model in analyzing the data contained in this report is fully justified. A possible exception is the coarse-silt longitudinal dispersion data for which justification is questionable on other grounds.

RELATIONSHIP OF DISPERSION COEFFICIENTS TO FLOW PARAMETERS

The dispersion coefficients determined from the data for the longitudinal dispersion of dye, the longitudinal dispersion of polyethylene particles, and the lateral dispersion of dye are shown in figure 51 as functions of y_nU_τ. The longitudinal dispersion coefficient for dye, which may be expressed by the formula

$$K_x=5.3y_nU_\tau, \tag{64}$$

is in excellent agreement with equation 34 of Elder (1959) for which the numerical coefficient, evaluated for $\kappa=0.42$, is 5.5.

The longitudinal dispersion coefficient for polyethylene particles floating on the water surface is expressed approximately by

$$K_{x_s}=0.59y_nU_\tau. \tag{65}$$

On the water surface the dispersion process is due mainly to turbulence, and there is no direct contribution from differential convection due to the velocity gradient. Therefore, the coefficients in equations 64 and 65 provide a basis for estimating roughly the relative contributions of convection and turbulence to the total longitudinal dispersion. The estimate is good only for an order of magnitude comparison, because the contribution due to turbulence, which is no doubt a function of depth, is specified by equation 65 only at the water surface. If it is assumed that the rate of longitudinal spread observed at the water surface is representative of the direct contribution by turbulence to the rate of longitudinal spread within the body of the flow, then the turbulence component of the longitudinal dispersion coefficient, K_{x_T}, can be estimated by making the appropriate correction for reference velocity. Using the ratio derived from the

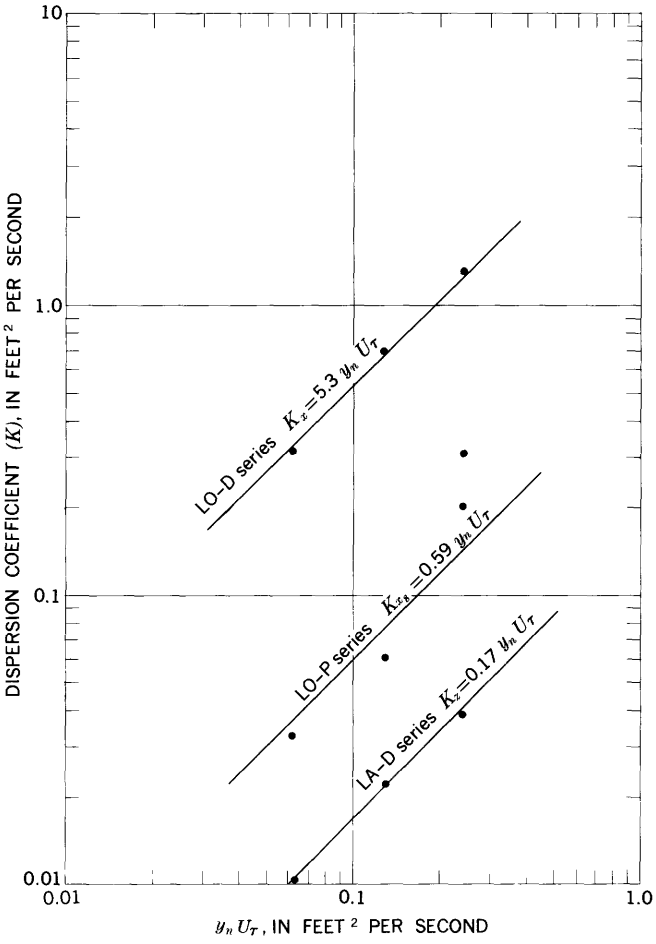

FIGURE 51.—Longitudinal and lateral dispersion coefficients as functions of y_nU_τ.

von Karman–Prandtl velocity distribution equation,

$$\frac{U_s}{\overline{U}}=1+\frac{U_\tau}{\kappa\overline{U}},$$

which has the average value 1.34 throughout the range of experimental flow conditions, the corrected coefficient is

$$K_{x_T}=\left(\frac{\overline{U}}{U_s}\right)^3K_{x_s}=0.25y_nU_\tau. \tag{66}$$

This is from three to four times as large as the coefficient given in equation 33, which was based on the assumption of isotropic turbulence. This result implies, therefore, that the turbulence in open channels is not isotropic.

The lateral dispersion coefficient for dye, expressed by the formula

$$K_z=0.17y_nU_\tau, \tag{67}$$

is the same for the three depths $y/y_n=0.25$, 0.50, and 0.75, provided that the same reference velocity $\overline{U}$, in equation 57, is used in all three cases. The experimental results of Batchelor, Binnie and Phillips (1955), in

which the mean velocity of neutrally buoyant particles in a sufficiently long reach of pipe was found to be equal to the mean flow velocity, regardless of the initial and final positions of the particles in the pipe cross section, indicate that $\overline{U}$ is the correct reference velocity for fluid particles.

Although the σ_z^2 versus x relationship for the lateral dispersion of polyethylene particles on the surface is shown by figure 48 to agree well with that for the dye, the lateral dispersion coefficient for the polyethylene particles should be $U_s/\overline{U}$ times as large to account for the difference in reference velocity. Thus, the equation for the lateral dispersion coefficient for particles floating on the surface is

$$K_{z_s}=\frac{U_s}{\overline{U}}K_z=0.23y_nU_\tau. \tag{68}$$

The coefficient in equation 68 agrees well with the coefficient 0.24 obtained by Sayre and Chamberlain (1964) for lateral dispersion of polyethylene particles in the same flume, but with a sand bed. The ratio of the longitudinal to the lateral dispersion coefficients for the polyethylene particles is 2.6, which agrees well with the ratio 2.5 obtained by Orlob (1961).

The results shown in figure 51 support the Taylor-Elder differential convection theory according to which the dispersion coefficients are proportional to the product y_nU_τ. In order to test this proportionality further, the longitudinal dispersion coefficients obtained by Krenkel (1960) and the lateral dispersion coefficients for polyethylene particles obtained by Orlob (1958) for runs with uniform flow are shown as functions of y_nU_τ in figure 52. These data, which were originally analyzed according to the local similarity theory, and later by Yotsukura, Smoot, and Cahal (1964), in terms of a functional relationship between the Schmidt number and the Reynolds number, also indicate a proportionality between the dispersion coefficients and y_nU_τ. However, the values of the coefficient are different from those in figure 51.

Considering first the longitudinal dispersion coefficient, Elder's analytically derived equation 34 states that K_x/y_nU_τ varies approximately inversely with the cube of the von Karman coefficient, κ, or in other words, that $K_x\kappa^3/y_nU_\tau\approx 0.404$. An estimated value of $\kappa=0.36$ for Krenkel's data was obtained by plotting the resistance function against normal flow depth as shown in figure 53. The value of $K_x\kappa^3/y_nU_\tau$ for Krenkel's data is 0.43 when $\kappa=0.36$. For the LO–D series in figure 51, where $\kappa=0.42$, $K_x\kappa^3/y_nU_\tau=0.39$. Both of these are in good agreement with the theoretical value in equation 34. Experimental evidence apparently bears out the theoretical prediction that K_x is extremely sensitive to small changes in κ. Additional confirmation of this is obtained if the velocity distribution function used by Taylor (1954) in deriving the equation

$$K_x=10.0r_0U_\tau, \tag{69}$$

where r_0 is the pipe radius, for turbulent flow in pipes, is approximated with a logarithmic velocity distribution as shown in figure 54. If $\kappa=0.32$, from figure 54, is substituted into the equation

$$K_x=\left[\frac{0.328}{\kappa^3}+\frac{\kappa}{6}\right]r_0U_\tau, \tag{70}$$

which is the counterpart of equation 34 for longitudinal dispersion in pipes, equation 70 becomes equal to equation 69. The coefficient 0.328 in equation 70 was determined by integrating the polar counterpart of equation 29, using the logarithmic velocity distribution function in figure 54.

Few experiments have been performed under conditions which conform to the requirements, set forth in the derivation of equation 34, of uniform two-dimensional flow with a logarithmic velocity distribution. When this requirement has been met, agreement has been good. If this requirement is not met, wide variations between predictions based on equation 34 and experimental results should not be surprising. Fischer (1964a) has shown, for example, that relatively slight deviations from a uniform lateral velocity distribution are capable of overwhelming all other effects which contribute to longitudinal dispersion.

Although it has not been established theoretically that the lateral dispersion coefficient K_z is proportional to y_nU_τ, the fact that the differential convection and eddy diffusivity theories indicate that both K_z and $\bar{\epsilon}_y$ are proportional to y_nU_τ suggests the same kind of relationship for K_z. Experimental evidence has borne this out to some extent; however, the proportionality coefficient has been found to vary somewhat from channel to channel. According to Yotsukura (written commun., 1965), values of K_z/y_nU_τ ranging from 0.1 to 0.4 for laboratory flumes, and up to 0.7 for natural channels, have been reported in the literature. Yotsukura's tabulation shows an apparent tendency for K_z/y_nU_τ to increase with boundary roughness. However, this tendency is not clearly defined, and it could depend mainly on other conditions under which the data were obtained, such as nonuniformity of flow, nonhomogeneity of the flow and turbulence structure in the lateral direction, differences in channel width, and whether the dispersant was floating on the surface (as in the LA–P series) or entrained in the flow (as in the LA–D series). It is likely that some of the small K_z/y_nU_τ values are due to a suppression of K_z caused

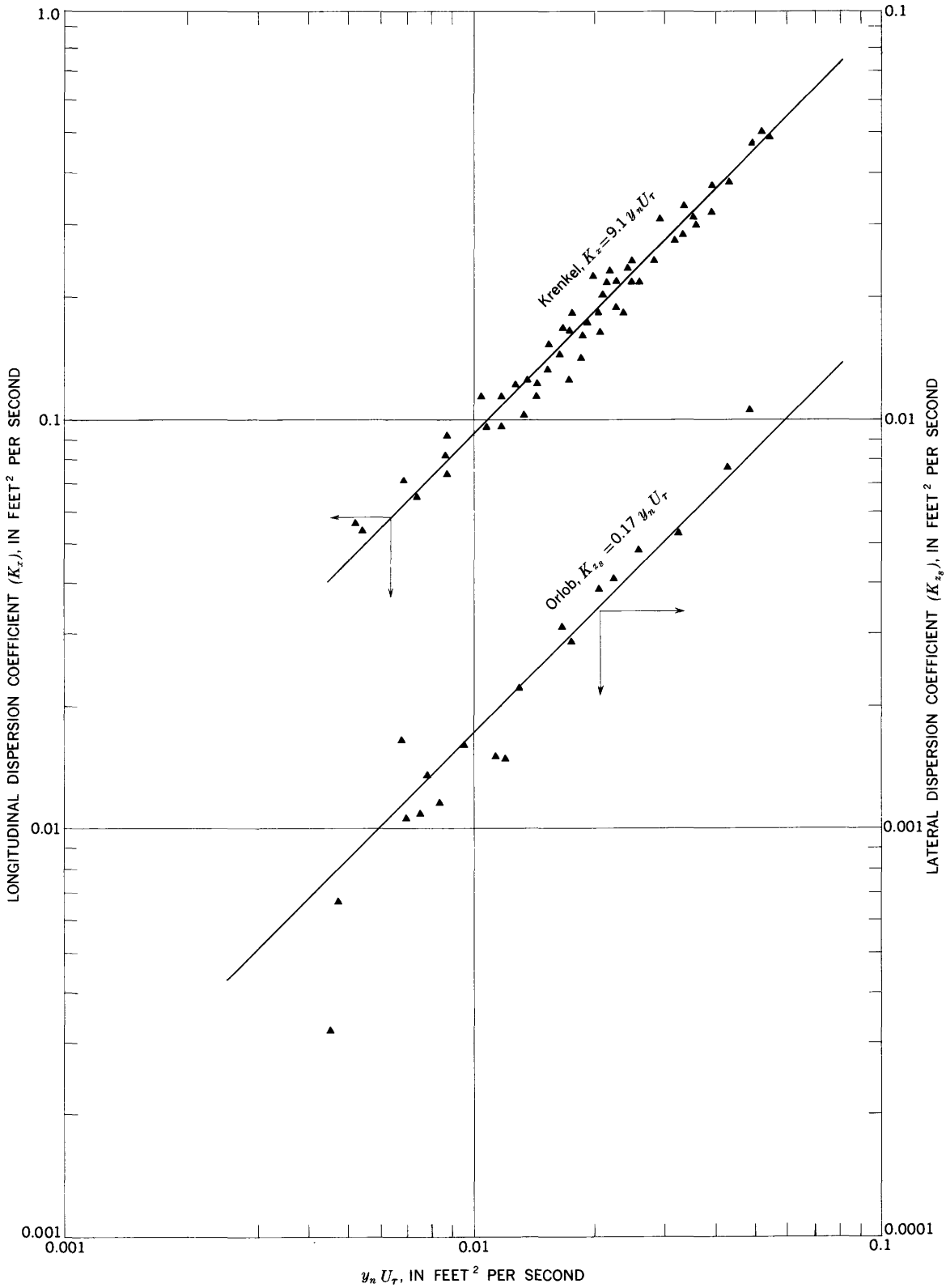

FIGURE 52.—Longitudinal and lateral dispersion coefficients as functions of $y_n U_\tau$ from Krenkel's and Orlob's data.

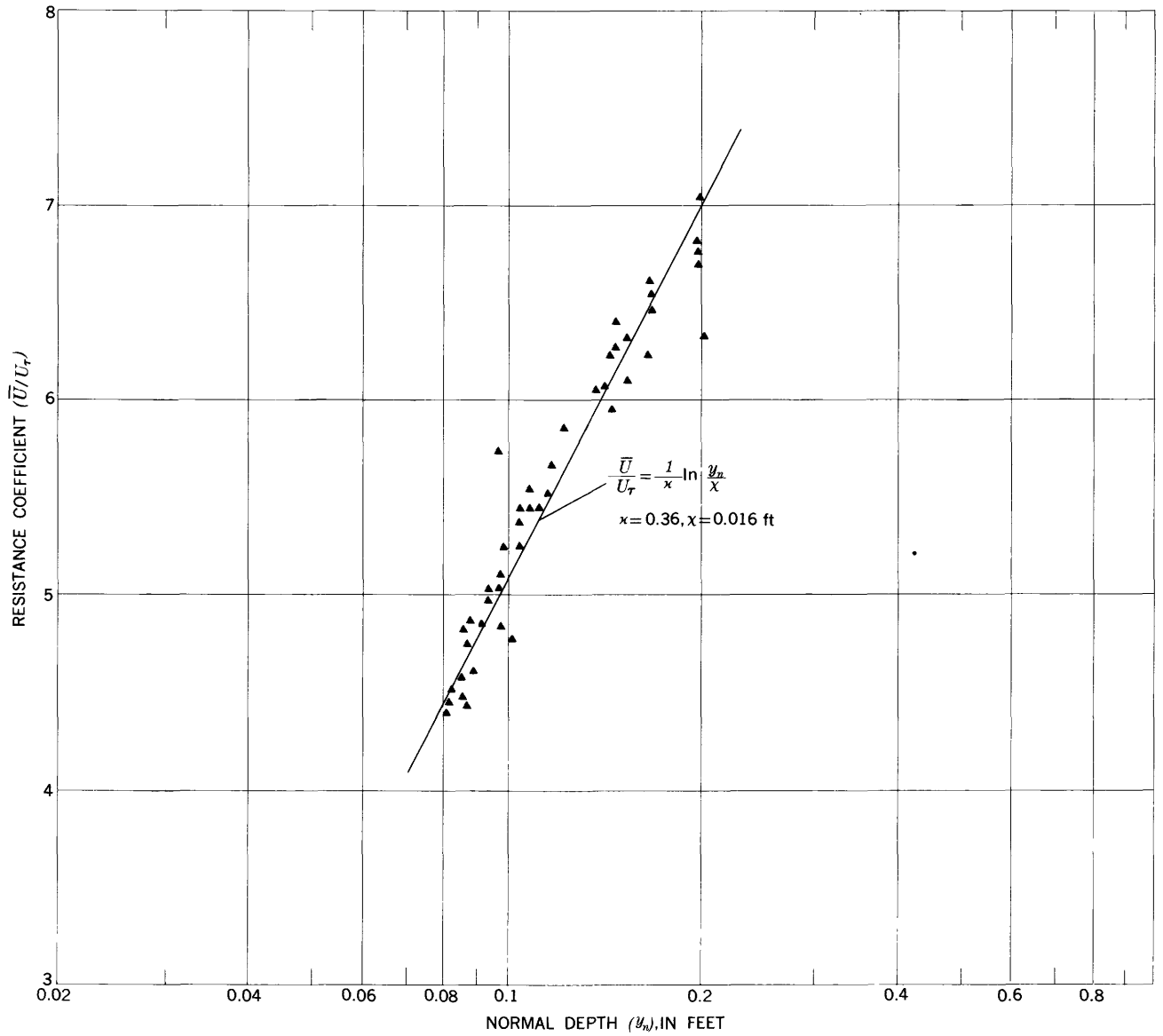

FIGURE 53.—Variation of resistance function with flow depth for Krenkel's data.

by a small width-to-depth ratio. However, except when B/y_n is very small, there does not appear to be any systematic correlation between K_z/y_nU_τ and B/y_n. The relationship between the lateral dispersion coefficients for floating and entrained dispersants given in equation 68 clearly depends on the resistance function $\frac{\overline{U}}{U_\tau}$, and hence on boundary roughness. However, this does not indicate the nature of the relationship of either K_z/y_nU_τ or K_{z_s}/y_nU_τ to boundary roughness.

Hino (1961), in an analysis based on the local similarity theory and a turbulence energy balance, showed that

$$K_{z_s}=\text{const}\ y_nU_\tau. \tag{71}$$

According to this result and equation 68, K_z/y_nU_τ should decrease with boundary roughness. This contradicts the apparent trend of the experimental results cited by Yotsukura. However, if it is assumed that equation 71 is correct, setting equation 71 equal to equation 26a results in the formula

$$L_z=\text{const}\ y_n\frac{U_s}{U_\tau}$$

$$=\text{const}\ y_n\left[\frac{\overline{U}}{U_\tau}+\frac{1}{\kappa}\right] \tag{72}$$

for the integral length scale of lateral turbulence components at the water surface. In figure 55 Orlob's data for runs with uniform flow and data from the alluvial-channel experiment of Sayre and Chamberlain (1964)

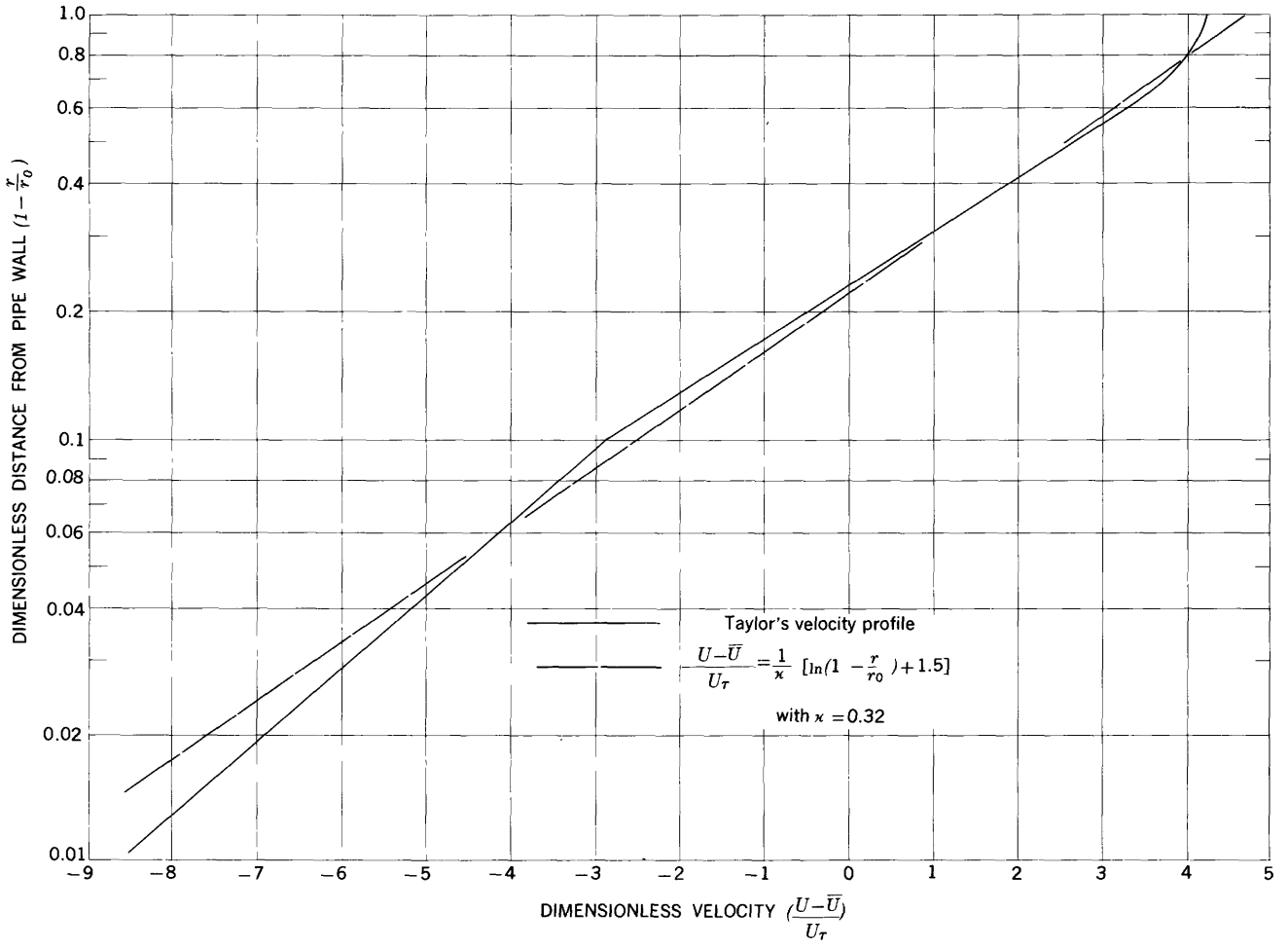

FIGURE 54.—Comparison of Taylor's and logarithmic velocity profiles.

are compared with equation 72. These data are described at least as well by equation 72 as by Orlob's (1958) empirical formula

$$L_z=7y_n^{4/3}.$$

Although the question of whether or not K_z/y_nU_τ varies with boundary roughness remains unsettled, equation 72 provides a useful link between the local similarity and eddy diffusivity theories of lateral dispersion.

Attempts at relating the variation in K_z/y_nU_τ to the von Karman turbulence coefficient, κ, and the absolute roughness, χ (as defined in eq 46), were also unsuccessful. The results are summarized in table 8.

DEFINITION OF DISPERSION COEFFICIENTS

The classical definition of the dispersion coefficient for a given quantity of dispersant, for which the spatial distribution is fixed at some initial instant, is that given in equation 20,

$$K_i\equiv\frac{1}{2}\operatorname*{Lim}_{t\to\infty}\frac{d\sigma_i^2}{dt}.$$

Fischer (1966) has shown that this definition is valid, regardless of the initial concentration distribution of dispersant, provided only that the dispersion process obeys a gradient-type diffusion law, for example, equation 6. Due to experimental considerations, it is difficult

TABLE 8.—*Lateral dispersion coefficients, von Karman coefficients, and absolute roughness*

Source of data	K_z/y_nU_τ	κ	χ (ft)	Remarks
Series LA-D	0.17	0.42	0.042	Dispersant entrained in flow. Flume with rough bed.
Series LA-P	.23	.42	.042	Dispersant floating on water surface. $U_s/\overline{U}\approx1.3$–$1.4$. Flume with rough bed.
Sayre-Chamberlain	.24	.38	.0012	Dispersant floating on water surface. $U_s/\overline{U}\approx1.2$. Flume with sand bed.
Orlob	.17	.40	.0058	Dispersant floating on water surface. $U_s/\overline{U}\approx1.3$–$1.5$. Flume with rough bed.

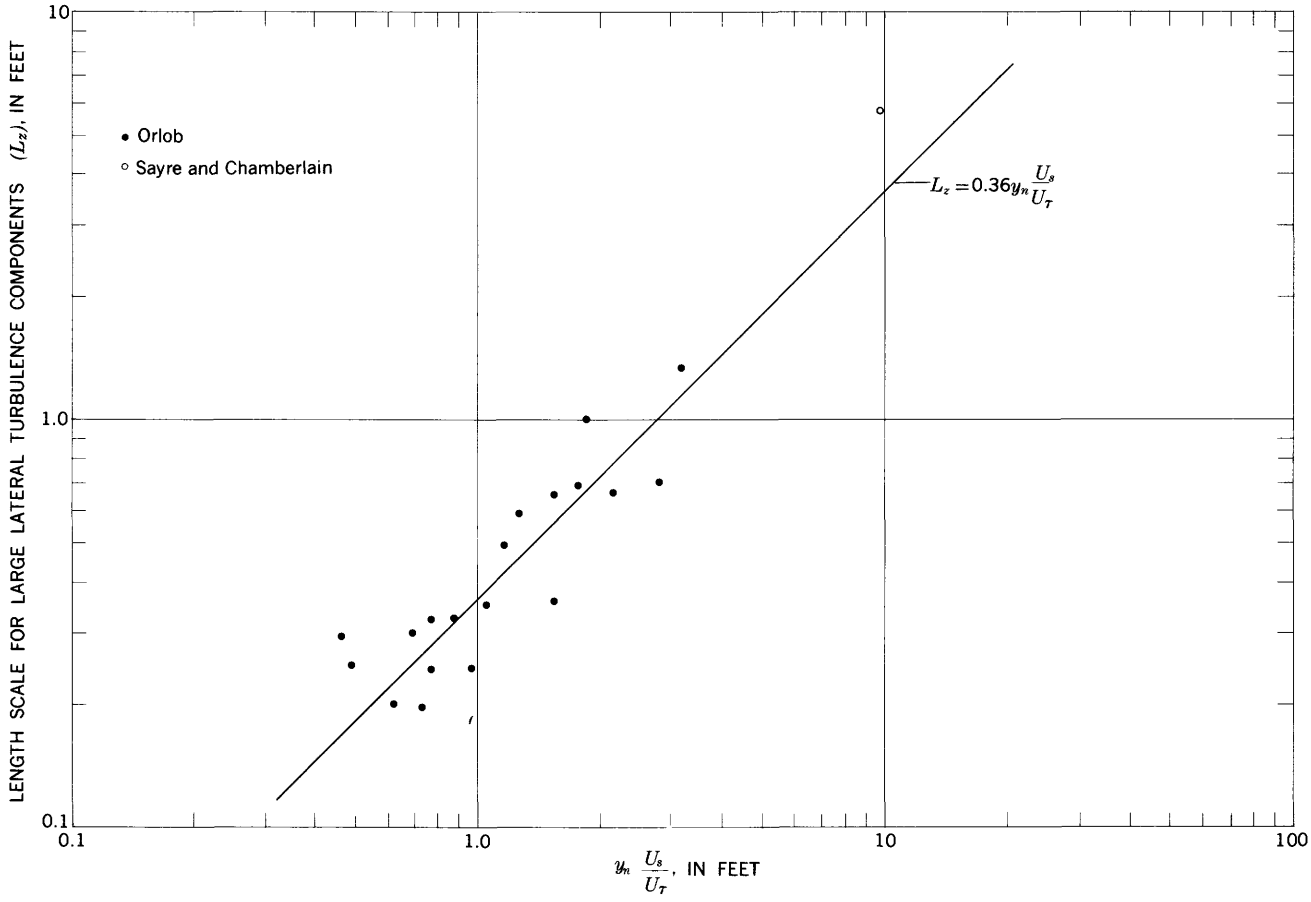

FIGURE 55.—Integral length scale of large lateral turbulence components at the water surface as a function of flow conditions.

to obtain instantaneous observations of the spatial concentration distributions as required by the classical definition. Therefore, relationships for which data are relatively easy to obtain such as

$$K_x = \frac{\overline{U}^3}{2} \operatorname*{Lim}_{x \to \infty} \frac{d\sigma_t^2}{dx},$$

for longitudinal dispersion from an instantaneous source (eq 50), and

$$K_z = \frac{\overline{U}}{2} \frac{d\sigma_z^2}{dx},$$

for lateral dispersion from a continuous source (eq 57), are generally used instead. It has been shown, for example, by Fischer (1964b), Levenspiel and Smith (1957), and Orlob (1961), that the values of the dispersion coefficients given by equations 50 and 57 are the same as those given by equation 20.

In principle, the most straightforward way of evaluating the variances in the above equations is by the method of moments—for example, eq 49. However, in practice, difficulties are sometimes encountered. A common difficulty is that of accurately fixing the points where the tails of the concentration-distribution curves become tangent to the background level. This difficulty is due to the extreme sensitivity of the second moment of a distribution curve to the length of the tails. If there is any appreciable fluctuation in background concentration, the difficulty is compounded. In the determination of lateral dispersion coefficients, complications arise in the method of moments when dispersant reaches the side of the channel and is reflected back toward the center.

Owing to difficulties such as these, indirect methods based on the properties of the normal probability law are sometimes used for estimating either the variance or the dispersion coefficient. Among these are methods based on the rate of attenuation of the peak relative concentration (eq 56), the width of the concentration-distribution curve at one-half the peak value (Taylor, 1954 and Elder, 1959), and the method based on the slope of a curve obtained by plotting log $(t^{1/2} f(t;x))$ against $(x - \bar{U}t)^2/t$ (Krenkel and Orlob, 1963). All of these methods give the same results if the concentration distribution follows closely the normal probability law. However, if there is any appreciable deviation from the normal probability law, results obtained by the different methods in general do not agree with one another.

Because the normal probability law gives, at best, only an approximate representation of actual concentration distributions, there has in fact been considerable difficulty in comparing the results of different investigators. The values of the dispersion coefficients obtained by the indirect methods are partially dependent on the initial concentration distribution and the early phases of the mixing process. The advantage of the direct methods, based on the rate of change of variance, is that the value of the dispersion coefficients so determined are independent of these effects after the initial mixing period.

Facilitating the comparison of data is, by itself, sufficient grounds for standardizing methods of evaluating dispersion coefficients from experimental data. It is recommended here that equation 50, with σ_t^2 determined by the method of moments (eq. 49), be used for evaluating the longitudinal dispersion coefficient. If there is a problem in locating the points where the concentration-distribution curve becomes tangent to the background level, both a minimum and a maximum probable variance for the distribution curve in question can be estimated by terminating the distribution curve at points which give, respectively, the minimum and maximum reasonable tail lengths. If this procedure is repeated for a series of distribution curves obtained at various dispersion distances, plotting both the minimum and maximum estimates of variance as a function of dispersion distance defines a band within which the correct σ^2 versus x relationship should lie. Increasing the range of dispersion distances with respect to the width of the band tends to minimize the error in the dispersion coefficient. Essentially the same method with equation 57 is recommended for evaluating lateral dispersion coefficients, except when reflection from the sides is a factor, in which case the peak attenuation method, with σ_t^2 calculated from equation 56, is recommended.

LONGITUDINAL DISPERSION OF SUSPENDED SILT-SIZE PARTICLES

No general analytical framework for the results of the longitudinal silt dispersion experiments has been found, because, as yet (1965), it has not been possible to either solve or simplify equation 38 in a manner that permits expression of the concentration distribution function, $C(x,t)$, or the moments thereof in terms of hydraulic and sediment parameters. A solution for the moments, $m_p(t)$, using Aris' (1956) eigenvalue method, was attempted; however this approach led to a system of ordinary differential equations with variable coefficients, for which there is no standard method of obtaining a formal solution. A numerical methods-type solution of these equations does, however, appear to be feasible and will be tried in the future.

Assuming that equation 38 in combination with appropriate boundary and initial conditions is capable of representing with good approximation the longitudinal dispersion of silt-size particles, the solution should indicate the combined effect of longitudinal dispersion owing to the velocity gradient and the tendency of the particles to settle. The settling of the particles should cause the development of a vertical concentration gradient which is weighted toward the slower moving flow near the bottom. In comparison with the dye, this should cause a retardation of the mean velocity and a tendency toward more rapid longitudinal spreading of the suspended particles. A comparison of the dye and silt data in general bears out these trends. The tendency for the particles to settle is clearly indicated in the recovery-ratio data, figures 39 and 40. The development of a vertical concentration gradient, although not clearly evident from the recovery-ratio data, is reflected in figures 33 and 34 where the mean velocity of the suspended coarse particles is seen to be slightly less than that of the flow. Figures 35 and 36 indicate that the longitudinal spread of the suspended coarse particles is characteristically greater than that of either the fine particles or the dye. Evidently with the fine particles there was not enough of a concentration gradient to cause a significant difference between the fine particle and dye data in figures 33 through 38.

From dimensional and physical considerations it would seem that the parameter $\beta=V_p/\kappa U_\tau$, which is an index of the vertical concentration distribution of suspended sediment under equilibrium conditions, should also be important in describing the longitudinal dispersion of suspended sediment particles under non-equilibrium conditions. The β values corresponding to the median fall velocities of the particles for the conditions of the experiments are given in table 9. The dispersion of the suspended fine particles agrees closely with the dispersion of the dye and is essentially independent of β. However, the β values for the coarse-particle experiments apparently do not correlate systematically with any of the index parameters for longitudinal dispersion, for example,

$$\overline{U}_p^3 \frac{d\sigma_t^2}{dx} \text{ or } U_p^3 \frac{d}{dx}[f(t;x)_{\max}]^{-2}.$$

This is seen in figure 56, where the data for the coarse-particle experiments consists of the four points farthest to the right. The curve in figure 56 is from Elder's equation 42. It is clear that the curve and the coarse-particle data do not follow the same trend.

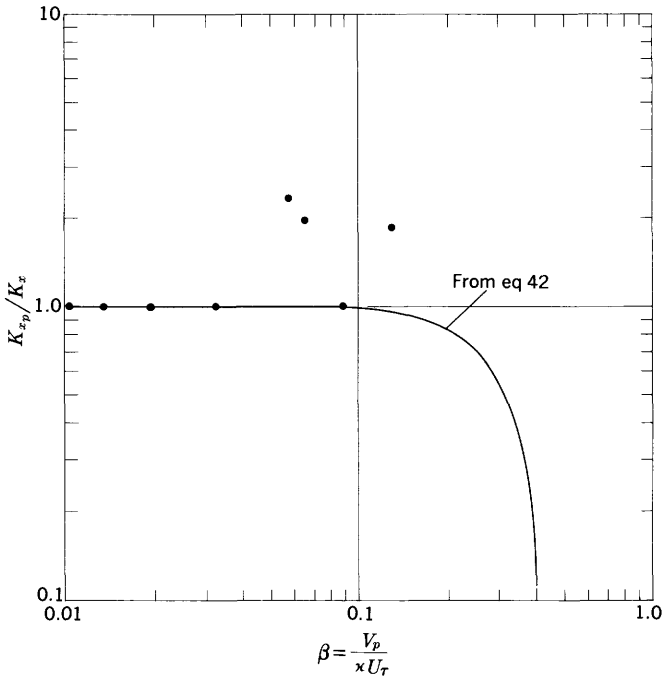

FIGURE 56.—Ratio of silt to dye longitudinal dispersion coefficients, K_{x_p}/K_x, as a function of β.

TABLE 9.—*Values of the parameter β and the median particle fall velocity in the silt dispersion experiments*

Run (LO-)	Particle size (μ)	T (°C)	V_p (ft per sec)	β
FS-1	15–30	20	0.00069	0.013
2	15–30	20	.00069	.010
CS-1	53–62	20	.0071	.13
FG-1	<44	7	.0017	.031
3	<44	6	.0016	.019
CG-1	53–62	5	.0047	.090
2	53–62	4	.0045	.066
3	53–62	6	.0048	.058

In the calculations for plotting the curve in figure 56, the legitimacy of the definition

$$K_{x_p} \equiv \frac{\overline{U}_p^3}{2} \operatorname*{Lim}_{x\to\infty} \frac{d\sigma_t^2}{dx}$$

was assumed. Strictly speaking, in view of the fact that the dispersion data for the coarse particles deviates significantly from the Fickian model, both in the skewness of the relative concentration versus time curves and in the nonlinearity of the σ_t^2 versus x relationship, there is no justification for supposing that the dispersion process for these particles can actually be characterized by means of a gradient-type diffusion model with a constant coefficient.

It would seem that the effect of particle size, as indicated by β, on the longitudinal dispersion of the coarse particles should become less going from flow 1 to flow 3, but the coarse-particle data lead to the opposite conclusion. Anomalies such as this one led to the investigation of the response characteristics of the concentration measuring systems, which is discussed at length in the section beginning on page E65. However, the corrections for system-response lag, even though relatively larger for the coarse particles than for the fine particles or the dye, did not appreciably change the pattern of the results.

It is noteworthy that whereas Camp's (1944, 1946) settling tank theory, in the form of equation 55 for the recovery ratio, agrees reasonably well with the trend of the experimental data, equations 42 and 45 for the longitudinal dispersion coefficient for suspended sediment particles do not. This is true, despite the fact that the implications introduced by assuming a parabolic velocity distribution are essentially the same in both cases. However, a fundamental difference, which probably accounts for this lack of agreement, is the assumption in the derivation of equations 42 and 45 of an equilibrium vertical distribution of suspended particles that is independent of x and t. A comparison of the relative concentration data in figures 25 through 32 for the different sampling depths shows clearly that the data contradict this assumption.

In considering some of the broader aspects of the transport and dispersion of a group of marked fluvial sediment particles, the significance of the recovery ratio data and Camp's settling tank theory extends beyond a material balance analysis. Let it be recalled that $\overline{A}_m/A_t$ is the ratio of the amount of sediment remaining in suspension as the dispersing cloud passes the sampling location x, to the amount which was originally in suspension at the source. Consequently,

$$1-\overline{A}_m/A_t = \int_0^x f_X(x')dx' \qquad (73)$$

represents the proportional amount of sediment deposited on the bed between the source and location x. In equation 73 $f_X(x)$ is a probability-density function which defines the longitudinal distribution of deposited particles. In a channel with an alluvial bed the deposited particles would become part of the bed-material load. The transport and dispersion of these particles would then proceed according to the manner postulated by Hubbell and Sayre (1964) and Sayre and Hubbell (1965) in which particle motion is described as an alternating sequence of steps and rest periods of random length and duration. The longitudinal deposition-distribution function, $f_X(x)$, would then become the initial source distribution function for the same group of particles in the bed-material dispersion process. Furthermore, even though the mechanics of entrainment are ignored, it is reasonable to suppose that the step length distribution function for those bed-material particles that are transported mainly in suspension should be closely related to $f_X(x)$. Indeed, if it is

assumed that they are the same, and the recovery ratio function is approximated by the exponential function

$$\frac{\overline{A}_m}{A_t}=e^{-k_1 x}, \tag{74}$$

then the corresponding probability-density function for the distribution of step lengths will be

$$f_x(x)=\frac{d}{dx}\left[1-\frac{\overline{A}_m}{A_t}\right]=k_1 e^{-k_1 x} \tag{75}$$

where $1/k_1$ is the mean step length. Equation 75 is identical to the step-length distribution function used by Hubbell and Sayre (1964) and Sayre and Hubbell (1965) in the development of their bed-material dispersion model. For small values of β ($\beta \lesssim 0.6$), Camp's settling tank equation (eq 55) can be closely approximated by equation 74 by making the substitution

$$k_1=\frac{V_p}{\overline{U}y_n}(0.8\beta+1). \tag{76}$$

The value of k_1 given by equation 76 differs by only 7 percent from the value determined experimentally for tracer particles in the North Loup River by Sayre and Hubbell (1965), under conditions where suspension was an important factor in the transport of the tracer particles. However, the value of k_1 determined by Hubbell and Sayre (1964) from a laboratory flume experiment in which there was no suspended load is approximately five times as large as that given by equation 76.

TREATMENT OF BOUNDARIES AS REFLECTING BARRIERS

In confined channels it has been assumed by some investigators (Diachishin, 1963; Nobuhiro Yotsukura, written commun., 1965) that surfaces such as the channel sides and bottom and the water surface behave as reflecting barriers for dispersing substances. Implications of this assumption are that the concentration gradient at any one of these surfaces, taken normal to the surface, is zero, and that a mirror image of that part of the concentration profile which would extend beyond the barrier, if the barrier were not present, is reflected back into the flow field. This is analogous to the concept of a perfectly insulated surface, adjacent to a conducting medium, which is commonly employed in heat diffusion theory.

Comparisons of the experimental lateral distribution curves for dye with the theoretical curves based on the Fickian model, equation 14, and the reflection principle, equation 18, which are given in figures 41–43, and in particular figure 46, indicate that application of the reflection principle here is indeed valid. These results are very encouraging because they support the acceptability of the reflecting barrier concept which greatly facilitates the solution of dispersion problems in confined channels. The vertical dispersion data are not sufficiently detailed to evaluate the applicability of the reflecting barrier concept at the water surface and channel bed. However, as seen in figure 50, the reflection principle seems to be reasonably adequate for predicting the dispersion distance required for uniform mixing in the vertical.

The utility of the reflecting barrier concept in the solution of dispersion problems is demonstrated in figure 57, where the maximum concentration in the cross section of a dispersant released continuously at the centerline is given as a function of mean flow velocity, channel width, K_z, and K_x. The curves were obtained from equations 14 and 15 using the reflection technique, equation 18. For comparison, experimental data are shown in figure 57 also. According to the curves dispersant reflected from the sides noticeably affects the centerline concentration at about $x=0.04\,\frac{\overline{U}B^2}{K_z}$, and uniform concentration across the channel is achieved at about $x=0.15\,\frac{\overline{U}B^2}{K_z}$.

CONCLUSIONS

The following conclusions are restricted to conditions of uniform, two-dimensional, turbulent flow in an open channel with a rough bed:

1. The longitudinal dispersion process for a dissolved dispersant can be represented with good approximation, except in the initial stages, by the one-dimensional Fickian diffusion equation.
2. The value of the longitudinal dispersion coefficient for a dissolved dispersant can be calculated with good accuracy by Elder's (1959) equation,

$$K_x=\left[\frac{0.404}{\kappa^3}+\frac{\kappa}{6}\right]y_n U_\tau,$$

   which is based on a coupling of turbulent dispersion with the differential convection rates due to a velocity gradient.
3. The length of the initial increment of dispersion distance, downstream from which the one-dimensional Fickian diffusion equation for the longitudinal dispersion of a dissolved dispersant should become applicable, is approximately

$$L_m=1.8\,\frac{y_n}{\kappa}\,\frac{\overline{U}}{U_\tau}.$$

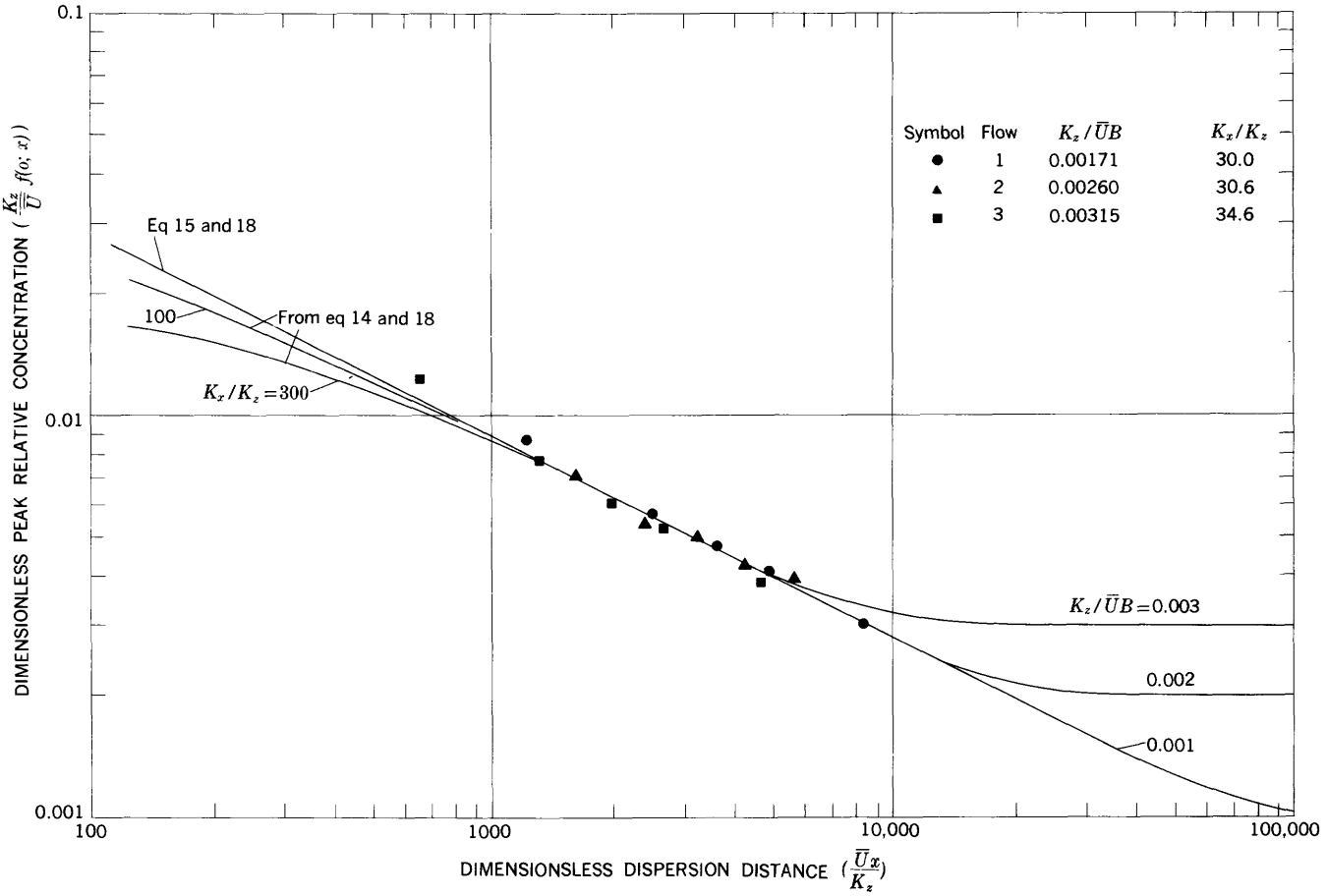

FIGURE 57.—Attenuation of peak concentration with dispersion distance in a rectangular channel of width B having a continuous point source at the centerline.

4. The longitudinal dispersion process for particles floating on the water surface can also be represented by the one-dimensional Fickian diffusion equation. The dispersion rate for floating particles is a function of turbulence at the water surface only. The value of the longitudinal dispersion coefficient for floating particles is approximately one-tenth the value of the coefficient for a dissolved dispersant that is distributed throughout the depth of flow.
5. The longitudinal dispersion process for suspended silt-size sediment particles differs from the process for a dissolved dispersant in that the particles tend to settle toward the slower moving flow near the bed and eventually deposit on the bed.
6. The longitudinal distribution of particles that are deposited along the channel can be calculated with satisfactory accuracy by a procedure based on Camp's (1944, 1946) theory of the influence of turbulence on sedimentation in settling tanks.
7. The lateral dispersion process for a dissolved dispersant released from a continuous point source can be represented with good approximation by the two-dimensional Fickian diffusion equation, provided that the dispersant is evenly distributed with respect to depth. The required minimum dispersion distance for uniform vertical distribution, if the source is at middepth, is approximately

$$L_m \approx 0.45 \frac{y_n \bar{U}}{\kappa U_\tau}.$$

8. The value of the lateral dispersion coefficient for a dissolved dispersant is approximately one-thirtieth that of the longitudinal dispersion coefficient.
9. The confining effect of the sidewalls on the lateral distribution of a dissolved dispersant can be satisfactorily accounted for by the reflection-superposition principle in which boundaries are treated analytically as reflecting barriers.
10. The lateral dispersion of floating particles released from an intermittent point source at the water surface can also be represented as a Fickian diffusion process. However, the dispersion pattern is somewhat distorted by the effects of secondary circulation. The rate of lateral dispersion per unit of dispersion distance is approximately the same for floating particles as for a dissolved dispersant

that is distributed evenly throughout the depth of flow.

The following conclusions are general insofar as they are not restricted to any particular type of channel or flow conditions:

11. If a dispersion process does not follow the Fickian diffusion law, different methods of evaluating dispersion coefficients may lead to significantly different results. In order to facilitate the comparison of results it is recommended that, insofar as possible, evaluations be based on equations of the type

$$K=\frac{1}{2}\frac{d\sigma^2}{dt},$$

where σ^2 is evaluated by the method of moments.

12. The Turner fluorometer, used as a nephelometer, provides a rapid and convenient means for measuring concentrations of suspended fine sediments. However, because the method is sensitive to surface characteristics and size of particles, a separate calibration must be performed for each type of sediment.
13. The response of concentration-measuring systems to rapidly changing concentrations can be evaluated by means of the convolution principle that permits the output of the system to be expressed as the convolution of the response function of the system and the input to the system. The response function of the system can be determined by experiment. From a knowledge of the response function, corrections for lag and distortion due to slow response can be made.

EXPERIMENTAL EVALUATION OF RESPONSE CHARACTERISTICS OF THE CONCENTRATION-MEASURING SYSTEMS

When the longitudinal dispersion data were being analyzed, some questions concerning the response characteristics of both the continuous and the discrete sampling systems were raised. With what degree of fidelity were the combined sampling and concentration-measuring systems indicating the rate of change of concentration actually occurring at the sampling nozzle? Was the response lag sufficient to cause an appreciable amount of distortion in the experimental-concentration versus time curves? Could a method be found for correcting the experimental data for the effects of response lag? These questions were investigated both analytically and experimentally. Because the problem of system response is common to many aspects of experimental hydraulics and because of the general applicability of the investigational methods, the results of these investigations are considered worth reporting here.

The investigations were based on the convolution principle, which according to Lee (1960), is universally applicable for determining the output of a linear system in terms of the system unit-impulse response and the input. For our problem, the principle may be stated in the form of a convolution integral,

$$C_O(t, x)=\int_0^t f_R(t-t_1)C_I(t_1, x)dt_1, \qquad (77)$$

where

$C_O(t, x)$ = output of combined sampling and concentration-measuring system with the sampling nozzle located at dispersion distance x,
$f_R(t-t_1)$ = response function of the sampling system to an instantaneous unit impulse occurring at the sampling nozzle at time t_1,
$C_I(t_1, x)$ = input to the system; that is, the concentration versus time relationship actually occurring at the sampling nozzle,
t = time registered by the output end of the system, and
t_1 = time of input; that is, the time of arrival at the sampling nozzle.

The convolution integral possesses various useful properties. The most important for this particular application is that it expresses the relationship between the probability-density functions of two independent random variables and the probability-density function of the sum of these random variables. Let I be a random variable that expresses the time required for a particle of dispersant to travel from an instantaneous plane source at $x=0$ to the sampling nozzle, and let I be distributed according to the probability-density function

$$f_I(t_1; x)=\frac{Q\gamma}{W}C_I(t_1, x).$$

Let R be a random variable, independent of I, which expresses the elapsed time between the arrival of a particle of dispersant at the sampling nozzle and the registration of the particle by the system, and let R be distributed according to the probability-density function $f_R(\tau)$ where $\tau=t-t_1$. Finally, let O be a random variable which expresses the total elapsed time from the release of a particle at the source until its registration by the system, and let O be distributed according to the probability-density function

$$f_O(t; x)=\frac{Q\gamma}{W}C_O(t, x).$$

According to the above interpretations, it is apparent that

$$O=R+I \tag{78}$$

and that

$$f_O(t;\,x)=f_{R+I}(t;\,x)=\int_0^t f_R(t-t_1)f_I(t_1;\,x)dt_1. \tag{79}$$

It is possible to determine $f_O(\cdot;\,x)$ and $f_R(\cdot)$ by means of experiment. However, $f_I(\cdot;\,x)$, which is the function of primary concern, cannot be so determined. Therefore, a means of expressing the unknown input function in terms of the known output and response functions would be highly desirable. Unfortunately, an expression of this type cannot readily be obtained unless the natures of the functions are specified mathematically, in which case $f_I(\cdot;\,x)$ can be determined from a knowledge of $f_O(\cdot;\,x)$, $f_R(\cdot)$, and their Fourier transforms. If, as is usually the case, a mathematical description of these functions is lacking, it nevertheless follows from equation 78 and elementary probability theory that the mean value of the output time is equal to the sum of the means of the response and the input times,

$$\bar{t}=\bar{\tau}+\bar{t}_1 \tag{80}$$

and likewise for the variances,

$$\sigma_O^2=\sigma_R^2+\sigma_I^2. \tag{81}$$

Thus, $\bar{\tau}$ and σ_R^2 can be considered, respectively, as indices of the lag time and distortion imposed on the input by the combined sampling and concentration measuring system. A particularly significant result of equation 81 is that, subject to possible restrictions on the assumptions in the foregoing analysis, values of the longitudinal dispersion coefficients obtained in the flume experiments were not influenced by the response characteristics of the system. This is because

$$K_x \propto \operatorname*{Lim}_{x\to\infty}\frac{d\sigma_I^2}{dx}=\operatorname*{Lim}_{x\to\infty}\frac{d\sigma_O^2}{dx}$$

since σ_R^2 is not a function of x.

The interpretation of I, O, and, for the discrete sampling system, R as random variables is straightforward. These variables are associated entirely with dispersion, either in the flume or in the feed tubes of the sampling system, and dispersion is essentially a random phenomenon. However, in the continuous system where the form of $f_R(\tau)$ is due to the combined effects of dispersion in the feed tube and the electronic characteristics of the fluorometer and recorder, the latter of which are essentially deterministic, the justification for interpreting R as a random variable is less clear. A partial justification is that $f_R(\tau)$ was shown by experiments to possess the necessary mathematical attributes of a probability-density function.

In order to obtain a quantitative measure of the effect of system response on the experimental longitudinal dispersion data, a series of experiments was performed in which $f_R(\tau)$ was determined under conditions closely approximating those in the flume experiments. Conditions which were duplicated are sampling velocity, length and diameter of sampling nozzles and feed tubes, and water temperature. The experimental setup, shown in schematic form in figure 58, consisted essentially of two 22-inch-diameter plexiglass tanks, each having a capacity of approximately 100 liters, a 4-way stopcock, the feed tubes, and either a continuous or a discrete sampling system. One of the tanks contained water with a known concentration of dispersant, and the other tank contained clean water. The dispersant tank was equipped with a hand-operated agitator, which when given an oscillating motion was capable of maintaining a steady concentration of suspended silt-size particles in the tank. By means of the 4-way stopcock the source of flow to the sampling system could be switched instantaneously

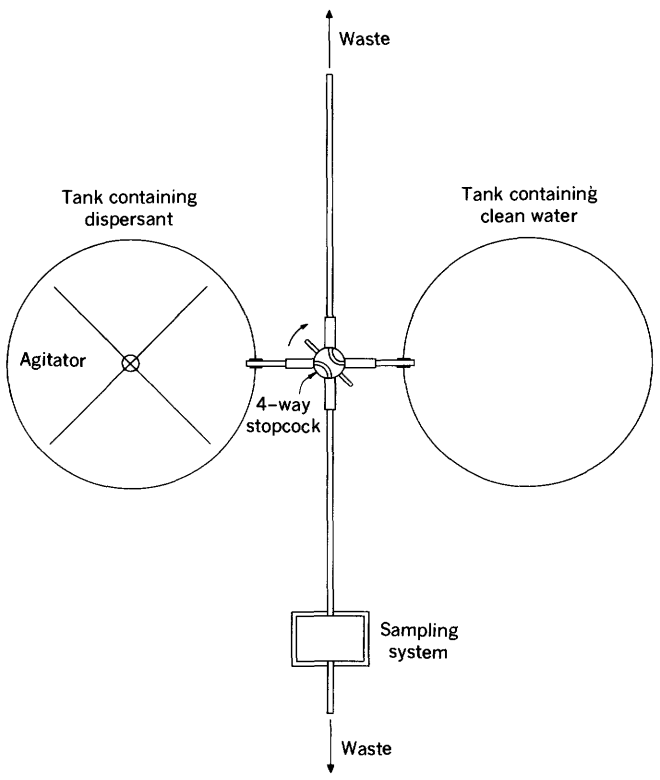

FIGURE 58.—Experimental setup for determining response characteristics of sampling systems.

from the clean-water tank to the dispersant tank or vice versa. The rate of flow in the feed tubes was controlled with tube clamps. The same rate of flow was maintained in both the sampling system and the waste feed tubes. The continuous sampling system consisted of the same Turner Model 111 Fluorometer and strip chart recorder that were used in the flume experiments. The discrete sampling system was a simplified version of that used in the flume experiments and consisted merely of a movable rack, containing 30 glass vials, which was passed under the outlet end of the feed tube so as to obtain discrete samples at one-second intervals.

In theory, $f_R(\tau)$ can be obtained either as a direct observation of the response of the system to an instantaneous unit pulse input or as the derivative with respect to time of a unit step function input. In the experiments, an instantaneous pulse was approximated by switching the source of flow to the sampling system from the clean-water tank to the dispersant tank for a period of 1 second and then switching it back. A step function input was obtained by switching the source from the clean-water tank to the dispersant tank until the response reached equilibrium with the concentration in the dispersant tank. In both cases $f_R(\tau)$ was put in the form of a probability-density function by normalizing the data to make $\int_0^\infty f_R(\tau)d\tau=1$. Good experimental agreement between the two methods was obtained. The pulse input method, despite the 1-second duration of the pulse, is considered to be the more reliable due to the inaccuracy inherent in graphically differentiating the response to the step function input, particularly for the first 1 or 2 seconds where the slope is very steep. Most of the data reported here were obtained by the pulse input method.

For some conditions, response experiments were repeated for different concentrations of dispersant in the dispersant tank. The results showed that a slight degree of dependence on concentration did in fact exist. For both the discrete system, with sediment as a dispersant, and the continuous system, with either dispersant, the tendency was toward a more sluggish response as the concentration of dispersant was in creased. The causes, however, were not the same. In the discrete system with sediment, the increase in sluggishness was due to a decreased capacity of the flow in the feed tube to transport all of the particles simultaneously in suspension at high concentrations. In the case of the continouus system with dye, the cause was associated with the electronics of the fluorometer and the recorder rather than intrinsically with concentration. That is, a response requiring a large instrument deflection was accomplished less rapidly than a response requiring a small deflection. In the continuous system with sediment, both causes were involved. As indicated previously, however, the degree of dependence of $f_R(\tau)$ on either the concentration of sediment or the required instrument deflection was found to be quite small and is therefore not considered sufficient to appreciably upset the assumption of system linearity or the contention that R and I are independently distributed, random variables.

A summary of the results obtained in the response experiments and associated supplementary data are given in table 10. The values of $\bar{\tau}$ and σ_R^2 were computed by the method of moments using the $f_R(\tau)$ curves and equations 48 and 49. It is immediately apparent that σ_R^2 for the sediment system-response curves is strongly dependent on the velocity in the feed tubes, but essentially independent of the Reynolds number, **R**, of the flow in the feed tubes despite the fact that the **R** values indicate flow conditions ranging from laminar to turbulent. This result contradicts estimates of the expected dispersion in the feed tubes, which were made prior to the flume experiments. Calculations based on Taylor's (1953, 1954) theories of longitudinal dispersion in laminar and turbulent pipe flow indicated that dispersion rates of dye in the feed tubes would be negligible in comparison to dispersion rates in the flume. As fall velocities of the silt-size sediment particles are on the order of 0.1 percent of the flow velocities in the feed tubes, it was assumed that this would be so for low concentrations of particles also. This assumption was borne out by the response experiments with a feed tube velocity of 2.5 feet per second, but not by those with a velocity of 1.3 feet per second. In retrospect, it seems likely that, at the lower velocity, forces such as those associated with molecular diffusivity, secondary circulation, and turbulence were capable of distributing the dye, but not the particles, over the cross section of the tube. This explanation is compatible with the long tails, which were typical of the response functions for sediment, obtained with the discrete system.

The results of the system-response experiments were used as a basis for estimating corrections to be subtracted from the values of $\bar{t}$ and σ_t^2 found in the flume experiments. Values of $\bar{\tau}$ and σ_R^2 used in making these corrections are listed in table 11.

Three typical system-response functions are shown in figure 59. These response functions were obtained under conditions closely approximating those in the flume experiments LO–D–2, LO–FS–2, and LO–CG–2. In order to illustrate more clearly the effect of the system-response characteristics on the longitudinal dispersion data, output curves are compared with hypothetical input curves for the same three runs in

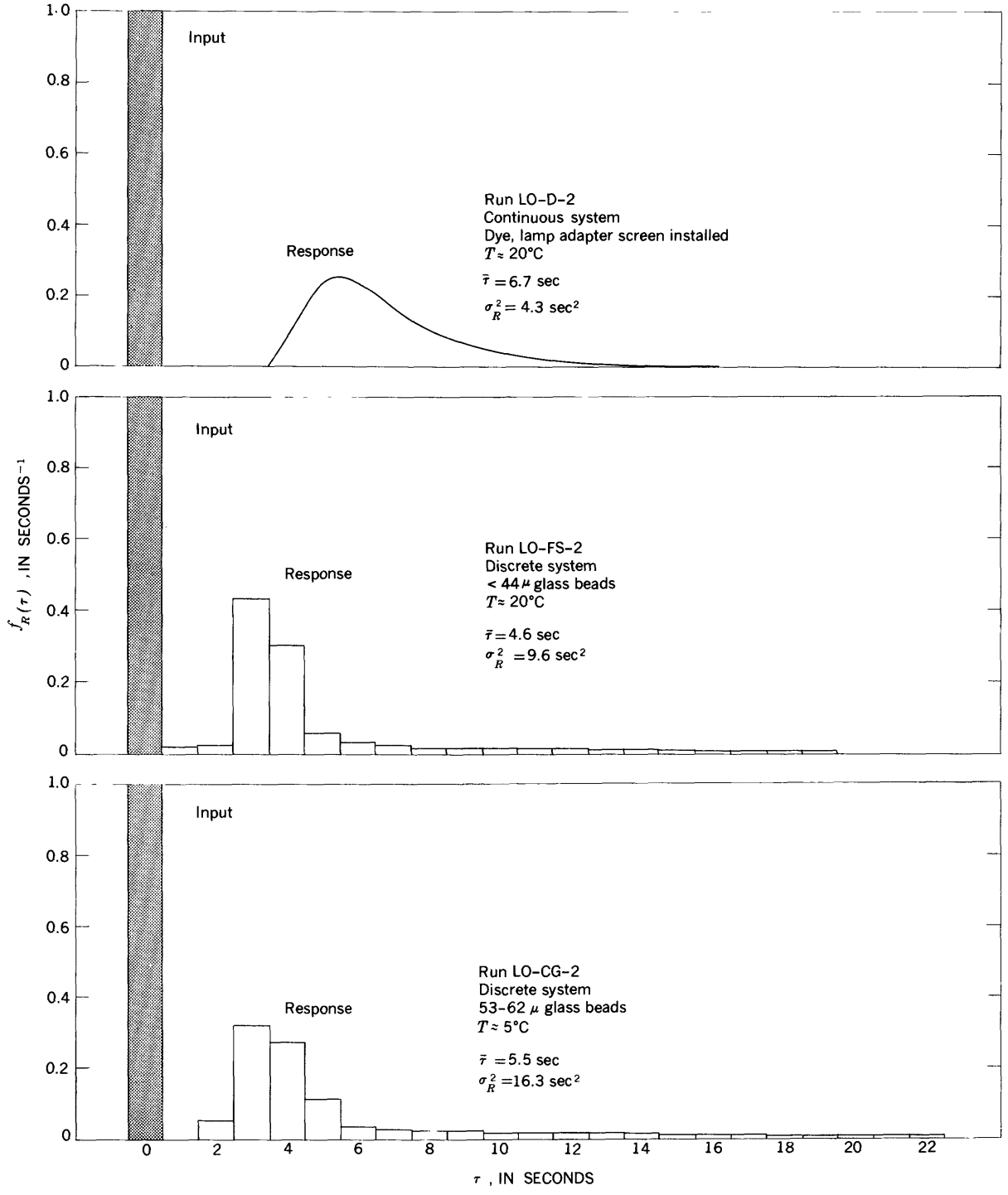

FIGURE 59.—Three typical system-response functions.

figure 60. The input curves were obtained from equation 9a with $t=t_1$, $x=65.6$ feet and $\bar{U}$ and K_x for the flow conditions in runs LO–D–2, LO–FS–2, and LO–CG–2. The output curves were determined by means of a numerical integration of equation 79 using the input curves, and the response functions in figure 59 with $\tau=t-t_1$ and $dt_1=\Delta t_1=1$ second. The results indicate that the distortion imposed on the longitudinal dispersion data by the response characteristics of the measuring systems is not great. Also, the values of the means and variances listed in figures 59 and 60 are in good agreement with equations 80 and 81, considering the fact that the moments for the response and output curves were calculated by the approximate method of numerical integration using equations 48 and 49.

TABLE 10.—*Summary of results of system-response experiments*

Dispersant	System	Velocity in sampling tube (ft per sec)	Temp. (°C)	R	Approximate initial concentration	Approx. F (fluorometer units per unit of concentration)	$\bar{\tau}$ (sec)	σ_R^2 (sec²)
Pontacyl Brilliant Pink B	Continuous	2.46	21.5	4730	18,38 ppb	4.9	5.5	1.7
	....do	2.54	4.0	2980	12 ppb	3.8	5.1	2.1
	....do.[1]	2.46	20.0	4560	18 ppb	15.0	6.7	4.3
	Discrete	1.28	4.0	1510	12 ppb	4.7	3.2	.8
	....do.[2]	1.35	21.5	2600	11 ppb	4.4	3.0	.5
	....do.[2]	1.28	4.0	1510	7.5 ppb	4.7	3.4	.7
<44μ glass beads	Continuous	2.46	23.0	4870	500 ppm	.147	5.5	1.7
	Discrete	1.32	23.0	2620	500 ppm	.101	4.6	9.6
53–62μ glass beads	Continuous	2.46	24.5	5020	1,000 ppm	.070	6.0	2.6
	....do	2.46	5.0	3000	1,000 ppm	.070	6.2	3.1
	Discrete	1.37	25.0	2820	1,000 ppm	.032	5.4	15.7
	....do	1.32	5.2	1610	1,000 ppm	.032	5.5	16.3

[1] Lamp adaptor screen in place.
[2] From derivative of step function response.

TABLE 11.—*Corrections for system-response lag which were applied to flume data*

Flume run (LO–)	System	$\bar{\tau}$ (sec)	σ_R^2 (sec²)	Remarks
D–1	Continuous	6.4	4.3	Lamp adaptor screen installed in fluorometer.
2	....do	6.4	4.3	Do.
3	....do	5.1	2.1	
3	Discrete	3.3	.7	
FS–1	....do	4.6	9.6	15–30μ silt assumed to behave as <44μ glass beads.
1	Continuous	6.4	4.3	Lamp adaptor screen installed in fluorometer.
2	Discrete	4.6	9.6	15–30μ silt assumed to behave as <44μ glass beads.
2	Continuous	6.4	4.3	Lamp adaptor screen installed in fluorometer.
CS–1	Discrete	5.4	15.7	53–62μ silt assumed to behave as 53–62μ glass beads.
1	Continuous	6.9	5.1	Lamp adaptor screen effect estimated.
FG–1	Discrete	4.8	10.1	Temperature effect estimated.
1	Continuous	5.5	2.1	Do.
3	Discrete	4.8	10.1	Do.
3	Continuous	5.5	2.1	Do.
CG–1	Discrete	5.5	16.3	
1	Continuous	6.2	3.1	
2	Discrete	5.5	16.3	
2	Continuous	7.2	5.6	Lamp adaptor screen effect estimated.
3	Discrete	5.5	16.3	
3	Continuous	6.2	3.1	

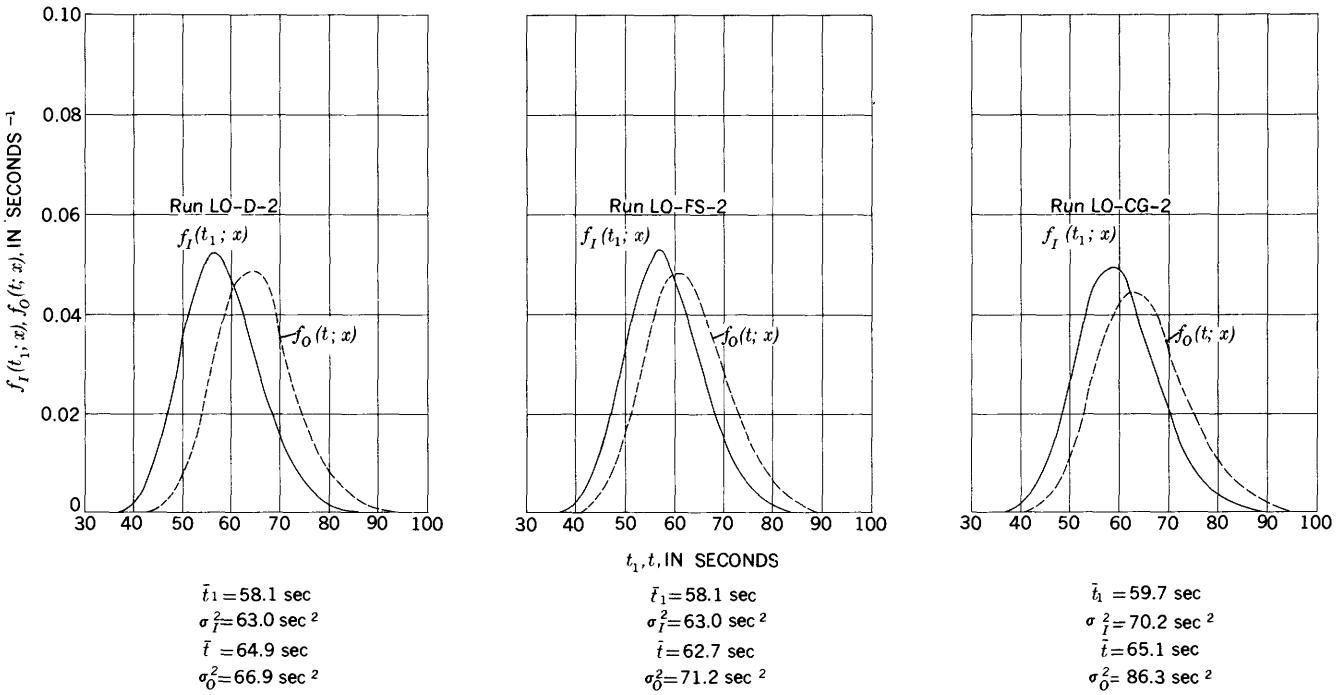

$\bar{t}_1 = 58.1$ sec
$\sigma_I^2 = 63.0$ sec²
$\bar{t} = 64.9$ sec
$\sigma_O^2 = 66.9$ sec²

$\bar{t}_1 = 58.1$ sec
$\sigma_I^2 = 63.0$ sec²
$\bar{t} = 62.7$ sec
$\sigma_O^2 = 71.2$ sec²

$\bar{t}_1 = 59.7$ sec
$\sigma_I^2 = 70.2$ sec²
$\bar{t} = 65.1$ sec
$\sigma_O^2 = 86.3$ sec²

FIGURE 60.—Comparisons between hypothetical input and output curves illustrating the effect of system-response characteristics on longitudinal dispersion data.

LITERATURE CITED

Al-Saffar, A. M., 1964, Eddy diffusion and mass transfer in open channel flow: California Univ., Ph.D. dissert., 138 p.

Aris, R., 1956, On the dispersion of a solute in a fluid flowing through a tube: Royal Soc. (London) Proc., Ser. A, v. 235, p. 67–77.

Batchelor, G. K., 1953, The theory of homogeneous turbulence: London, Cambridge Univ. Press, 197 p.

Batchelor, G. K., Binnie, A. M., and Phillips, O. M., 1955, The mean velocity of discrete particles in turbulent flow in a pipe: Physical Soc. [London] Proc., v. 68, Sect. B, p. 1095–1104.

Batchelor, G. K., and Townsend, A. A., 1956, Turbulent diffusion, *in* G. K. Batchelor, and R. M. Davies, eds., Surveys in mechanics: London, Cambridge Univ. Press, p. 352–399.

Brush, L. M., Jr., 1962, Exploratory study of sediment diffusion: Jour. Geophys. Research, v. 67, no. 4, p. 1427–1435.

Camp, T. R., 1944, Discussion of "Effect of turbulence on sedimentation": Am. Soc. Civil Engineers Trans., v. 109, p. 660–667.

———1946, Sedimentation and the design of settling tanks: Am. Soc. Civil Engineers Trans., v. 111, p. 895–958.

Diachishin, A. N., 1963, Waste disposal in tidal waters: Am. Soc. Civil Engineers Proc., v. 89, no. SA4, Paper no. 3602, p. 23–43.

Dobbins, W. E., 1944, Effect of turbulence on sedimentation: Am. Soc. Civil Engineers Trans., v. 109, p. 629–678.

Elder, J. W., 1959, The dispersion of marked fluid in turbulent shear flow: Jour. Fluid Mechanics, v. 5, pt. 4, p. 544–560.

Ellison, T. H., 1960, A note on the velocity profile and longitudinal mixing in a broad open channel: Jour. Fluid Mechanics, v. 8, pt. 1, p. 33–40.

Feuerstein, D. L., and Selleck, R. E., 1963, Tracers for dispersion measurements in surface waters: California Univ., Berkeley, Sanitary Engineering Research Lab. Rept. 63–1, 69 p.

Fischer, H. B., 1964a, Longitudinal dispersion by velocity gradients in open channel flow: Pasadena, California Inst. Technology, W. M. Keck Lab. Hydraulics and Water Resources Tech. Memo. 64–4, 12 p.

———1964b, Determination of dispersion coefficients by the change in moment method: Pasadena, California Inst. Technology, W. M. Keck Lab. Hydraulics and Water Resources Tech. Memo. 64–6, 22 p.

———1966, A note on the one-dimensional dispersion model: Internat. Jour. Air and Water Pollution, v. 10, no. 6/7, p. 443–452.

Glover, R. E., 1964, Dispersion of dissolved or suspended materials in flowing streams: U.S. Geol. Survey Prof. Paper 433–B, 32 p.

Godfrey, R. G., and Frederick, B. J., 1963, Dispersion in natural streams: U.S. Geol. Survey open-file rept., 75 p.

Hino, Mikio, 1961, Discussion of "Eddy diffusion in homogeneous turbulence": Am. Soc. Civil Engineers Trans., v. 126, pt. 1, p. 417–419.

Hinze, J. O., 1959, Turbulence: New York, McGraw-Hill Book Co., 586 p.

Hubbell, D. W., and Sayre, W. W., 1964, Sand transport studies with radioactive tracers: Am. Soc. Civil Engineers Proc., v. 90, no. HY4, Paper no. 3900, p. 39–68.

Kalinske, A. A., and Pien, C. L., 1944, Eddy diffusion: Industrial and Engineering Chemistry, v. 36, p. 220–223.

Karman, T. von, and Lin, C. C., 1949, On the concept of similarity in the theory of turbulence: Rev. Modern Physics, v. 21, p. 516–519.

Kolmogoroff, A. N., 1941, The local structure of turbulence in incompressible viscous fluid for very large Reynolds numbers: Acad. Sci. URSS Comptes rendus (Doklady), v. 30, no. 4, p. 301–305.

Korn, G. A., and Korn, T. M., 1961, Mathematical handbook for scientists and engineers: New York, McGraw-Hill Book Co., 943 p.

Krenkel, P. A., 1960, Turbulent diffusion and the kinetics of oxygen absorption: California Univ., Ph. D. dissert., 142 p.

Krenkel, P. A., and Orlob, G. T., 1963, Turbulent diffusion and the reaeration coefficient: Am. Soc. Civil Engineers Trans., v. 128, pt. III, p. 293–334.

Lee, Y. W., 1960, Statistical theory of communication: New York, John Wiley & Sons, 509 p.

Levenspiel, Octave, and Smith, W. K., 1957, Notes on the diffusion-type model for the longitudinal mixing of fluids in flow: Chemical Engineering Science, v. 6, p. 227–233.

Mickelsen, W. R., 1960, Measurements of the effect of the molecular diffusivity—turbulent diffusion: Jour. Fluid Mechanics, v. 7, pt. 3, p. 397–400.

Nemenyi, P. F., 1946, Discussion of "Transportation of suspended sediment by water": Am. Soc. Civil Engineers Trans., v. 111, p. 116–125.

Orlob, G. T., 1958, Eddy diffusion in open channel flow: California Univ., Sanitary Engineering Research Lab., Contr. 19, 144 p.

——— 1961, Eddy diffusion in homogeneous turbulence: Am. Soc. Civil Engineers Trans., v. 126, pt. 1, p. 397–438.

Patterson, C. C., and Gloyna, E. F., 1963, Radioactivity transport in water—the dispersion of radionuclides in open channel flow: Univ. Texas, Environmental Health Engineering Research Lab. Tech. Rept. to U.S. Atomic Energy Comm., 87 p.

Richardson, L. F., 1920, Some measurements of atmospheric turbulence: Royal Soc. London Philos. Trans., v. 221A, p. 1–28.

Richardson, L. F., and Stommel, H., 1948, Note on eddy diffusion in the sea: Jour. Meteorology, v. 5, p. 238–240.

Sayre, W. W., and Albertson, M. L., 1963, Roughness spacing in rigid open channels: Am. Soc. Civil Engineers Trans., v. 128, pt. 1, p. 343–427.

Sayre, W. W., and Chamberlain, A. R., 1964, Exploratory laboratory study of lateral turbulent diffusion at the surface of an alluvial channel: U.S. Geol. Survey Circ. 484, 18 p.

Sayre, W. W., Guy, H. P., and Chamberlain, A. R., 1963, Uptake and transport of radionuclides by stream sediments: U.S. Geol. Survey Prof. Paper 433–A, 35 p.

Sayre, W. W., and Hubbell, D. W., 1963, Transport of radionuclides in fresh water—Dispersal of bed sediments, *in* U.S. Atomic Energy Comm., Transport of radionuclides by fresh water systems: U.S. Atomic Energy Comm. TID–7664, p. 327–352.

——— 1965, Transport and dispersion of labeled bed material, North Loup River, Nebraska: U.S. Geol. Survey Prof. Paper 433–C, 48 p.

Task Committee on Preparation of Sedimentation Manual, 1963, Sediment transportation mechanics—suspension of sediment: Am. Soc. Civil Engineers Proc., v. 89, no. HY5, Paper no. 3636, p. 45–87.

Taylor, G. I., 1921, Diffusion by continuous movements: London Math. Soc. Proc., Ser. 2, v. 20, p. 196–211.

Taylor, G. T., 1953, Dispersion of soluble matter in solvent flowing slowly through a tube: Royal Soc. (London) Proc., Ser. A, v. 219, p. 186–203.

——— 1954, The dispersion of matter in turbulent flow through a pipe: Royal Soc. (London) Proc., Ser. A, v. 223, p. 446–468.

Tchen, C. M., 1947, Mean value and correlation problems connected with the motion of small particles suspended in a turbulent fluid: Delft Tech. Univ. Lab. Aero-and Hydrodynamics Rept. 51.

Vanoni, V. A., 1946, Transportation of suspended sediment by water: Am. Soc. Civil Engineers Trans., v. 111, p. 67–133.

Yotsukura, Nobuhiro, 1963, Turbulent dispersion of miscible materials in open channels: *in* U.S. Atomic Energy Comm., Transport of radionuclides in fresh water systems: U.S. Atomic Energy Comm. TID–7664, p. 311–326.

Yotsukura, Nobuhiro, and Fiering, M. B., 1964, Numerical solution to a dispersion equation: Am. Soc. Civil Engineers Proc., v. 90, no. HY5, Paper no. 4046, p. 83–104.

——— 1966, Closure to "Numerical solution to a dispersion equation": Am. Soc. Civil Engineers Proc., v. 92, no. HY3, p. 67–72.

Yotsukura, Nobuhiro, Smoot, G. F., and Cahal, D. I., 1964, Dispersion in open channel flow: U.S. Geol. Survey open-file report, 19 p.

U.S. GOVERNMENT PRINTING OFFICE : 1968—O–281–661